Cinvestav del IPN

Doctoral Dissertation

Adaptive Sliding Mode Techniques with Aerospace Applications

Author:
M. Sc. Sajjad Keshtkar

Supervisor:
Dr. Alexander Poznyak

A thesis submitted in fulfilment of the requirements for the degree of Doctor of Science

in the

Department of Automatic Control

June 2016

CINVESTAV DEL IPN

Abstract

Department of Automatic Control

Doctor of Science

Adaptive Sliding Mode Techniques with Aerospace Applications

by M. Sc. Sajjad KESHTKAR

In this dissertation, the adaptive techniques based on sliding mode are studied to be implemented in operation, orientation and observation of the aerospace systems. The adaptation is directed to the observed feedback control and the chattering effect reduction for nonlinear satellite-ground stabilization and tracking particulary for *tethered satellite systems* and *parabolic Cassegrian radio-telescope antennas*.

The tethered satellite system is a set of spacecrafts, connected by long cables (tethers), orbiting around the Earth. The large length, compared to conventional satellites, makes a strong interaction of these systems with external fields of the planet through which allows to resolve a wide range of tasks related to space exploration. The ground tracking task of these satellite systems is resolved by a dual reflector radio-telescopes with movable secondary mirror which uses a Stewart platform as a positioner. The nonlinear mathematical models of the named mechanisms are developed in the presence of external perturbations, model uncertainty and neglected dynamics.

The unusual structure and complicity of the named mechanisms and the high accuracy needed for their operation on leads to use a new robust and effective controllers and observers. The set of methods developed in this work deal firstly with the adaptive sliding mode control with the adaptation of the gain matrix providing the reduction of undesirable chattering effect and near-singularity phenomenon while the second one represents a feedback sliding mode controller with the observation based on high order sliding mode. The behavior of proposed methods on the performance of the system are obtained numerically via simulation.

Resumen

En la tesis se estudiaron las técnicas adaptivas de control con base en modos de deslizamiento que se aplicaron en la operación, la orientación y la observación de los sistemas aeroespaciales. La adaptación se dirige al control retroalimentado para la estabilización y seguimiento de un sistema no lineal satélite-tierra que incluye un sistema de satélites atados y una antena de radiotelescopio parabólico tipo Cassegrain como su seguidor.

El sistema de satélites atados es un conjunto de naves espaciales, conectadas por cables largos (ataduras), que orbitan alrededor de la Tierra. La longitud grande, en comparación con los satélites convencionales, hace una fuerte interacción de estos sistemas con campos externos del planeta a través del cual permite resolver una amplia gama de tareas relacionadas con la exploración del espacio. La tarea de seguimiento desde la Tierra para estos sistemas de satélites se realizó mediante un radio-telescopio con doble reflector con el reflector (espejo) secundario móvil que utiliza una plataforma de Stewart como su posicionador. Los modelos matemáticos de los mecanismos nombrados han sido desarrollados en presencia de perturbaciones externas, y dinámicas internas desconocidas.

La estructura inusual y la complicidad de los mecanismos nombrados y la alta precisión requerida para su funcionamiento requieren una atención detallada para la elección y diseño de controladores. Por otro lado la complejidad de los sistemas hace imposible la medición de todos los estados, que impide el uso de un observador de estado capaz de estimar estos estados en presencia de perturbaciones. Algunos nuevos diseños de controladores y observadores eficaces basados en modos deslizantes han sido propuestos para las tareas mencionadas. El conjunto de métodos desarrollados en el trabajo se tratan en primer lugar con un control adaptable basado en modos deslizantes con la adaptación de la matriz de ganancias que proporciona la eleminación de la singularidad del sistema de posicionador. La segunda parte de la tesis representa la retroalimentación de un controlador clásico basado en modos deslizantes con la observación basada en Super-Twisting. El comportamiento de los métodos propuestos en el rendimiento del sistema se comprobó a través de la simulación numérica.

Acknowledgements

Firstly, I would like to express my sincere gratitude to my advisor Prof. *Alexander Poznyak* for the continuous support of my Ph.D study and related research, for his patience, motivation, and immense knowledge. His guidance helped me in all the time of research and writing of this thesis. I could not have imagined having a better advisor and mentor for my Ph.D study.

Besides my advisor, I would like to thank the rest of my thesis committee: Dr. *Wen Yu*, Dr. *Rafael Martínez*, Dr. *Fernando Castaños*, Dr. *Alberto Luviano* and Dr. *Eusebio Hernandez* for their insightful comments and encouragement, but also for the hard question which incented me to widen my research from various perspectives.

My sincere thanks also goes to my teachers, colleagues and friends in *CINVESTAV* and *ESIME Ticomán*. Without their precious support it would not be possible to conduct this research.

Special thank to the *National Council of Science and Technology (CONACYT)* of Mexico who supported my Ph.D study and research.

Finally my deepest gratitude goes to my family for their unflagging love and unconditional support throughout my life and my studies.

Contents

List of Figures

Chapter 1

Introduction

At the present time, there is an intense exploration of space, which is conducted on a broad scale, including numerous flights to the Earth orbit as well as to other planets of the solar system. There are also many experimental and perspective concepts of spacecrafts with unusual structure and architecture, which promise an easy and cheap access to the space and the interplanetary travels. For the successful implementation of these operations, the orientation and stabilization of spacecrafts and their trackers are necessary and inevitable. The solution of this task lays on the orientation and stabilization systems, the technical and operational features of which can guarantee the success of the scientific experiments. Thereby, reliable and effective control systems, which provide a long trouble-free operating time, become necessary.

Control in outer space varies appreciably from the control in the terrestrial conditions. Firstly, the conditions, existing in the space, differs the Earth by the presence of the gravity, intensive radiation, rarefaction near to absolute vacuum, and, consequently, almost the total lack of natural damping. These factors complicate the construction and exploitation of the orientation and stabilization subsystems and make their computational and experimental modelling exceedingly difficult. Secondly, in outer space the disturbing moments, acting on the spacecraft, are very small and usually there is no need to use a large magnitude of restoring moments, produced by the control system. However, these small disturbing moments in the condition of almost absolute vacuum and absence of natural damping exert an essentially influence on the movement of spacecraft. This acquires a great significance to the question of dynamic of stabilization and orientation systems.

The first spacecrafts were turning in the space, without any orientation [1, 2]. Later spacecraft mission designs used passive spin stabilization to hold one axis relatively fixed by spinning the spacecraft around it (usually the axis of maximum moment of inertia). The spin stabilization was mostly used due to the limited control actuation and lack of sophisticated computer technology to implement complex control laws. The spin-stabilized spacecrafts are very stable but they have to be sensitively balanced and every component has to be designed and located with spacecraft balance in mind. This can be extremely difficult to accomplish the required accuracy. In most cases the last few weights are added and adjusted only after actual flight hardware is delivered and installed, and the spacecraft is experimentally spin tested. Allowances must also be made for everything onboard that can move during flight [1].

In view of the absence of natural damping in outer space it is required to create damping moments by artificial way with the help of a special mechanism. Actually for the orientation systems the special devices based on natural forces of circular fields, electromagnetic and centrifugal forces among all are designed and successfully exploited. The dynamic characteristics and precision of the spacecraft operation depends of the choice, design and operation of these devices.

In the modern era advancements in sensors, actuators, and computer processors allow the three-axis stabilized spacecraft designs, although spinners are still used to this day for many missions. Attitude control law theory also has been extensively studied and advanced, allowing for guaranteed control stability even with nonlinear attitude dynamics. However, the control of spacecraft and its tracking devices still poses a difficult problem. These difficulties include the highly nonlinear characteristics of the governing equations, control rate, saturation constraints and limits, and incomplete state knowledge due to sensor failure or omission [2].

Together with the launch of artificial satellites of earth (first on October 4 in 1957 by URRS)the fast development the radioelectrinic–space communication initiated. The centers of space communication with unique full revolving antennas, powerful transmitters and high–sensitive receivers, high-performance computer were built. These facilities allowed to control the flight and receive the information from satellites and objects, situated in the hundreds of million of kilometers from the Earth's surface. At the same time the large number of station are under construction for tracking and observing the satellites

and the communication between terrestrial stations via satellites; the question of antenna-installations guidance towards the satellite and practically their round-the-clock tracking independently of meteorologic conditions transforms into a comparatively sophisticated technical problem.

The development of radio-astronomy would not be possible without the big-area antennas with low temperature noise. This fact forced the engineers to come up with the new designs of antennas, new principles of reflecting surfaces, rotary supports and high-precise automatic guidance and control systems.

The principal designation of automatic control system of antenna installations for the space communication is to point the main maximum diagram of orientability of the antenna to the given direction in the space and to move the diagram in compliance with the real movement of satellite. In all process it is important to take into account the deformation of the antenna construction and external perturbations.

Since the orbits of space objects or satellites, which are observed by antenna, are usually well known, then the main working regime of the automatic control system is given by programs. Nevertheless the modern automatic control systems must provide the search regimes, auto-tracking, combined guidance and manual distance pointing (for example, for the execution of works adjusting preventive repair works [3].

1.1 Control of aerospace systems

The specialists, who are working on the design of spacecraft's control system, use two principals in their practical works: "orientation" and "stabilization", although they are not interchangeable [1].

Orientation is a process, in the result of which the spacecraft takes a defined place or a the sequence of defined locations in space. As a general rule, the orientation system, by removing the initial deviation, combines the connected and base coordinate systems together; the later is tasked by the control system on the board of aircraft and can be realized by active or passive devices.

Stabilization is the process of elimination of angular deviations between the connected and base coordinate systems occurred during the flight. The stabilization system gives to the spacecraft the possibility of either restoring to the initial position, damaged by the external as well internal perturbations, or to be resistant and robust to these perturbations.

The named control tasks can be accomplished by either open-loop or closed-loop schemes. Open-loop schemes usually require a pre-determined pointing maneuver and are typically determined using optimal control techniques, which involve the solution of a two-point boundary value problem (e.g. the time optimal maneuver problem). Open-loop schemes are sensitive to system parameter uncertainties and unexpected disturbances. Closed-loop systems can account for parameter uncertainties and disturbances, and thus provide a more robust design methodology [4].

For many years now, much effort has been devoted to the closed-loop design of aerospace system controllers. In [5] a number of simple control schemes are derived using quaternion and angular velocity (rate) feedback. Asymptotic stability is shown by using a Lyapunov function analysis for all cases. Reference [6] expands upon these formulations by deriving simple control laws based on both a Gibbs vector parameterization and a modified Rodrigues parametrization, each with rate feedback. Lyapunov functions are shown for all the controllers developed in this work as well.

Other full state feedback techniques have been developed that are based on variable-structure (sliding mode) control, which uses a feedback linearizing technique and an additional term aimed at dealing with model uncertainty. This type of control has been successfully applied for large angle maneuvers using a Gibbs vector parametrization, a quaternion parametrization, and a modified Rodrigues parametrization [7]. Another robust control scheme using a nonlinear H1 control methodology has been developed in [8]. This scheme involves the solution of Hamilton-Jacobi-Isaacs inequalities, which essentially determines feedback gains for the full state feedback control problem so that the spacecraft is stabilized in the presence of uncertainties and disturbances. Robust control can be thought of as an online policy capable of regulating aerospace systems whose dynamics may contain bounded (in some sense) uncertainties. Such algorithm often utilizes feedback-feed forward state-output connections to generate appropriate control inputs so that the plant output moves along the prescribed trajectories [9].

1.2 Criteria for feedback control election

We often start with a mathematical model that resembles the process of interest in a selected domain of operation. The model may or may not be accurate in capturing significant and other effects in the process dynamics. In order to overcome potential modeling deficiencies, we seek a robust solution, designed based on the model, yet capable of controlling the real process, and not just the model. We would also want a controller whose performance "gracefully degrades" in the presence of uncertainties. The graceful degradation property is highly desirable, since it becomes the only assurance that the controller would not abruptly break down, if and when the system encounters slightly unprecedented events during its intended operation.

Embedding robustness properties into a control solution should be treated as one of the main criteria in any design. For example, achieving closed-loop stability and tracking performance, while providing adequate stability margins, are the main goals, especially when dealing with very adequate aerospace systems.

On the other hand the aforementioned techniques all utilize full state knowledge (i.e. orientation and rate feedback). The problem of controlling a spacecraft without full state feedback is more complex. The basic approaches used to solve this problem can be divided into methods which estimate the unmeasured states using a filter algorithm and methods which develop control laws directly from output feedback. A more direct technique is need to be developed in, which solves the orientation problem without rate knowledge. This method should be based on a passivity approach, which replaces the rate feedback by a nonlinear observer.

Sliding mode technique can satisfy the above listed requirements. This method [4, 10] is a robust technique that alters the dynamics of a nonlinear system by the application of a switching control. The feature of this approach is that it has the so called *sliding mode* on the switching surface. Within the sliding mode, the system remains intensive to parameter variation and disturbances and its trajectories lie in the switching surface. The sliding phenomenon do not depend on the system parameters and have a stable property. The combination of the sliding mode controller/observer presented in this work can be the adequate feedback control for the named tasks.

1.3 Applications of designed controls

It will be presented how to design and analyze practical control algorithms for two practical systems with nonlinear and uncertain dynamics. The application of the suggested controllers are illustrated for the orientation of a tethered satellite system and the sub-reflector of a radiotelescope that follows the movement of the satellites.

1.3.1 Tethered Satellite Systems

Firstly to illustrate the effectiveness of the suggested technique in outer-space conditions consider the, so-called, *Tethered Satellite System* (TSS). This system consists of two or more bodies connected with long high-strength cable accomplishing orbital flight. Tethered satellite systems are not a new concept, however, and in fact have been studied since well before the dawn of human space flight. In addition to the various theoretical studies of TSS that have been performed in the past, a number of TSS missions have already own in space, providing a solid foundation for the design of future missions and the further development of the theory underlying the behavior of TSS. The concept of a TSS was first proposed by Tsiolkovsky in 1895. In his work, Tsiolkovsky proposed a means of generating artificial gravity that involves connecting a spacecraft to a counterweight with a long chain and spinning the entire system. Because of its architecture (see Fig. 4.1 [11]) the TSS can offer numerous advantages comparing with the traditional space systems. Among them we can mention: generation of artificial gravity, in-space interferometry, orbital maneuvering of spacecraft by means of momentum transfer energy production, propellantless launch, orbital transfer, Earth observation, deep space exploration, and etc. [12].

The main problem discussed in this work is the spinning TSS orientation and stabilization in the orbit. The TSS system is a highly stable but with a rough orientation facility. Additionally it is evident that the dynamics of spinning and electrodynamic TSS can be quite complicated and rich. The analysis and design of any TSS mission requires more than the qualitative insights discussed thus far, and the literature contains a vast amount of detailed analysis of various types of TSS.

The problem can be resolved by creating the desired control torque; due to the interaction with in/out plane angles, we can achieve both high accuracy of stabilization and attitude

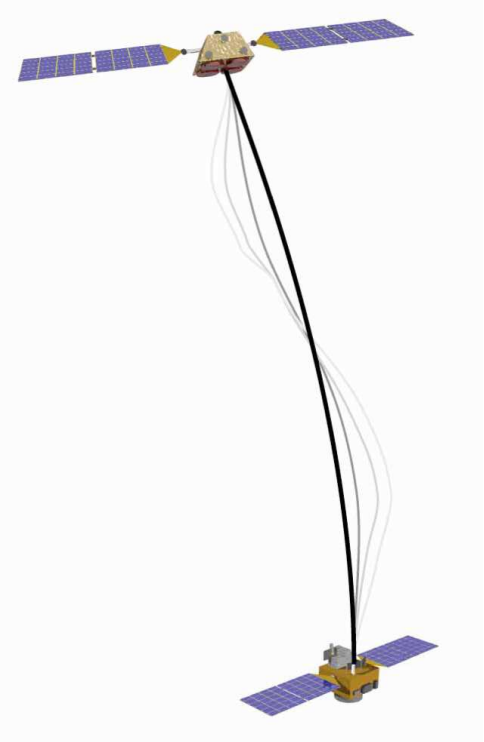

FIGURE 1.1: The tethered space system representation.

control systems. Thus, the introduction of a system with active control points, opens up the possibility of creating a new generation of high-precision orientation and stabilization TSS.

1.3.2 Radio-Telescope Subreflector

The radio-telescope antenna is a device that is used to receive radio-frequency radiation emitted by extraterrestrial sources and satellites. Radio telescopes vary widely, but depending on their design they can be divided in one and dual reflector antennas. In dual-reflector (Cassegrian) antennas a parabolic reflector is used as the mail reflector and a hyperboloid of revolution as the sub-reflector (secondary mirror) as shown in Fig. 1.2. This antenna has a number of advantages over a single-dish. In dual-reflector antenna the feed can be positioned close to the primary reflector. This simplifies the supplying of the power to the feed, shortens the length of the supply line and facilitate the mounting of the line and the feed. Shortening the supply line leads to a reduction of the losses and reduces the noise temperature of the power path.

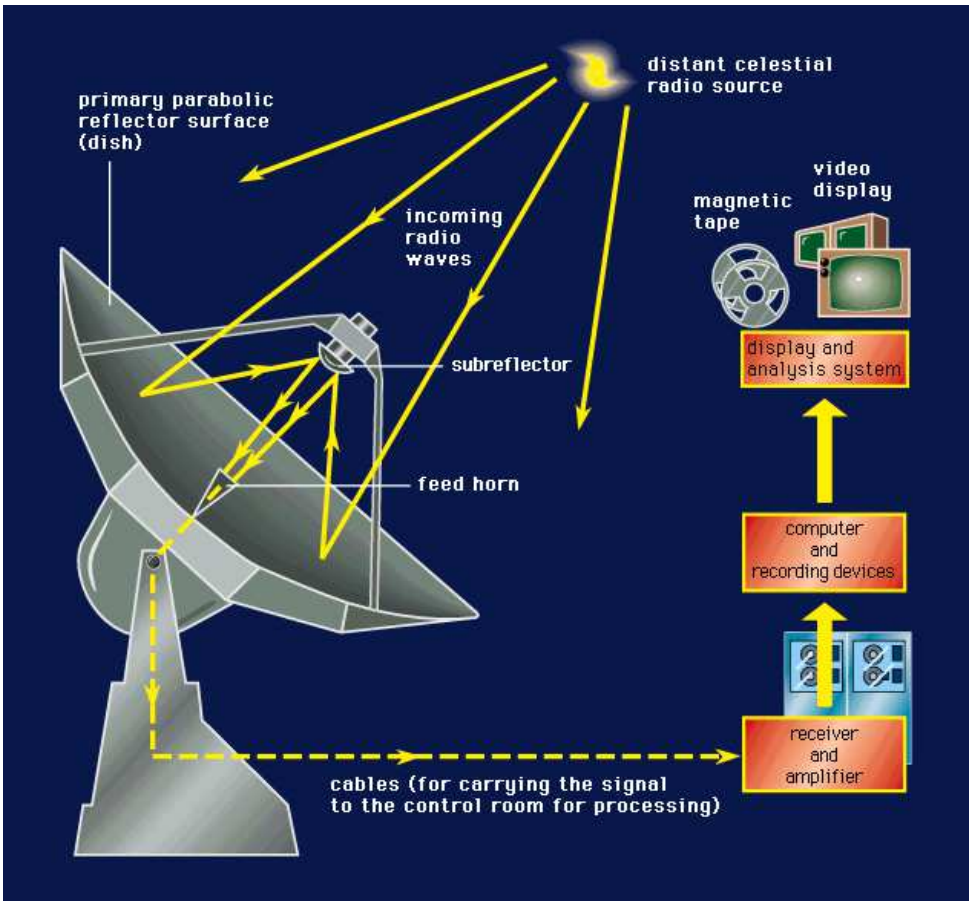

FIGURE 1.2: The Radio telescope with a Cassegrain antenna.

The performance of a radio telescope is limited by various factors: the accuracy of reflecting surfaces that may depart from the ideal shape because of manufacturing irregularities; the effect of wind load; thermal deformations that cause differential expansion and contraction; and deflections due to changes in gravitational forces as the antenna is pointed to different parts of the sky.

In this work a Stewart platform is used to obtain desired pointing accuracy (1 arcsec) of the subreflector (secondary mirror) in the required position and orientation. These highly position and attitude requirements encompass six independent degrees of freedom. The platform consists of a stationary base, the mirror mounted on a movable platform, and six prismatic actuators. The main problem here is to design the control laws that provides the desired positioning task in the presence of disturbances/uncertainties.

1.4 Contribution of the dissertation

Although a great deal of research has already been conducted on the dynamics and control of aerospace systems, there exist a number of topics that remain to be addressed. The purpose of this dissertation is to address some of these open areas of study, and in this section we present an overview of the original contributions made by this work.

First, the orientation tasks of a tethered satellite system and a radiotelescope subreflector are resolved using a sliding mode controller for both regulation and tracking cases. Then, the the chattering and near-singularity problems are discussed and the elimination approaches are shown.. An example from a real plants, the Large Millimetric Radiotelescope, is shown for tracking task. finally, the feedback control is discussed using a sliding mode observer. This is followed by.

Chapter *2* is solely devoted to adaptive control method based on "equivalent control" for nonlinear systems with perturbations/uncertainties. The near-singularity phenomenon of the systems is also discussed in the second section of this chapter.

Chapter *3* covers a new topic in feedback control method design with observer and controller both based on sliding mode techniques in a progressive complexity. For the unmeasured state estimations the realization of a classical high-order sliding mode needs to be designed as an adaptive one.

The mathematical model of dynamic systems to be used in positioning and orientation tasks are then described in Chapter *4*. Most of the previous research on the dynamics of spinning TSS has used simplified system models in which the out-of-plane pendular motion of the tether is neglected. A typical spinning TSS nominally spins in the orbit plane, so it is reasonable to neglect the out-of-plane motion in a preliminary study of spinning TSS dynamics; however, a complete picture of spinning TSS dynamics requires a rigorous analysis of the out-of-plane pendular motion of the system. Such an analysis is one of the main contributions of this work. A simplified system model is used to study the stability of small out-of-plane pendular motion of the tether, and to determine approximate solutions for stable out-of-plane pendular motion. These results obtained using a simplified system model are validated using numerical solutions determined using the top-level computational model.

Chapter *5* is devoted to show the performance of the proposed approach through the numerical simulations. Concluding remarks and recommendations for future work are offered in Chapter *6*.

The publications based on the research of this dissertation is devoted in the last page.

Chapter 2

Adaptive Sliding Mode Control

Control systems must provide stability and performance in the presence of model uncertainty and neglected dynamics. This has proven to be a significant challenge, and as our understanding of dynamics and control has improved, aerospace has been able to develop new aircraft designs that are faster, have greater performance, and perform robustly in very large flight envelopes. These advancements built upon the foundation created by classical methods but were powered by computer-aided design tools which greatly expanded the engineer's ability to solve larger and more complex problems using advanced techniques.

In general, designing flight control systems using conventional (classical) analytical methods involves iterative single-loop design analyses that are costly in time and manpower. These systems were often designed by discretizing the flight envelope at specific points, designing the control system at these points, and guaranteeing robustness to parameter variations by designing large single-loop stability margins and evaluating the design through simulation.

The control system is called *adaptive*, if the online information in it, in addition to the elaboration of the control action, is used also to change the control algorithm. In the usual (nonadaptive) control systems the current information just is used for the formation of control action.

The adaptive controls are used, when with the help of usual systems the proposed task can not be handled. This usually happens when the initial information about the object

is not enough or during the operation the object's characteristics changes widely in an unexpected way.

The researches about the design of adaptive control systems began at the early 50s in connection with the construction of the autopilots for new airplanes with wide rate of velocity and height [1]. However, the first attempts of using the adaptive control for the autopilot ended in failure, which led to a decrease of interest in adaptive control for some time. After a short break, the study of adaptive control continued. Especially intensively the theory of adaptive control was developed at the end of the last century, and while great achievements have been achieved in this direction.

Initially the practical application of developed adaptive control algorithms were restrained because of their complexity. However recently thanks to big capacities of actual computing devices, the adaptive control methods found a practical use in a field, as robotics, aeronautics, energetic system and complex technological process control [13].

There are many systems in which the use of adaptive control is recommended and even necessary. For example for in the aerospace devices like airplanes and aircrafts, their aerodynamic characteristics depend on the velocity and the height of the plane and the atmosphere conditions of flight. Additionally during the flight, some particular parameters, defining the dynamic property of the airplane, could change in ten times. In this conditions the common autopilots can not handle the high quality control task.

The models of technological process in metallurgy, chemistry, petrochemistry are very complex. Because of a priori information their parameters and structures are not always available. Moreover, these parameters can change during the fluxion of of the technological process in the named areas. Therefore the common control systems in a lot of cases can not provide a high quality, and sometimes just a simple stable control of these process [13].

In the development of the unified regulator for a wide class of objects the parameters of regulator can not be accurately calculated and established in advance. Therefor if these regulators are nonadaptive, then with their use in each specific case there will be a need for tuning. The application of adaptive regulators relieve the users from these procedures, which allows to save the time and energy.

In most cases the adaptive control aims to neutralize the parametric uncertainty or the inevitable parameter changes in the object. However in some cases, particulary for controlling the technological process, when hundreds of outline controllers can be presented, the adaptive control also is used to reduce the number of design variables of manual tuning and at the same time increase the performance and practicality of the control system.

Summarizing, it can be proved, that the use of adaptive control allows to:

- provide the optimum behaviour of the control system in conditions of uncomplete information;
- provide the workability of the control system in conditions of the objects with widely changing dynamic properties;
- create a unified regulator for wide class of objects;
- reduce the systems' design and tuning time.

2.1 Adaptive and robust control with sliding mode

The Sliding Mode Control is a very popular strategy for control of nonlinear uncertain systems, with a very large frame of applications fields [4, 10]. Due to the use of the discontinuous function, its main features are

- the robustness of closed-loop system
- and the finite-time convergence.

However, its design requires the knowledge of the bound on the uncertainties, which could be, from a practical point of view, a hard task: it often follows that this bound is overestimated, which yields excessive gain. Then, the main drawback of the sliding mode control, the well-known chattering phenomenon, is important and could damage actuators and systems. A first way to reduce the chattering is the use of a boundary layer: in this case, many approaches have proposed adequate controller gains tuning. A

second way to decrease the effect of the chattering phenomenon is the use of higher order sliding mode controller [14–16]. However, in both these control approaches, knowledge of the bound on the uncertainties is required. As the objective is the non-requirement of the uncertainties bound, another way consists in using adaptive sliding mode, the goal being to ensure a dynamic adaptation of the control gain to be as small as possible whereas sufficient to counteract the uncertainties and perturbations.

The basic idea of the Adaptive Control Approach consists in designing the systems exhibiting the same dynamic properties under uncertainty conditions based on utilization of current information. It involves modifying the control law used by a controller to cope with the fact that the parameters of the system being controlled are slowly time-varying or uncertain. Even more, adaptive control implies improving dynamic characteristics while properties of a controlled plant or environment are varying [17]. Without adaptation the original SMC demonstrates robustness properties with respect to parameter variations and disturbances [10]. The first attempts to apply the ideas of adaptation in Sliding Mode Control (SMC) were made in the 60's (for example, see [18]): the control efficiency was improved by changing the position or equation of the discontinuity surfaces without any information on a plant parameters. The design idea might be formulated as follows: if sliding mode exists, then the coefficients of switching plane can be varied to improve the system dynamics.

However those early publications did not take into account the main obstacle for SMC application - the chattering phenomenon which is inherent in sliding motions. This phenomenon is well-known from literature on power converters and referred to as "ripple". Then the efforts of the researchers were oriented to the application of adaptability principles to reduce the effect of chattering.

Since the amplitude of chattering is proportional to discontinuity magnitude in control, one of possible adaptation methods is related to reducing this magnitude to the minimum admissible value dictated by the conditions for SM to exist. So, in [19] the control gain depended on the distance of system state to a discontinuity surface. The tracks of adaptability can be found in the first publications about variable structure systems with SM with the control gain proportional the system state. As recalled previously, this problem is an exciting challenge for applications given that, in many cases, gains are also overestimated, which gives larger control magnitude and larger chattering.

In [20] gain dynamics directly depends on the tracking error (sliding variable): the control gain is increasing since sliding mode is not established. Once this is the case, gain dynamics equals zero. The main drawback of this approach is the gain over-estimation with respect to uncertainties bound. Furthermore, this approach is not directly applicable, but requires modifications for its application to real systems: thus, the sign function is replaced by a saturation function where the boundary layer width affects accuracy and robustness.

Furthermore, no boundary layer width tuning methodology is provided. A method proposed in [16] in order to limit the switching gain must be mentioned. The idea is based on use of equivalent control: once sliding mode occurs, disturbance magnitude is evaluable and allows an adequate tuning of control gain. However, this approach requires the knowledge of uncertainties/perturbations bounds and the use of low-pass filter, which introduces signal magnitude attenuation, delay and transient behavior when disturbances are acting. In [21] a gain-adaptation algorithm is proposed by using sliding mode disturbance observer. The main drawback is that the knowledge of uncertainties bounds is required to design observer-based controller. There exist also adaptive SMC (ASMC) algorithms that allow adjusting dynamically the control gains without knowledge of uncertainties/perturbations bounds. In particular, several adaptive fuzzy SMC algorithms were proposed. However, they do not guarantee the tracking performance or overestimate the switching control gains as in . Of course, another efficient tool to suppress chattering is the application of state observers, but for this method the plant parameters are assumed to be known.

2.2 Conventional Sliding Mode Design

Consider the following controlled uncertain system represented by the state space equation

$$\dot{x}(t) = f(x,t) + g(x_1,t)\,u(x,t) + \xi(x,t) \tag{2.1}$$

- $x(t) := \left(x_1^\top(t), x_2^\top(t)\right)^\top \in \mathbb{R}^{2\times n}$;

- $x_1(t)$, $x_2(t) \in \mathbb{R}^n$ are states of the system at time $t \in \mathbb{R}_+$;

- $u \in \mathbb{R}^n$ is a control to be designed;

- $\xi(x,t) \in \mathbb{R}^n$ is unmeasurable term including the external as well as internal perturbations and uncertainties;

- $f(x,t) \in \mathbb{R}^n$, $g(x_1,t) \in \mathbb{R}^{n\times n}$ are supposed to be exactly known.

$$\|\xi(x,t)\| \leq L$$

where L is assumed *a* priory.

The problem is to design a feedback control law $u(x,t)$ that derives the states $x(t)$ (angular positions) to required positions and their derivatives $\dot{x}(t)$ (angular velocities) to zero i.e.,

$$\lim_{t\to\infty}(x_1, x_2, ..., x_n) = x_1^*, x_2^*, ..., x_n^*$$

$$\lim_{t\to\infty}(x_{n+1}, x_{n+2}, ..., x_{2n}) = 0$$

The control, which we are interested in, is apparently a challenging one, since asymptotic convergence is to be achieved in the presence of the bounded disturbance $\xi(x,t)$. First, let us introduce new variables $\sigma_n(x)$ in the state space of the system, which define the sliding surfaces

$$\begin{gathered}
\sigma_1(x) := \dot{x}_1 + c_1(x_1 - x_1^*) = x_3 + c_1(x_1 - x_1^*) = 0 \\
\sigma_2(x) := \dot{x}_2 + c_2 x_2 = x_4 + c_2(x_2 - x_2^*) = 0 \\
\vdots \\
\sigma_n(x) := \dot{x}_n + c_n x_n = x_{2n} + c_n(x_n - x_n^*) = 0 \\
\sigma(x) := \begin{pmatrix} \sigma_1(x) \\ \sigma_2(x) \\ \vdots \\ \sigma_n(x) \end{pmatrix} \in R^n
\end{gathered} \tag{2.2}$$

Here $x_1^*, ..., x_n^*$ are desired angular positions and $c_1, ..., c_n$ are positive constants. $x_{n+1}, ..., x_{2n}$ define the angular velocities and in this chapter are assumed to be measured.

Using the candidate Lyapunov function

$$V(x) := \frac{1}{2}\left\|\sigma\left(x\right)\right\|^2 = \frac{1}{2}\left[\sigma_1^2\left(x\right) + \sigma_2^2\left(x\right) + ... + \sigma_n^2\left(x\right)\right]$$

it derives to:

$$\begin{gathered}\frac{d}{dt}V(x) = \sigma^{\intercal}\left(x\right)\dot{\sigma}\left(x\right) = \sigma^{\intercal}\left(x\right)\left[\frac{\partial}{\partial x}\sigma\left(x\right)\right]\dot{x}\left(t\right) = \sigma^{\intercal}\left[g\left(x_1,t\right)u\left(x,t\right) + h(x)\right] \\ h(x) = f\left(x,t\right) + \xi\left(x,t\right)\end{gathered} \tag{2.3}$$

Let us design the *control action* as

$$\begin{gathered}u\left(x\right) = -k\left[g\left(x\right)\right]^{-1}\mathrm{Sign}\left(\sigma\left(x\right)\right) \\ \mathrm{Sign}\left(\sigma\right) := \left(\mathrm{sign}\left(\sigma_1\right), \mathrm{sign}\left(\sigma_2\right), ..., \mathrm{sign}\left(\sigma_n\right)\right)^{\intercal}\end{gathered} \tag{2.4}$$

where $k > 0$ and

$$\mathrm{sign}\left(z\right) = \begin{cases} 1 & if \quad z > 0 \\ -1 & if \quad z < 0 \\ \in \left[\ -1, \ \ 1\ \right] & if \quad z = 0 \end{cases}$$

Substituting of (2.4) into (2.3) implies

$$\frac{\mathrm{d}}{\mathrm{d}t}V(x) = \sigma^{\intercal}\left(x\right)h(x) - k\sigma^{\intercal}\left(x\right)\mathrm{Sign}\left(\sigma\left(x\right)\right)$$

$$= \sigma^{\intercal}\left(x\right)h(x) - k\left(\left|\sigma_1\left(x\right)\right| + \left|\sigma_2\left(x\right)\right| + ... + \left|\sigma_n\left(x\right)\right|\right)$$

By the inequality

$$\left|\sigma_1\right| + \left|\sigma_2\right| + ... + \left|\sigma_n\right| \geq \sqrt{\sigma_1^2 + \sigma_2^2 + ... + \sigma_n^2} = \left\|\sigma\right\|$$

we get

$$\sigma^{\intercal}(x)\, h(x) - k\left(|\sigma_1(x)| + |\sigma_2(x)| + ... + |\sigma_n(x)|\right) \leq$$

$$\|\sigma(x)\|\, \|h(x)\| - k\,\|\sigma(x)\| = -\,\|\sigma(x)\|\,(k - \|h(x)\|)$$

Finally, selecting the control gain k as

$$k = \|h(x)\| + \rho,\ \rho > 0$$

we obtain

$$\frac{d}{dt}V(x) \leq -\rho\,\|\sigma(x)\| = -\rho\sqrt{2}\sqrt{V(x)}$$

which leads to

$$2\left(\sqrt{V(x(t))} - \sqrt{V(x(0))}\right) \leq -\rho\sqrt{2}t$$

and

$$\sqrt{V(x(t))} \leq \sqrt{V(x(0))} - \frac{\rho}{\sqrt{2}}t$$

The reaching time t_{reach} when $V(x(t))$ becomes to be equal to zero is

$$t_{reach} = \frac{\sqrt{2}}{\rho}\sqrt{V(x(0))} = \frac{1}{\rho}\sqrt{\sigma_1^2(x(0)) + \sigma_2^2(x(0))} \tag{2.5}$$

Consequently, a control law $u(x,t)$ (referred to as the sliding mode controller) is given by

$$u(x,t) = (\|h(x)\| + \rho)\,[g(x)]^{-1}\,\mathrm{Sign}(\sigma(x)),\ \rho > 0 \tag{2.6}$$

2.3 Adaptation Based on the "Equivalent Control"

Using this method, we want to handle simultaneously two interconnected phenomena of application of the SMC: chattering and high activity of control action. It is well known that the amplitude of chattering is proportional to the magnitude of a discontinuous control.

These two problems can be handled simultaneously if the magnitude is reduced to a minimal admissible level defined by the conditions for the sliding mode to exist. Here the adaptation methodology, based on the *equivalent control*, is discussed to obtain the minimum possible value of control. The control objective is associated with dynamic adaptation of Sliding Mode Controllers (under known uncertainty bounds) where the adaptation process is continued during sliding mode, using the current estimates of the corresponding equivalent control, that leads to the minimization of chattering effect.

In the previous works, following to [19], the adaptation process with the varying magnitude of the control gain terminates in the moment when the sliding mode starts. In [22] the authors tried to continue the adaptation process during sliding mode estimating the corresponding equivalent control. However, none of the above algorithms resulted in minimum possible value of the discontinuous control. Finding the solution of this problem under uncertainty conditions is the objective of this section.

2.3.1 Main Assumptions

Let us consider a nonlinear second order system[1]

$$\dot{x}(t) = f(x,t) + g(x_1,t)\,u(x,t) + \xi(x,t) \tag{2.7}$$

we assume that

1. the control $u = u(x,t)$ enforces sliding mode on some surface

$$\sigma(x) = 0$$

[1] for the linear case look [23]

and is in the following form

$$u(x,t) = -k(t)\left(1+\lambda\sqrt{\|x\|^2+\varsigma}\right)\operatorname{sign}(\sigma(x)) \tag{2.8}$$

$$\lambda \geq 0,\ \varsigma > 0,\ k(t) \in [\mu, k^+],\ \mu > 0$$

As one can see the control gain k (t) is a time varying function governed by the adaptation procedure.

2. the uncertain functions $f(x,t)$ and $g(x_1,t)$ satisfy the conditions

$$\|f(x,t)\| \leq f_0 + f_1\|x\|$$

$$0 < b_0 \leq \nabla^\top \sigma(x)\, g(x_1,t) \tag{2.9}$$

$$\|f(x,t)\| \leq g^+,\ \ \|\nabla\sigma(x)\| \leq \sigma^+$$

$$\Phi(x,t) := \frac{\nabla^\top \sigma(x)\, f(x,t)}{\nabla^\top \sigma(x)\, g(x_1,t)}$$

$$\left\|\nabla^\top \Phi(x,t)\right\| \leq \Phi_0 + \Phi_1\|x\| \tag{2.10}$$

$$\left\|\frac{\partial}{\partial t}\Phi(x,t)\right\| \leq \varphi_0 + \varphi_1\|x\|$$

All coefficients in the right-hand sides of these inequalities are constant and positive. The function $\sigma(x)$ and its time derivative

$$\dot{\sigma}(x) = \nabla^\top \sigma(x)\, f(x,t) -$$

$$\nabla^\top \sigma(x)\, f(x,t)\, g(x_1,t)\, k(t)\, \lambda_1 \operatorname{sign}(\sigma(x)) \tag{2.11}$$

$$\lambda_1 = 1 + \lambda\sqrt{\|x\|^2+\varsigma}$$

should have opposite signs ($\sigma(x)\,\dot{\sigma}(x) < 0$ if $\sigma(x) \neq 0$) for sliding mode to exist on the superface $\sigma(x) = 0$. The sufficient condition for this follows from (2.9–2.11):

$$\begin{aligned}\sigma(x)\dot{\sigma}(x) &= \sigma(x)\nabla^{\top}\sigma(x) f(x,t) - \nabla^{\top}\sigma(x) g(x_1,t) k(t) \lambda_1 |\sigma(x)| \\ &\leq \left[\nabla^{\top}\sigma(x) g(x_1,t)\right] |\sigma(x)| \times [\Phi(x,t) - k(t)\lambda_1] < 0\end{aligned} \tag{2.12}$$

The last inequality implies if the second part is negative, e.g.

$$\Phi(x,t) - k(t)\lambda_1 < 0$$

which is always hold when

$$\lambda \geq f_1/f_0,\ \mu > f_0\sigma^{+}/g_0,\ k(t) \in \left[\mu, k^{+}\right] \tag{2.13}$$

in view of the relation

$$|\Phi(x,t)| - k(t)\lambda_1 \leq f_0 \frac{\sigma^{+}(1 + \|x\| f_1/f_0)}{g_0} - \mu(1 + \lambda\|x\|)$$

To derive the sliding mode equation the function $\text{sign}(\sigma(x))$ should be replaced by the solution of the equation $\sigma(x) = 0$ with respect to the term $\text{sign}(\sigma(x))$, called the *equivalent control*:

$$[\text{sign}(\sigma(x))]_{eq} := \begin{cases} \dfrac{\Phi(x,t)}{k(t)\lambda_1} & \text{if} \quad \sigma(x(t)) = 0 \\ \\ \text{sign}(\sigma(x)) & \text{if} \quad \sigma(x(t)) \neq 0 \end{cases} \tag{2.14}$$

satisfying (in view of (2.12)) in the sliding mode ($\sigma(x(t)) = 0$)

$$\left|[\text{sign}(\sigma(x))]_{eq}\right| < 1 \tag{2.15}$$

Note that the state-depended magnitude of discontinuity is the conventional tool to minimize chattering. Indeed, in the course of approaching the origin $x = 0$ it is decreasing automatically. Similarly the term

$$1 + \lambda\sqrt{\|x\|^2 + \varsigma}$$

may also affect the amplitude of chattering appearing on sliding mode phase. The necessity of this term in (2.8) is related with the considered class of nonlinear function satisfying

$$\|f(x,t)\| \leq f_0 + f_1 \|x\|$$

if $f_1 = 0$ (nonlinear function is bounded satisfying $\|f(x,t)\| \leq f_0$) similarly to the example we may take $\lambda = 0$, and, in the case, the term λ_1 does not affect a chattering amplitude. It is important, that this methodology is oriented to the worst case - sliding mode should exist for all values of unknown functions or parameters from some range. The method of the paper guarantees the minimal magnitude for their current values of unknown functions and parameters.

In general, we may add the term λ_1 to the gain multiplying the discontinuous function $\sigma(x)$ to enforce sliding mode when $f(x)$ is unbounded. This term in the form $\varsigma = 0$ (in the form $1 + \lambda \|x\|$) can solve this problem as well. However, the adaptation algorithm implies existence of the gradient of this term, but it does not exist for the last case.

Below we will show that in the general case the adaptation of the gain-parameter $k(t)$ only is sufficient to minimize the chattering effect on sliding mode phase since the suggested "learning law" for $k(t)$ variation automatically takes into account the presence of this term.

2.3.2 Adaptation procedure

$$\dot{x}(t) = f(x,t) + g(x_1,t)\, u(x,t) + \xi(x,t) \tag{2.16}$$

Consider the system (2.7). The adaptation (learning) law for the control gain $k(t)$ can be represented as

$$\dot{k}(t) = \begin{cases} \gamma_0 k(t) \operatorname{Sign}(\theta(t)) - M[k(t) - k^+]_+ + M[\mu - k(t)]_+ \\ \text{if } 0 < \mu \leq k(t) \leq k^+ \\ \\ 0 \text{ otherwise} \end{cases} \tag{2.17}$$

where

$$\begin{gathered} \theta(t) := \left\| [\operatorname{Sign}(\sigma_t)]_{eq} \right\| - \varrho, \\ \varrho \in \left(\sqrt{2} - \upsilon, \sqrt{2}\right), \quad \gamma_0, \mu > 0 \end{gathered} \tag{2.18}$$

The gain k can vary in the range $[\mu, k^+]$ where $\mu > 0$ is a preselected minimal value of k, $M > \rho k^+$, $\rho > 0$.

The function $[z]_+$ represented above can be defined as

$$[z]_+ := \left\{ \begin{array}{l} 1 \text{ if } z \geq 0 \\ 0 \text{ if } z < 0 \end{array} \right\}, \; M > \rho k^+, \; \rho > 0$$

The vector-function $v := [\operatorname{Sign}(X(t))]_{eq}$ is an average value, or a slow component of discontinuous function $\operatorname{Sign}(x(t))$ switching at high frequency and can be easily obtained by a low pass filter, which filters out the high frequency component [24]:

$$\mu \dot{v} + v = \operatorname{Sign}(\sigma(x))$$

fulfilling

$$v \simeq [\operatorname{Sign}(\sigma(x))]_{eq}$$

Certainly, the component values of vector v is in the range $[-1, 1]$.

To justify the workability of the control algorithm (2.4) with the gain $k(t)$, given by (2.17), notice that on the sliding surface $\sigma(x) = 0$ the "*equivalent control*" (see [25]) can be found from the equation

$$\dot{\sigma}\left(x\left(t\right)\right)=\left[\frac{\partial}{\partial x}\sigma\left(x\right)\right]\dot{x}=g\left(x_1,t\right)u\left(x,t\right)+h\left(x\right)=0$$

which leads to

$$0=g\left(x_1,t\right)u\left(x,t\right)+h\left(x\right)=-k(t)\left[\mathrm{Sign}\left(\sigma\left(x\right)\right)\right]_{eq}+h\left(x\right)$$

and, as the result, to

$$\left[\mathrm{Sign}\left(\sigma\left(x\right)\right)\right]_{eq}=\left[\begin{array}{c}\mathrm{sign}\left(\sigma_1\left(x\right)\right)\\ \mathrm{sign}\left(\sigma_2\left(x\right)\right)\\ \vdots\\ \mathrm{sign}\left(\sigma_n\left(x\right)\right)\end{array}\right]_{eq}=\frac{1}{k(t)}h\left(x\right)$$

Hence, the vector $\left[\mathrm{Sign}\left(\sigma\left(x\right)\right)\right]_{eq}$ is differentiable so that

$$\frac{\mathrm{d}}{\mathrm{d}t}\left\|\left[\mathrm{Sign}\left(\sigma\left(x\right)\right)\right]_{eq}\right\|=-\frac{\dot{k}}{k^2}\left\|h\left(x\right)\right\|+\frac{1}{k(t)}\frac{\mathrm{d}}{\mathrm{d}t}\left\|h\left(x\right)\right\|$$

In finite time we obligatory obtain the regime when $\mu\leq k\left(t\right)\leq k^{+}$ and

$$\dot{k}=\gamma_0 k\left(t\right)\mathrm{sign}\left(\theta\left(t\right)\right)$$

implying

$$\frac{\mathrm{d}}{\mathrm{d}t}\left\|\left[\mathrm{Sign}\left(\sigma\left(x\left(t\right)\right)\right)\right]_{eq}\right\|=\frac{1}{k(t)}\left[-\gamma_0\left\|h\left(x\right)\right\|\mathrm{sign}\left(\theta\left(t\right)\right)+\frac{\mathrm{d}}{\mathrm{d}t}\left\|h\left(x\right)\right\|\right]\tag{2.19}$$

Therefore for $V\left(\theta\left(t\right)\right)=\frac{1}{2}\theta^2\left(t\right)$ we have

$$\begin{aligned}\dot{V}&=\theta\dot{\theta}=\theta\frac{\mathrm{d}}{\mathrm{d}t}\left\|\left[\mathrm{Sign}\left(\sigma\left(x\right)\right)\right]_{eq}\right\|\\ &=\frac{1}{k(t)}\theta\left[-\gamma_0\left\|h\left(x\right)\right\|\mathrm{Sign}\left(\theta\left(t\right)\right)+\frac{\mathrm{d}}{\mathrm{d}t}\left\|h\left(x\right)\right\|\right]\end{aligned}\tag{2.20}$$

from the assumptions $(1-2)$ in the previous subsection one may conclude that

$$\|h(x)\| \leq h^{+} < \infty, \ \frac{\mathrm{d}}{\mathrm{d}t}\|h(x)\| \leq h(x)^{+}_{der} < \infty$$

Moreover, by (2.20) if $\theta(t_0) = 0$, then for any $t \geq t_0$ one has $\theta(t) = 0$, $k(t) \in [\mu, k^{+}]$ and then by (2.18)

$$\theta(t) := \left\| [\mathrm{Sign}(\sigma(x))]_{eq} \right\| - \varrho = 0$$

implying

$$\left\| [\mathrm{Sign}(\sigma(x))]_{eq} \right\| = \frac{\|h(x)\|}{k(t)} = \varrho$$

and

$$\frac{\|h(x)\|}{\varrho} = k(t) \geq \mu$$

Hence

$$\|h(x)\| \geq \varrho\mu$$

and

$$\dot{V} = \frac{1}{k(t)}\theta\left[-\gamma_0\|h(x)\|\,\mathrm{Sign}(\theta) + \frac{\mathrm{d}}{\mathrm{d}t}\|h(x)\|\right] \leq$$

$$-\frac{1}{k(t)}\gamma_0\|h(x)\|\,|\theta| + \frac{1}{k(t)}|\theta|\,h^{+}_{der} \leq -\frac{\varrho\mu}{k^{+}}\gamma_0|\theta| + \frac{1}{\mu}|\theta|\,h^{+}_{der} =$$

$$-\frac{\varrho\mu}{k^{+}}\gamma_0|\theta|\left(1 - \frac{k^{+}h^{+}_{der}}{\varrho\mu^2\gamma_0}\right)$$

Taking

$$\gamma_0 > \frac{k^+ h^+_{der}}{\varrho \mu^2}$$

fulfilling

$$\varkappa := \frac{\varrho \mu}{k^+} \gamma_0 \left(1 - \frac{k^+ h^+_{der}}{\varrho \mu^2 \gamma_0} \right) > 0$$

we finally, obtain

$$\dot{V} \leq -\varkappa |\theta| = -\varkappa \sqrt{2V}$$

resulting to

$$V(\theta(t)) = 0 \text{ for all } t \geq t_{reach} = \frac{\sqrt{2}}{\varkappa} \sqrt{V(x)}$$

Notice that in (2.14)

$$\frac{|\Phi(x,t)|}{\lambda_1} < k$$

and, moreover,

$$\frac{|\Phi(x,t)|}{\lambda_1} \leq \frac{\sigma^+ (f_0 + f_1 \|x\|)}{h_o (1 + \lambda \|x\|)} =$$

$$\sigma^+ \frac{f_0}{h_o} \left[1 + \frac{\sigma^+ \left(f_0^{-1} f_1 - \lambda \right) \|x\|}{1 + \lambda \|x\|} \right] \leq \sigma^+ \frac{f_0}{h_o}$$

select in (2.17)

$$k^+ > \sigma^+ \frac{f_0}{h_o}$$

and the gain $k(t)$ will be equal to k^+ which results in the occurrence of this motion in the surface $\sigma(x) = 0$.

2.4 Near Singularity Problem

Here we resolve another principal problems for the realization of the sliding mode control, which causes by the inverse of $g(x_1, t)$ (2.4) in the control action designing. Singular configurations are particular poses of the end-effector, for which parallel robots lose their inherent infinite rigidity, and in which the end-effector will have uncontrollable degrees of freedom.

In this section the near-singularity condition of the platform is handled by implementation of a new control law based on sliding mode with an inner regularization procedure. The finite-time convergence of the closed-loop system by the designed control in the presence of the external as well as internal disturbances/uncertainties is proved.

2.4.1 Near Singularity Analysis

Singularity is an important phenomenon in order to provide success in the motion of the robots in terms of accomplishing the desired task. Singularity analysis of robots should be performed before giving a task to the robot including the desired motion.

Compared with its serial counterparts, a parallel manipulator (or a closed-chain mechanism or system) has a much more complex structure in terms of its kinematics, dynamics, planning and control. In particular, the configuration space of a parallel manipulator is not even explicitly known, it is implicitly defined by a set of constraint functions introduced by the manipulator's closure constraints. A parallel manipulator also has, in addition to the usual end-effector singularities, different types of singularities such as configuration space singularities and actuator singularities. Understanding the intrinsic nature of the various types of singularities and their relations with the kinematic parameters and the configuration spaces is of ultimate importance in design, planning and control of the system

The importance of singularities from an engineering perspective arises for several reasons [26]:

Loss of freedom The derivative of the kinematic mapping or forward kinematics represents the conversion of joint velocities into generalized end-effector velocities, i.e.

linear and angular velocities. This linear transformation is generally referred to as the manipulator Jacobian in the robotics literature. A drop in rank reduces the dimension of the image, representing a loss of instantaneous motion for the end-effector of one or more degrees.

Workspace When a manipulator is at a boundary point of its workspace, the manipulator is necessarily at a singular point of its kinematic mapping, though the converse is not the case. Interior components of the singular set separate regions with different numbers or topological types of inverse kinematics. These are usually associated with a change of posture in some component of the manipulator. Therefore knowledge of the manipulator singularities provides valuable information about its workspace.

Loss of control A variety of control systems is used for manipulators. Rate control systems require the end-effector to traverse a path at a fixed rate and therefore determine the required joint velocities by means of the inverse of the derivative of the (known) forward kinematics. Near a singularity, this matrix is ill-conditioned and either the control algorithm fails or the joint velocities and accelerations may become unsustainably great. Conversely, force control algorithms, well-adapted for parallel manipulators, may result in intolerable joint forces or torques near singularities of the projection onto the joint space.

Mechanical advantage Near a singular configuration, large movement of joint variables may result in small motion of the end-effector. Therefore there is mechanical advantage that may be realised as a load-bearing capacity or as fine control of the end-effector . Another aspect of this is in the design of mechanisms possessing trajectories with specific singularity characteristics.

The search for singular configurations rests on the study of the singularities of the full inverse kinematic jacobian matrix, which is usually obtained through a velocity analysis or through an analysis of the mechanical equilibrium (see [26]). A direct analysis will thus involve the calculation of the determinant of matrix the J^{-1} , which may be a complicated task, even with symbolic computation software.

Researchers like Fichter [27] have intuitively analyzed particular cases of singularity for the inverse jacobian matrix of a 6-degrees of freedom robot, and have obtained a certain

number of cases. But intuition has its limits, and since the direct method is not satisfactory, researchers have suggested methods based on the degeneracy of the screws that are associated with the robot links [28]. These methods are equivalent to the geometric approach that we will present, but may be more difficult to use. A preliminary result on the geometry of the singularities was obtained by Cauchy [29]; this shows that the singularity of an articulated octahedron could be obtained only for concave configurations [2].

Using the conventional sliding mode, the values of this matrix in the operational space explode in the inverse calculation. It does not mean that the matrix is singular, but the determinate of $g(x_1, t)$ on some time-intervals becomes very small and reaches the so-called near-singularity condition, requiring the large control signals.

Near-singularity or ill-conditioned systems arise in many problems in modeling and simulation of physical, engineering, socio-economic and biological systems. These systems are very sensitive to roundoff errors and, therefore, may pose problems during computation of the solution. During computing process, these errors induce small changes in the coefficients which, in turn, result a large error in the solution. In [30] the well-known modified (underrelaxed, damped) Newton method is extended in such a way as to apply to the solution of ill-conditioned systems of nonlinear equations. In [31] the solution of ill-conditioned systems of linear and/or non-Linear equations are tested via *genetic algorithms*. The study of approximate input-output linearization of non-linear system with fail to have a well defined relative degree is studied in [32]. For such systems, they provided a method for constructing approximate systems that are input-output linearizable.

2.4.2 Regularization of SMC

Consider the system (2.7)

$$\dot{x}(t) = f(x, t) + g(x_1, t)\, u(x, t) + \xi(x, t) \tag{2.21}$$

Here

[2] To see the geometry analysis of the singularities see 5

$$g\left(x_1\right) g^{\intercal}\left(x_1\right) > 0 \quad \text{for} \quad \text{all} \quad x_1 \in \mathbb{R}^n$$

but $\det\left[g\left(x_1\right) g^{\intercal}\left(x_1\right)\right]$ may be very close to zero provoking the near-singularity effect during the SMC realization. The problem is to design a feedback control law $u\left(x\right)$ that derives the angular positions to desired values, that are the cartesian coordinate and angular positions of the moving platform x^*:

$$\lim_{t\to\infty} x(t) = x^*$$

First, let us introduce new variable vector $\sigma\left(\delta\right)$ in the state space of the system, named sliding surfaces

$$\sigma = C\delta_1 + \delta_2,\ C = \operatorname{diag}\left\{C_1 ... C_6\right\},\ C_i > 0 \tag{2.22}$$

where

$$\delta = x - x^* = \begin{pmatrix} \delta_1 \\ \delta_2 \end{pmatrix},\ \delta_1,\ \delta_2 \in \mathbb{R}^n$$

For the system (2.21), the control signal

$$u_t = -g^{\intercal}\left(gg^{\intercal} + \varepsilon^2 I\right)^{-1}\left[\left(\xi^+ + \rho\right)\operatorname{Sign}\left(\sigma\right) + C\delta_2 + f\left(x,t\right)\right] \tag{2.23}$$

$$\operatorname{Sign}\left(\sigma\right) = \left(\operatorname{sign}\left(\sigma_1\right), ..., \operatorname{sign}\left(\sigma_n\right)\right)^{\intercal}$$

$$\operatorname{sign}\left(z\right) = \begin{cases} 1 & \text{if} \quad z > 0 \\ -1 & \text{if} \quad z < 0 \\ \in \left[\ -1, \quad 1\ \right] & \text{if} \quad z = 0 \end{cases}$$

avoids the near-singularity problem and provides the desired behavior $\sigma = 0$ (2.22) in finite time. Let T be an orthogonal matrix transforming $gg^{\intercal}$ to the diagonal form, i.e.,

$$T^{\intercal}GG^{\intercal}T = \Lambda,\ T^{\intercal}T = TT^{\intercal} = I$$

Then

$$gg^{\intercal}\left(gg^{\intercal}+\varepsilon I\right)^{-1} = \left(gg^{\intercal}+\varepsilon I-\varepsilon I\right)\left(gg^{\intercal}+\varepsilon I\right)^{-1} =$$

$$I-\varepsilon\left(gg^{\intercal}+\varepsilon I\right)^{-1} = I-\varepsilon\left[TT^{\intercal}\left(gg^{\intercal}+\varepsilon I\right)TT^{\intercal}\right]^{-1} =$$

$$I-\varepsilon\left[T\left(\left(T^{\intercal}gg^{\intercal}T+\varepsilon I\right)\right)T^{\intercal}\right]^{-1} = I-\left[T\left(\Lambda+\varepsilon I\right)T^{\intercal}\right]^{-1} =$$

$$I-\varepsilon T\left(\Lambda+\varepsilon I\right)^{-1}T^{\intercal} = I-T\begin{bmatrix} \dfrac{\varepsilon}{\lambda_1+\varepsilon} & 0\cdots & 0 \\ & & \\ 0 & \ddots & 0 \\ 0 & 0\cdots & \dfrac{\varepsilon}{\lambda_n+\varepsilon} \end{bmatrix}T^{\intercal} = I-\Xi\left(\varepsilon\right)$$

Then the closed-loop system becomes

$$\begin{aligned} \dot{\delta}_1 &= \delta_2 \\ \dot{\delta}_2 &= f\left(x,t\right)-\left[I-\Xi\left(\varepsilon\right)\right]\left[\left(\eta^{+}+\rho\right)\mathrm{Sign}\left(\sigma_t\right)+C\delta_2+f\left(x,t\right)\right]+\xi\left(x,t\right) \end{aligned} \tag{2.24}$$

where $0<\varepsilon\ll 1$ and

$$\Xi\left(\varepsilon\right) := T\begin{bmatrix} \dfrac{\varepsilon}{\lambda_1+\varepsilon} & 0\cdots & 0 \\ 0 & \ddots & 0 \\ \vdots & & \vdots \\ 0 & 0\cdots & \dfrac{\varepsilon}{\lambda_n+\varepsilon} \end{bmatrix}T^{\intercal} \tag{2.25}$$

$$\left\|\Xi\left(\varepsilon\right)\right\| \leq \max_{i=\overline{1,n}}\frac{\varepsilon}{\lambda_i+\varepsilon} = \frac{\varepsilon}{\min\limits_{i=\overline{1,n}}\lambda_i+\varepsilon} = m\left(\varepsilon\right)$$

2.4.3 Stability analysis

Using the candidate of the Lyapunov function $V(t) = \frac{1}{2}\|\sigma(\delta(t))\|^2$ it drives to

$$\dot{V} = \sigma^\top \dot{\sigma} = \sigma^\top (C\dot{\delta}_1 + \dot{\delta}_2) =$$

$$\sigma^\top \left(C\delta_2 + F - [I - \Xi(\varepsilon)]\left[k\mathrm{Sign}(\sigma_t) + C\delta_2 + F\right] + \xi\right)$$

Denoting

$$\eta = \Xi(\varepsilon)\left(k\mathrm{Sign}(\sigma_t) + C\delta_2 + F\right) + \xi$$

we derive

$$\begin{aligned} \dot{V} &= -k\sum_{i=1}^{6}|\sigma_i| + \sigma^\top \eta \leq -k\|\sigma\| + \|\sigma\|\,\|\eta\| \\ &\leq -\|\sigma\|\left(k\left[1 - 6m(\varepsilon)\right] - m(\varepsilon)\left(C\delta_2^+ + F\right) - \xi^+\right) \end{aligned} \tag{2.26}$$

Taking the control gain k as

$$k = \frac{m(\varepsilon)\left(C\delta_2^+ + F\right) + \xi^+ + \rho}{[1 - 6m(\varepsilon)]}$$

for small enough ε it follows

$$k = \xi^+ + \rho + O(\varepsilon) > \xi^+ + \rho,\ \ \rho > 0$$

Then (2.26) becomes

$$\dot{V} \leq -\rho\|\sigma\| = -\rho\sqrt{2V}$$

implying for a given V_0

$$0 \leq \sqrt{V} \leq \sqrt{V_0} - \frac{\rho}{\sqrt{2}}t$$

Hence after

$$t_f = \|\sigma\| / \rho$$

it will result to $V(t) = 0$ for all $t \geq t_f$.

2.5 Solution of ODE with discontinuous right-hand side

As is known, a solution of the differential equation

$$\frac{dx}{dt} = f(t, x)$$

with a continuous right-hand side is a function $x(t)$, which has a derivative and satisfies this equation everywhere on a given interval. This definition is not, however, valid for differential equations with discontinuous right-hand sides. As can be seen in the sliding mode the *sign* has the following characteristics:

$x = \text{sign}(t)$. For $t < 0$ we have $x = -1$, the solution being given by $x = -t + c_1$; for $t > 0$ we have $x = 1$, the solution being $x = t + c_2$ (Fig. 2.1).

Proceeding from the requirement of solution continuity for $t = 0$, we obtain

$$x(0) = \lim_{t \to -0}(-t + c_1) = \lim_{t \to +0}(t + c_2) \qquad x(0) = c_1 = c_2$$

Consequently the solution is expressed by the formula $x(t) = |t| + c$. For $t = 0$ the derivative $\dot{x}(t)$ does not exist.

Thus, the consideration of differential equations with discontinuous righthand side requires a generalization of the concept of solution. In cases where the right-hand side of

the equation $\dot{x} = f(t, x)$ is continuous in x and discontinuous only in t, it usually proves possible to generalize the concept of solution using only a mathematical argument. In cases where the right-hand side of the equation is discontinuous in x, such simple mathematical arguments are often insufficient. Then the solution is defined by means of a limiting process taking into account the physical meaning of a given problem.

The generalization of the concept of solution must necessarily meet the following requirements:

1) For differential equations with a continuous right-hand side the definition of a solution must be equivalent to the usual one.

2) For the equation $\dot{x} = f(t)$ the solutions must be the functions $x(t) = \int f(t)dt + c$ only.

3) Under any initial data $x(t_0) = x_0$ in a given region of the solution must exist (at least for $t > t_0$) and continue to the boundary of this region or to infinity, i.e. $(t, x) \to 0$.

4) The definition of a solution must serve as a description of a fairly wide class of processes in physical systems. In order that equations with discontinuous right-hand sides be investigated by the well-known methods, the following conditions should also be satisfied:

5) The limit of a uniformly convergent sequence of solutions must be a solution.

6) Under the commonly-used changes of variables a solution must be transformed into a solution.

Many results from the theory of differential equations have already been extended (sometimes with necessary alterations) to differential equations with discontinuous right-hand sides. Such equations are usually analyzed by the same methods as differential equations with continuous right-hand sides.

Filippov and Utkin (see [33], [10]) have proposed two different approaches to define the solution of these dynamical systems. In case of linear systems, these two approaches are equivalent, but in case of nonlinear systems, the ways to extend the vector field on the sliding surface is generally different.

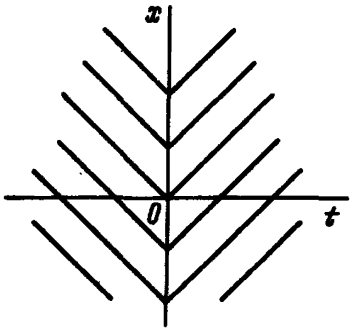

FIGURE 2.1: The solution of $\dot{x} = sign(t)$

2.5.1 Filippov solution for sliding mode dynamics

Consider the discontinuous differential system:

$$\dot{x}(t) = f(x(t)) = \begin{cases} f_1(x(t)) & , \quad h(x) < 0 \\ f_2(x(t)) & , \quad h(x) > 0 \end{cases}, \qquad x(0) = x_0 \in \mathbb{R}^n \tag{2.27}$$

Above, and henceforth, we suppose that the state space $\Re^n$ is split into two subspaces $\sum_1$ and $\sum_2$ by a surface such that $\mathbb{R}^n = \sum_1 \cup \sum \cup \sum_2$. $\sum$ is defined by the scalar event function $h : \mathbb{R}^n \to \mathbb{R}$, so that the subspaces $\sum_1$ and $\sum_2$, and the $\sum$, are characterized as

$$\begin{aligned} \textstyle\sum_1 &= \{x \in \mathbb{R}^n \,|h\,(x) < 0\,\} \\ \textstyle\sum_2 &= \{x \in \mathbb{R}^n \,|h\,(x) > 0\,\} \\ \textstyle\sum &= \{x \in \mathbb{R}^n \,|h\,(x) = 0\,\} \end{aligned} \tag{2.28}$$

We will also assume throughout that the gradient $\nabla h(x) \neq 0$ at all $x \in \sum$, and write $n(x) = \frac{\nabla h(x)}{\|\nabla h(x)\|}$ for the unit normal to $\sum$.

In (2.27), the right-hand side $f(x)$ can be assumed to be smooth on $\sum_1$ and $\sum_2$ separately, but it is usually discontinuous across $\sum$. More precisely, we will assume that f_1 is C^k; $k \geq 2$, on $\sum_1 \cup \sum$ and f_2 is C^k; $k \geq 2$ on $\sum_2 \cup \sum$.

As long as $x \neq 2$, (2.27) is a standard differential equation. The interesting case is when $x \in \sum$. In this case, if the condition

$$\left[n^{\top}(x)f_1(x)\right] > 0 \text{ and } \left[n^{\top}(x)f_2(x)\right] < 0 \tag{2.29}$$

is satisfied at $x \in \sum$, then one has so-called (attractive) sliding motion on $\sum$. Filippov defines this sliding motion as the solution of the differential system

$$\dot{x}(t) = \begin{cases} f_1(x(t)) & , \quad h(x) < 0 \\ f_F(x(t)) & , \quad h(x) = 0 \\ f_2(x(t)) & , \quad h(x) > 0 \end{cases} \tag{2.30}$$

where the vector field on the surface is taken to be in the convex hull $\text{co}(f_1, f_2)$ of f_1, f_2, that is:

$$f_F(x) = \left[\varpi f_2(x) + (1-\varpi) f_1(x)\right], \qquad x \in \sum,$$

and $\varpi(x) \in [0;1]$ chosen so that $n^{\top}(x)f_F(x) = 0$, that is

$$\varpi(x) = \frac{n^{\top}(x)f_1(x)}{n^{\top}(x)\left(f_1(x) - f_2(x)\right)} \tag{2.31}$$

We remark that Filippov's construction defines the vector field on the sliding surface as that vector in $\text{co}(f_1, f_2)$ which is tangent to $\sum$.

We stress that there is one unknown in Filippov's contraction, the scalar valued ϖ function in (2.31).

2.5.2 Utkin solution for sliding mode dynamics

To introduce Utkin's approach, we need to consider a system of the type (2.27), with additional control variables. To be precise, we consider the system

$$\dot{x} = f(x,u) \quad \text{where} \quad \begin{cases} u(x) = u_1(x) & \text{when} \quad h(x) < 0 \\ u(x) = u_2(x) & \text{when} \quad h(x) > 0 \end{cases} \tag{2.32}$$

where u_1 and u_2 are C^k functions of x defined on $\sum_1 \cup \sum$ and $\sum_2 \cup \sum$, respectively, and taking values in $\mathbb{R}^p$. Notice that the system in (2.32) has the same functional form of f,

and discontinuity in the vector field arises because of the discontinuous control. Again, the interest is in the case of attracting sliding motion, when $x \in \sum : [n^\top(x) f(x; u_1(x))] > 0$ and $[n^\top(x) f(x; u_2(x))] < 0$.

The problem can be trivially recast in the form of (2.27). In fact, letting $f_1(x) = f(x; u_1)$ and $f_2(x) = f(x; u_2)$, one obtains a system formally of the form (2.27). So doing, the Filippov extension in the case of sliding motion will be the same as before, that is:

$$\dot{x} = \begin{cases} f_1(x) = f(x, u_1(x)), & h(x) < 0 \\ f_F(x), & h(x) = 0 \\ f_2(x) = f(x, u_2(x)), & h(x) > 0 \end{cases} \tag{2.33}$$

where

$$f_F(x) = [\varpi f(x, u_2(x))] + (1 - \varpi) f(x, u_1(x)) \tag{2.34}$$

and ϖ is such that $n^\top(x) f_F(x) = 0$, as in (2.31).

On the other hand, Utkin (see [10]) proposed a different way to deal with this problem, the equivalent control approach. For sliding motion (that is, for $x \in \sum$), he proposes to take the vector field obtained by choosing $f(x, u)$ so that $f(x, u)$ will lie in the tangent plane to $\sum$ at x. Formally, Utkin's construction is as follows:

$$\dot{x} = \begin{cases} f_1(x) = f(x, u_1(x)), & h(x) < 0 \\ f_U(x) = f(x, u_{eq}(x)), & h(x) = 0 \\ f_2(x) = f(x, u_2(x)), & h(x) > 0 \end{cases} \tag{2.35}$$

where the equivalent control u_{eq} must be chosen so that $f(x, u_{eq}(x))$ lies in the tangent plane to $\sum$ at $x : n^\top(x) f(x, u_{eq}(x)) = 0$. In general (i.e., when $u \in \mathbb{R}^p$, $p > 1$), this is an underdetermined system. Utkin's approach is to choose u_{eq} in the convex hull of u_1 and u_2:

$$u_{eq}(x) = \varpi u_2(x) + (1 - \varpi) u_1(x) \tag{2.36}$$

and $\varpi \in [0; 1]$ is chosen so that (this is a nonlinear system to be solved)

$$n^\top(x) f_U(x) = 0$$

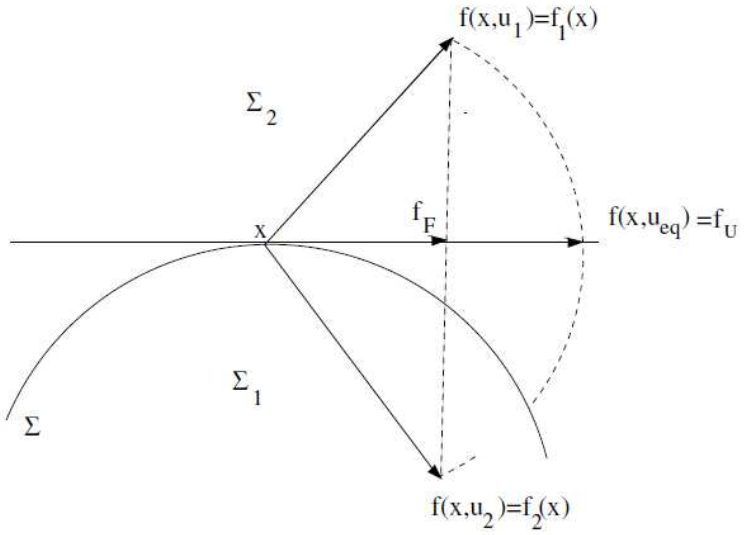

FIGURE 2.2: Filippov's and Utkin's approach.

So, there is one unknown in Utkin's construction, the scalar valued function in (2.36) which must be found by solving a (single) nonlinear equation.

Utkin's approach is geometrically different from Filippov's approach. Among the vectors in $\{f(x;u)\,|u = \mathrm{co}(u_1, u_2)\}$, Utkin takes the one tangent to at x (see Figure 2.2). In general, Filippov's and Utkin's vector are different. They coincide directionally in case the convex hull is a straight line, and also in magnitude when f is linear with respect to the control u.

Chapter 3

Feedback Sliding Mode Observer-Controller

In this chapter an implementation of the proposed adaptive type of high order sliding mode controller-observer help us to provide a high performance nonlinear feedback control for the system manipulation in presence of unmodelled dynamics and perturbations. The novelly observer for velocity estimation is designed on the base of the classical second-order (super-twist) algorithm [34]. This observer provides a high accuracy of estimate the velocity values of the system guarantying the convergence of the state error estimates and tracking this error into a small zone containing the origin. To orient the system in presence of unmodelled dynamics and perturbations and in order to achieve chattering attenuation a high efficiency adaptive sliding mode controller is used [25, 34, 35].

In this chapter

- The SM controller, which uses the state estimates obtained on-line by the adaptive Super-Twisting observer, is presented.
- The gain parameters $k = k(\hat{x}, t)$ of the controller as well as $\lambda = \lambda(\hat{x}, t)$ of the observer are admitted to be time-varying and depending on available current measurements. In view of that the considered controller is referred to as an *adaptive* one.

- It is shown that the deviations of the generated state estimates from real state values together with a distance of the closed-loop system trajectories to a desired sliding surface reach the, so-called, μ-zone around the origin in finite time.
- It is shown that μ-zone may be done as small as we wish by the corresponding regularizing parameters selection (fulfilling some constrains) of the adaptation mechanism.
- It is shown that the initial values of the observer should not be so far from the real states of the dynamic plant; this admissible zone for initial estimates value is calculated analytically.
- The application of the suggested controller is illustrated by the orientation of a tethered satellite system in a required position. The presented simulation results demonstrate very high efficiency of the suggested approach.

3.1 Feedback control design

The designed control law provides the desired performance of the corresponding nonlinear model in the presence of disturbances/uncertainties. This work deals with a new adaptive SMC feedback design when the angular velocities are not measured directly and are estimated on-line by the second-order *Sliding Mode* (SM) observer. Such approach for designing of orientation control can reduce the cost of the controlled system, avoid the fragility of angular velocity sensors, and eliminate the difficulty of the sensors installation in the satellite system. However, due to the high-order multiple variables and nonlinearity of the considered system, the estimation of angular velocities in the presence of disturbances and uncertainties still remains very challenging.

Recently the design of such observers for nonlinear systems has received a great deal of attention: the standard Luenberger [36, 37] ,the SM observers [34, 38, 39], the extended Kalman filter [40, 41] and H_∞ observers [42]. Among them, adaptive SM observers provide an attractive technology due to its robustness against disturbances, parameter deviations and measurement noise [34]. The SM observers found a wide use in different fields. Some works [43–45] propose the adaptive SM observer for sensorless induction motor drive. In [38] the adaptive SM observer - controller system was proposed for the induction machine control design under unknown parameters and partial state variable information.

The papers [39, 46] consider the application of a particular SM observer to the problem of fault detection and isolation. In [47] the fault detection and estimation issues for a class of nonlinear systems with uncertainty were considered based on the equivalent output error injection approach. There the particular design of SM observer was presented where its parameters satisfy some LMI constraint. In [48] the authors proposed a feedback linearization-based controller with a high-order SM observer running parallel and applied to a quadrotor unmanned aerial vehicle. The high-order SM observer works as an observer and estimator of the effect of the external disturbances such as wind and noise.

The problem treated in this section can be described as follows:

- *first*, estimate on-line unknown variables

- *second*, use these estimates to design a SM controller.

The parameters of the controller as well as the observer are admitted to be time-varying and depending on available current measurements.

Consider the state space representation in the vector form:

$$\begin{aligned} \dot{x}_1(t) &= x_2(t) \\ \dot{x}_2(t) &= f(x,t) + g(x_1,t)\,u(x,t) + \xi(x,t) \\ y(t) &= x_1(t) \end{aligned} \tag{3.1}$$

- $x_1(t)$, $x_2(t) \in \mathbb{R}^n$ are the state of the system at time $t \in \mathbb{R}_+$;

- $x(t) := \left(x_1^\top(t), x_2^\top(t)\right)^\top \in \mathbb{R}^{2n}$;

- $y(t) \in \mathbb{R}^n$ is a measurable output at time $t \geq 0$;

- $u(x,t) \in \mathbb{R}^n$ is a control to be designed;

- $\xi(x,t) \in \mathbb{R}^n$ is unmeasurable term including the external as well as internal perturbations and uncertainties;

- $f(x,t) \in \mathbb{R}^n$, $g(x_1,t) \in \mathbb{R}^{n\times n}$.

Notice that in the model (3.1) only the half of coordinates ($x_1(t)$) are available in time.

3.1.1 Velocity estimation

To estimate the non-measurable coordinate $x_2(t)$ in (3.1) we apply a popular second-order sliding mode (super-twisting) observer [34]:

$$\begin{aligned} \dot{\hat{x}}_1 &= \hat{x}_2 + \lambda \left\| y - \hat{x}_1 \right\|^{1/2} \mathrm{Sign}\left(y - \hat{x}_1\right) \\ \dot{\hat{x}}_2 &= f(x,t) + g(\hat{x},t)\, u + \alpha \mathrm{Sign}\left(y - \hat{x}_1\right) \end{aligned} \tag{3.2}$$

where the scalar positive parameters α and λ are assumed to be constant in the original publications. The vector function $\mathrm{Sign}(z)$ is defined as follows

$$\begin{aligned} \mathrm{Sign}(z) &:= \left(\mathrm{sign}(z_1), ..., \mathrm{sign}(z_n)\right)^\top \\ \mathrm{sign}(z_i) &:= \begin{cases} 1 & if \quad z_i > 0 \\ -1 & if \quad z_i < 0 \\ \in [-1,1] & if \quad z_i = 0 \end{cases} \end{aligned} \tag{3.3}$$

Define the new variable $e := (x - \hat{x})$ which characterizes the error of estimated state and is governed by the following equations:

$$\begin{aligned} \dot{e}_1 &= e_2 - \lambda \left\| e_1 \right\|^{1/2} \mathrm{Sign}(e_1) \\ \dot{e}_2 &= f_e(t, x_1, x_2, \hat{x}_2) - \alpha \mathrm{Sign}(e_1) \end{aligned} \tag{3.4}$$

where

$$f_e(t, x_1, x_2, \hat{x}_2) = f(x,t) + \xi(x,t) \tag{3.5}$$

describes unmodelled dynamics and external perturbation effects. Obviously, it is unmeasurable. Notice that vector

$$e_1 = x_1 - \hat{x}_1 = y - \hat{x}_1 \tag{3.6}$$

is measurable and available in time.

3.1.2 Control design

Sliding surface The problem which we are interested in is to design a feedback control law $u(\hat{x}, t)$ that derives the states $x(t)$ of the systems to desired values. i.e.,

$$\lim_{t\to\infty} x_1 = x_1^*, \ \lim_{t\to\infty} x_2 = 0$$

These requirements may be expressed in another way using *Sliding Mode Approach*. To do that let us introduce new variable $\sigma(x)$ in the state space of the system, defining the *"ideal"* sliding surface [10]:

$$\sigma(x) := \dot{x}_1 + C(x_1 - x_1^*) = x_2 + C(x_1 - x_1^*) = 0 \tag{3.7}$$

where x_1^* is desired state value and $C = diag(c_1, c_2, ..., c_n)$ is a diagonal matrix with positive elements. Arriving to this surface making $\sigma(x(t)) \to 0$ when $t \to \infty$, the system will slide to the origin with exponential rate.

3.2 Sliding mode controller and observer adaptation

For the following ideal sliding surfaces:

$$\sigma(x) = [\sigma_1(\hat{x}), ..., \sigma_n(\hat{x})]^\top$$

$$\text{Sign}(\sigma(\hat{x})) = [\text{sign}(\sigma_1(\hat{x})), ..., \text{sign}(\sigma_n(\hat{x}))]^\top \tag{3.8}$$

$$\sigma_i(\hat{x}) = \hat{x}_{2,i} + c_i\left(\hat{x}_{1,i} - x_{1,i}^*\right), \ i = 1, ..., n$$

we need to define the positive adaptation parameters

$$k(\hat{x}, t), \ \lambda(\hat{x}, t), \ \alpha(\hat{x}, t) \tag{3.9}$$

which provide the attainment in a finite time.

To resolve this problem we propose an **adaptive sliding mode controller** $u(\hat{x},t)$ as follows

$$u(\hat{x},t) = -k(\hat{x},t)\left[g(\hat{x},t)\right]^{-1}\mathrm{Sign}\left(\sigma(\hat{x})\right) \tag{3.10}$$

where the state estimates $\hat{x}$ are generated by the observer (3.2) with varying parameters:

$$\begin{aligned}\dot{\hat{x}}_1 &= \hat{x}_2 + \lambda(\hat{x},t)\left\|y-\hat{x}_1\right\|^{1/2}\mathrm{Sign}\left(y-\hat{x}_1\right)\\ \dot{\hat{x}}_2 &= f(\hat{x},t) + g(\hat{x},t)\,u + \alpha(\hat{x},t)\,\mathrm{Sign}\left(y-\hat{x}_1\right)\end{aligned} \tag{3.11}$$

3.2.1 Resulting algorithms

If under the assumptions that $f(x,t)$ and $g(x,t)$ are Lipschitzian with respect to the first argument and measurable on t the adaptive parameters $k = k(\hat{x},e_1,t)$ (3.9) in the controller (3.10) and $\lambda(\hat{x},t)$, $\alpha(\hat{x},t)$ in the observer (3.11) are designed as

$$\left.\begin{aligned} k = k(\hat{x},e_1,t) &:= (p_0)^{-1}\left(\rho+\kappa(\hat{x},e_1,t)+\gamma\sqrt{\tfrac{p_0}{2}}\right),\ \rho \geq \sqrt{\tfrac{p_0}{2}}\\ \kappa(\hat{x},e_1,t) &:= \left\|f(\hat{x},t)+\alpha\mathrm{Sign}(e_1)+C\left[\hat{x}_2+\lambda\left\|e_1\right\|^{1/2}\mathrm{Sign}(e_1)\right]\right\|\end{aligned}\right\} \tag{3.12}$$

and

$$\left.\begin{aligned}\lambda(\hat{x},t) := \begin{cases}\frac{\eta_1(\gamma)+\sqrt{\frac{p_1}{2}}}{p_1\sqrt{\|e_1\|}} & \text{if} \quad \sqrt{\|e_1\|} \geq \epsilon > 0\\ \\ \frac{\eta_1(\gamma)+\sqrt{\frac{p_1}{2}}}{p_1\epsilon} & \text{if} \quad \sqrt{\|e_1\|} < \epsilon\end{cases}\\ \alpha(\hat{x},t) := \alpha > 0\end{aligned}\right\} \tag{3.13}$$

then we may guarantee that the "storage" function

$$V(t) := V\left(\sigma\left(\hat{x}\left(t\right)\right), e_1\left(t\right), e_2\left(t\right)\right) = \frac{p_0}{2}\left\|\sigma\left(\hat{x}\left(t\right)\right)\right\|^2 + \frac{p_1}{2}\left\|e_1\left(t\right)\right\|^2 + \frac{p_2}{2}\left\|e_2\left(t\right)\right\|^2$$
$$p_0,\ p_1,\ p_2\ > 0 \text{ and } p_0 + p_1 + p_2 = 1 \tag{3.14}$$

approaches to μ-zone in the finite time t_f, that is, for all $t \geq t_f = \gamma^{-1}\sqrt{2W\left(0\right)}$ we have

$$W\left(t\right) := \left[\sqrt{V\left(t\right)} - \mu\right]_+^2 = 0 \tag{3.15}$$

where

$$\eta_0\left(\alpha\right) := p_2 e_2^+\left(\alpha\sqrt{n} + \sqrt{2}\xi^+ + \sqrt{2L_f}e_2^+\right) + \gamma\sqrt{\frac{p_2}{2}}$$

$$\eta_1\left(\gamma\right) := \gamma\sqrt{\frac{p_1}{2}} + \left(p_1 + \sqrt{2L_f}p_2\right)e_2^+,\ \gamma > 1$$

$$e_2^+ = \frac{2c}{\sqrt{b^2 + 4ac} + b} = \frac{2}{\sqrt{\left(\frac{b}{c}\right)^2 + 4\frac{a}{c}} + \frac{b}{c}} = \tag{3.16}$$

$$\frac{2}{\sqrt{\left(\frac{\sqrt{2}}{(\gamma-1)}\sqrt{p_1} + \left[\frac{2\sqrt{L_f}}{(\gamma-1)} + \frac{(\alpha\sqrt{2n}+2\xi^+)}{(\gamma-1)\epsilon\frac{10}{27}}\right]\frac{p_2}{\sqrt{p_1}}\right)^2 + \frac{216\sqrt{L_f}}{(\gamma-1)10\epsilon}\frac{p_2}{p_1}} + \frac{\sqrt{2}}{(\gamma-1)}\sqrt{p_1} + \left[\frac{2\sqrt{L_f}}{(\gamma-1)} + \frac{(\alpha\sqrt{2n}+2\xi^+)}{(\gamma-1)\epsilon\frac{10}{27}}\right]\frac{p_2}{\sqrt{p_1}}}$$

$$\mathcal{F}_1\left(p_1\right) := \sqrt{p_1}r_1 + \frac{p_2}{\sqrt{p_1}}r_2 + \sqrt{\left(\sqrt{p_1}r_1 + \frac{p_2}{\sqrt{p_1}}r_2\right)^2 + \frac{p_2}{p_1}r_3}$$

where

$$r_1 = \frac{\sqrt{2}}{(\gamma - 1)}$$

$$r_2 = \frac{2\sqrt{L_f}}{(\gamma - 1)} + \frac{\left(\alpha\sqrt{2n}+2\xi^+\right)}{(\gamma - 1)\,\epsilon^{\frac{10}{27}}}$$

$$r_3 = \frac{216\sqrt{L_f}}{(\gamma - 1)\,10\epsilon}$$

and

$$\begin{gathered}
\mu_0 := \tfrac{2}{\mathcal{F}_1}\left[\sqrt{2L_f}p_2\tfrac{2}{\mathcal{F}_1} + p_2\left(\alpha\sqrt{n}+\sqrt{2}\xi^+\right)\right] + \tfrac{\gamma\epsilon\sqrt{2}10}{27}\sqrt{p_1} \\
\mu_1(\epsilon) := \sqrt{\tfrac{p_2}{2}} + \epsilon^{\frac{10}{27}}\left(p_1 + \sqrt{2L_f}p_2\right) \\
\mu := \mu_0\left(\alpha, \gamma, e_2^+\right) + \mu_1(\epsilon)\, e_2^+ = \mathcal{F}_2 \\
\frac{2}{\mathcal{F}_1}\left[\sqrt{2L_f}p_2\frac{2}{\mathcal{F}_2} + p_2\left(\alpha\sqrt{n}+\sqrt{2}\xi^+\right)\right] + \frac{\gamma\epsilon\sqrt{2}10}{27}\sqrt{p_1}+ \\
r_4 + \frac{r_5}{\mathcal{F}_1} + \frac{r_6}{\mathcal{F}_1^2}
\end{gathered} \tag{3.17}$$

where

$$r_4 = \frac{\gamma\epsilon\sqrt{2}10}{27}\sqrt{p_1}$$

$$r_5 = 2\left[p_2\left(\alpha\sqrt{n}+\sqrt{2}\xi^+\right) + \sqrt{\tfrac{p_2}{2}} + \epsilon^{\frac{10}{27}}\left(p_1 + \sqrt{2L_f}p_2\right)\right]$$

$$r_6 = 4\sqrt{2L_f}p_2$$

and

The initial values of the observer $\hat{x}_2(t_0)$ should not be so far from the real values $x_2(t_0)$ thus fulfilling

$$\|x_2(t_0) - \hat{x}_2(t_0)\| \leq e_2^+$$

3.2.2 Proof of the main result

A) Calculating the time derivative of the storage function (3.14) on the trajectories of the considered dynamics we get (omitting the arguments dependence)

$$\dot{V} = p_0\sigma(\hat{x})^\top \dot{\sigma}(\hat{x}) + p_1 e_1^\intercal \dot{e}_1 + p_2 e_2^\intercal \dot{e}_2 = p_0\sigma(\hat{x})^\top \left(\tfrac{d}{dt}\hat{x}_2 + C\tfrac{d}{dt}\hat{x}_1\right)$$

$$+ p_1 e_1^\intercal \left[e_2 - \lambda \|e_1\|^{1/2} \operatorname{Sign}(e_1)\right] + p_2 e_2^\intercal \left[F_e - \alpha \operatorname{Sign}(e_1)\right] \leq -k p_0 \sigma(\hat{x})^\top \operatorname{Sign}(\sigma(\hat{x})) +$$

$$p_0\sigma(\hat{x})^\top \left[f(\hat{x},t) + \alpha \operatorname{Sign}(e_1) + c_1\left(\hat{x}_2 + \lambda\|e_1\|^{1/2}\operatorname{Sign}(e_1)\right)\right] +$$

$$p_1 e_1^\intercal e_2 - \lambda p_1 \|e_1\|^{3/2} + \sqrt{2} p_2 \|e_2\| \left(\sqrt{L_f}\|e\| + \xi^+\right) + \alpha p_2 \sqrt{n}\|e_2\|$$

which leads to

$$\dot{V} \leq \|\sigma(\hat{x})\|\left[-k p_0 + \varkappa(\hat{x}, e_1, t)\right] - \lambda p_1 \|e_1\|^{3/2} +$$

$$\|e_2\|\left[p_1\|e_1\| + \sqrt{2}p_2\sqrt{L_f}\left(\|e_1\| + \|e_2\|\right) + p_2\left(\alpha\sqrt{n} + \sqrt{2}\xi^+\right)\right]$$

where

$$\varkappa(\hat{x}, e_1, t) := \left\| f(\hat{x},t) + \alpha \operatorname{Sign}(e_1) + C\left[\hat{x}_2 + \lambda\|e_1\|^{1/2}\operatorname{Sign}(e_1)\right]\right\|$$

Adding and subtracting the term

$$\gamma\left[\sqrt{p_0/2}\,\|\sigma(\hat{x}(t))\| + \sqrt{p_1/2}\,\|e_1(t)\| + \sqrt{p_2/2}\,\|e_2(t)\|\right]$$

which is more or equal to $\gamma\sqrt{V}$ $(\gamma > 0)$, we derive

$$\dot{V} \leq -\gamma\sqrt{V} + \|\sigma(\hat{x})\| \left[-kp_0 + \varkappa(\hat{x}, e_1, t) + \gamma\sqrt{\tfrac{p_0}{2}}\right] - \|e_1\| \left(\lambda p_1 \sqrt{\|e_1\|} - \gamma\sqrt{\tfrac{p_1}{2}}\right)$$

$$+ \|e_2\| \left[p_1 \|e_1\| + p_2\sqrt{2L_f}\,(\|e_1\| + \|e_2\|) + p_2\left(\alpha\sqrt{n} + \sqrt{2}\xi^+\right) + \gamma\sqrt{\tfrac{p_2}{2}}\right]$$

If in time $t \geq 0$ we may guarantee that

$$\|e_2(t)\| \leq e_2^+ \tag{3.18}$$

then from the last inequality we obtain

$$\begin{aligned} \dot{V} \leq -\gamma\sqrt{V} - \|\sigma(\hat{x})\| \left[-kp_0 + \varkappa(\hat{x}, e_1, t) + \gamma\sqrt{\tfrac{p_0}{2}}\right] \\ - \|e_1\| \left[\lambda p_1 \sqrt{\|e_1\|} - \eta_1\left(\gamma, e_2^+\right)\right] + \eta_0\left(\alpha, e_2^+\right) \end{aligned} \tag{3.19}$$

with

$$\begin{aligned} \eta_0\left(\alpha, e_2^+\right) &:= e_2^+ \left[\sqrt{2L_f} p_2 e_2^+ + p_2\left(\alpha\sqrt{n} + \sqrt{2}\xi^+\right)\right] \\ \eta_1\left(\gamma, e_2^+\right) &:= \left(p_1 + \sqrt{2L_f} p_2\right) e_2^+ - \gamma\sqrt{\tfrac{p_1}{2}} \end{aligned} \tag{3.20}$$

Taking $\rho > 0$ and defining $k = k(\hat{x}, e_1, t)$ as in (3.12), from (3.19) we obtain

$$\begin{aligned} \dot{V} \leq -\gamma\sqrt{V} - \rho\|\sigma(\hat{x})\| \\ - \|e_1\| \left[\lambda p_1 \sqrt{\|e_1\|} - \eta_1\left(\gamma, e_2^+\right)\right] + \eta_0\left(\alpha, e_2^+\right) \end{aligned} \tag{3.21}$$

where $\eta_0(\alpha)$ and $\eta_1(\gamma)$ are defined in (3.20). Introduce the Lyapunov function

$$W := \left[\sqrt{V} - \mu\right]_+^2, \ \mu > 0 \tag{3.22}$$

for which (in view of (3.21)) we have

$$\dot{W} = \frac{dW}{dV}\dot{V} = -\gamma\left[\sqrt{V}-\mu\right]_+ + \frac{1}{\sqrt{V}}\left[\sqrt{V}-\mu\right]_+ \times$$
$$\left[-\rho\left\|\sigma\left(\hat{x}\right)\right\| - \left\|e_1\right\|\lambda p_1\sqrt{\left\|e_1\right\|} + \left\|e_1\right\|\eta_1\left(\gamma, e_2^+\right) + \eta_0\left(\alpha, e_2^+\right)\right] \tag{3.23}$$

Let us try to select positive λ,α, ρ, μ such that

$$\Phi := \left[\sqrt{V}-\mu\right]_+\left[-\rho\left\|\sigma\left(\hat{x}\right)\right\| - \left\|e_1\right\|\lambda p_1\sqrt{\left\|e_1\right\|}\right.$$
$$\left. + \left\|e_1\right\|\eta_1\left(\gamma, e_2^+\right) + \eta_0\left(\alpha, e_2^+\right)\right] \le 0 \tag{3.24}$$

If $\rho \ge \sqrt{p_0/2}$, then $\rho\left\|\sigma\left(\hat{x}\right)\right\| + \sqrt{p_1/2}\left\|e_1\left(t\right)\right\| + \sqrt{p_2/2}\left\|e_2\left(t\right)\right\| \ge \sqrt{V}$

and

$$\Phi \le -\sqrt{V}\left[-\left[\mu\right]_+ - \left(\eta_0 + \sqrt{p_2/2}e_2^+ + \left\|e_1\right\|\left(\eta_1 + \sqrt{p_2/2} - \lambda p_1\sqrt{\left\|e_1\right\|}\right)\right)\right] \tag{3.25}$$

Select λ as follows

$$\lambda = \begin{cases} \frac{\eta_1\left(\gamma, e_2^+\right) + \sqrt{p_1/2}}{p_1\sqrt{\left\|e_1\right\|}} & \text{if} \quad \sqrt{\left\|e_1\right\|} \ge \epsilon > 0 \\ \\ \frac{\eta_1\left(\gamma, e_2^+\right) + \sqrt{p_1/2}}{p_1\epsilon} & \text{if} \quad \sqrt{\left\|e_1\right\|} < \epsilon \end{cases} \tag{3.26}$$

Then

$$\left\|e_1\right\|\left(\eta_1\left(\gamma, e_2^+\right) + \sqrt{p_1/2} - \lambda p_1\sqrt{\left\|e_1\right\|}\right) =$$
$$\begin{cases} 0 & \text{if} \quad \sqrt{\left\|e_1\right\|} \ge \epsilon \\ \\ \left\|e_1\right\|\left(\eta_1\left(\gamma, e_2^+\right) + \sqrt{p_1/2}\right)\left(1 - \sqrt{\left\|e_1\right\|}/\epsilon\right) & \text{if} \quad \sqrt{\left\|e_1\right\|} < \epsilon \end{cases}$$

Taking into account that $x - x^{3/2} \le 10/27$ for all $x \ge 0$ with $x = \left\|e_1\right\|$ we obtain

$$\|e_1\|\left(\eta_1\left(\gamma,e_2^+\right)+\sqrt{p_1/2}\right)\left(1-\sqrt{\|e_1\|}/\epsilon\right)\leq\epsilon 10/27\left(\eta_1\left(\gamma,e_2^+\right)+\sqrt{p_1/2}\right)$$

which by (3.5) implies

$$\Phi\leq-\left[\sqrt{V}-\mu\right]_+\left[\sqrt{V}-\left(\eta_0\left(\alpha,e_2^+\right)+\sqrt{p_1/2}e_2^+ +\epsilon 10/27\left(\eta_1\left(\gamma,e_2^+\right)+\sqrt{p_1/2}\right)\right)\right]$$

Taking μ as in (20) the last inequality becomes

$$\Phi\leq-\left[\sqrt{V}-\mu\right]_+\left[\sqrt{V}-\mu\right]=-\left[\sqrt{V}-\mu\right]_+^2\leq 0$$

fulfilling (3.24). Based on (3.23) we get

$$\dot{W}\leq-\gamma\left[\sqrt{V}-\mu\right]_+=-\gamma\sqrt{W} \tag{3.27}$$

implying $W_t=0$ for all $t\geq t_f=2\gamma^{-1}\sqrt{W\left(0\right)}$.

B) To complete the proof we need to show that if (3.18) is fulfilled in time t_0, it will be valid for any other time more than t_0. By (3.27) we have

$$\sqrt{W\left(t_0+\Delta t\right)}\leq\sqrt{W\left(t_0\right)}-\gamma\Delta t/2$$

or, equivalently,

$$\left[\sqrt{V\left(t_0+\Delta t\right)}-\mu\right]_+\leq\left[\sqrt{V\left(t_0\right)}-\mu\right]_+-\gamma/2\Delta t<\left[\sqrt{V\left(t_0\right)}-\mu\right]_+$$

a) If $\sqrt{V\left(t_0\right)}\leq\mu$ we have $\sqrt{V\left(t_0+\Delta t\right)}\leq\mu$ for any small $\Delta t>0$ and, as the result,

$$\|e_2\left(t_0+\Delta t\right)\|\leq\sqrt{2/p_2}\sqrt{V\left(t_0+\Delta t\right)}\leq\sqrt{2/p_2}\left[\mu_0\left(\alpha,\gamma,e_2^+\right)+\mu_1\left(\epsilon\right)e_2^+\right]$$

To fulfill

$$\sqrt{2/p_2}\left[\mu_0\left(\alpha,\gamma,e_2^+\right)+\mu_1\left(\epsilon\right)e_2^+\right]:=e_2^+$$

it is sufficient to realize

$$\sqrt{2L_f}p_2\left(e_2^+\right)^2+\left[\epsilon\tfrac{10}{27}\left(p_1+\sqrt{2L_f}p_2\right)+p_2\left(\alpha\sqrt{n}+\sqrt{2}\xi^+\right)\right]e_2^+=\left(\gamma-1\right)\epsilon\tfrac{10}{27}\sqrt{\tfrac{p_1}{2}}$$

selecting e_2^+ as in (3.16). This means that for $t_0=0$ the initial values of the observer should satisfies $\|x_2\left(t_0\right)-\hat{x}_2\left(t_0\right)\|\leq e_2^+$.

b) If $\sqrt{V\left(t\right)}>\mu$, then

$$\sqrt{\tfrac{p_2}{2}}\left\|e_2\left(t+\Delta t\right)\right\|\leq\sqrt{V\left(t+\Delta t\right)}\leq\sqrt{V\left(t\right)}-\frac{\gamma}{2}\Delta t<\sqrt{V\left(t\right)}$$

and one can take

$$e_2^+:=\sqrt{\tfrac{2}{p_2}V\left(0\right)}\leq\sqrt{\left(\tfrac{p_0}{p_2}\left\|\sigma\left(\hat{x}\left(0\right)\right)\right\|^2+\tfrac{p_1}{p_2}\left\|e_1\left(0\right)\right\|^2+\left(e_2^+\right)^2\right)}$$

which is valid for any e_2^+. This means that the selection of e_2^+ as in (3.16) covers both cases a) and b). Theorem is proven.

3.2.3 Optimization of the controller parameters

The control algorithm (3.12) contains three free parameters p_0,p_1,p_2 which should be selected in such a way that the resulting behavior would be as better as possible. Without loss of generality we may select the parameters p_0, p_1 and p_2 of the controller as follows

$$p_0+p_1+p_2=1$$

implying

$$p_2=1-p_1-p_0 \tag{3.28}$$

Indeed, since

$$\arg\min_{u\in U_{adm}} V = \arg\min_{u\in U_{adm}} \frac{1}{p_0+p_1+p_2} V$$

the multiplication of the function V by any positive constant does not change the optimal control parameters. If we fix the value $p_0 \in (0,1)$, then in view of (3.28) we have only one free parameters $p_1 \in (0,1)$ which should be selected to fulfill the following optimality requirements:

1) to make the "workability zone" $e_2^+ = \dfrac{2}{\mathcal{F}_1(p_1)}$ as much as possible which corresponds to the minimization of the function

$$\mathcal{F}_1(p_1) := \sqrt{p_1} r_1 + \frac{1-p_1-p_0}{\sqrt{p_1}} r_2 + \sqrt{\left(\sqrt{p_1} r_1 + \frac{1-p_1-p_0}{\sqrt{p_1}} r_2\right)^2 + \frac{1-p_1-p_0}{p_1} r_3} \to \min_{p_1\in(0,1)}$$

2) to make the convergence zone μ minimal possible one which corresponds to the minimization of the function

$$\mu = \mathcal{F}_2(p_1) := r_1 + \frac{r_2}{\mathcal{F}_1(p_1)} + \frac{r_3}{\mathcal{F}_1^2(p_1)} \to \min_{p_1\in(0,1)}$$

One can see that we deal with the multi-functional optimization problem

$$\begin{aligned} \mathcal{F}_1(p_1) &\to \min_{p_1\in(0,1)} \\ \mathcal{F}_2(p_1) &\to \min_{p_1\in(0,1)} \end{aligned}$$

and it is clear that simultanious optimization two different functions by the same arguments p_1 is impossible. That's why we need to apply the, so-called, "*Pareto-set approach*" [49]. A standard technique for generating the Pareto set in multicriteria optimization problems is to minimize (convex) weighted sums of the different objectives for various different settings of the weights. *Pareto efficiency*, or *Pareto optimality*, is a state of allocation of resources in which it is impossible to make any one individual better off without making at least one individual worse off. The term is named after Vilfredo Pareto (1848–1923), an Italian engineer and economist who used the concept in his studies of economic efficiency and income distribution. Many real-world problems involve simultaneous optimization of several incommensurable and often competing objectives. Usually, there is

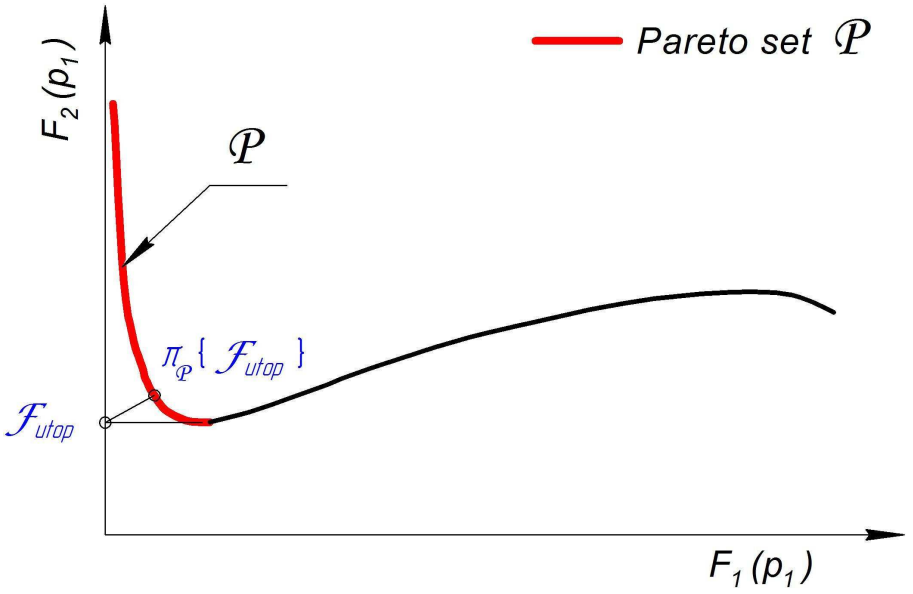

FIGURE 3.1: The set of Pareto optimal points.

no single optimal solution, but rather a set of alternative solutions. These solutions are optimal in the wider sense that no other solutions in the search space are superior to them when all objectives are considered. They are known as *Pareto-optimal solutions*. The concept has applications in academic fields such as economics, engineering, and the life sciences [50].

In our case the Pareto set looks as in the Fig.3.1.

It this figure

$\mathcal{P}$ is the Pareto set,

$\mathcal{F}_{utop} = \left(\min\limits_{p_1 \in (0,1)} \mathcal{F}_1(p_1), \min\limits_{p_1 \in (0,1)} \mathcal{F}_2(p_1) \right)$ is the utopia point,

$\pi_{\mathcal{P}}\{\mathcal{F}_{utop}\}$ is the projection of the utopia point $\mathcal{F}_{utop}$ to the pareto set.

Definition. *The parameters p_1^* and p_2^*, corresponding to the point $\pi_{\mathcal{P}}\{\mathcal{F}_{utop}\}$ on the Pareto set, we will referred to as the* ***optimal parameters*** *of the control algorithm.*

Chapter 4

Description of Mechanical Systems

4.1 Tethered Satellite Systems

Traditionally launch vehicles are used for the delivery of a payload from Earth to a desired orbit. In recent decades, several alternative delivery schemes were suggested. Their main goal is to reduce the cost of delivery operation by refusing to use the last stage of the launch vehicle or totally ignore the usage of carrier rockets. Recently many works discussing several methods of transfer of payload into a higher orbit using TSS's were published [12].

They consist of two or more bodies connected with long high-strength tethers accomplishing orbital flight ability to transfer energy and momentum from one object to another, and, as a result, they can be used to provide space propulsion without consuming propellant.

TSS varies from traditional spacecraft with three main features. The first is a large length providing a stable orientation that is aligned along the local vertical in orbit and on the ends of the system and creates a small artificial gravity. The second feature is a changeable configuration flexibility: the ability to change the length of the cables for the realization of different operations. This allows adjusting the relative position and orientation of devices, attaching and detaching objects from tethers, moving payloads along the tether, etc. The third difference is the active interaction of the conductive tether with the external environment, primarily with the magnetic field of the Earth and

the ionosphere, allowing TSS to work in different operation regimes like generator, motor, electricity transmission and radiative modes. Creation of carbon nano-tubes (a material with the strength of two times more than steel with five times lower specific gravity) provides realization of projects until recently had seemed fantastic [51].

The most ambitious and unwieldy project for payload delivery to orbits is the space elevator, which consists in a TSS that connects the Earth's surface with the space station located in the geostationary orbit. The centrifugal force ensures the stability of the structure. The payload delivers to an orbit by moving along the tether lift [12]. More realistic are the concepts of space escalator and momentum exchange tether. The escalator is a radially oriented TSS constantly in an orbit. The concept is to bring off the satellite into low orbit, where attaches to the lower end of the escalator, then special lifter attracts it along tether to other top. There the satellite undocks and continues its mission in higher orbit. In momentum exchange TTS as in the previous method, we should firstly transport the payload from the ground to some intermediate point in the upper atmosphere. There, instead of escalator, we use an orbiting spinning TSS. The difference is that rotating TSS catches a payload in a low Earth orbit, carries it for a short time, and then throws it into a higher energy orbit. These systems minimize, and perhaps, even eliminate, the use of rockets for Earth-to-orbit launch of satellite payloads and even passengers [52].

Recently, a combined concept of *Momentum eXchange* and *Electrodynamic Reboost*, named MXER, was proposed for propellantless orbital transfer. To provide the tether facility to boost multiple payloads, TSS has electrodynamic reboosting system that gives TSS the capability to restore its orbital energy and momentum after each payload transfer operation. The idea is to generate thrust through electrodynamic interactions of tether facility with a portion of the conducting wire with the Earth's magnetic field. By properly controlling the tether current during an orbit, the tether facility can reboost itself to its original orbit [52].

The main problems discussed in this paper is the TSS orientation in the orbit. Rotating TSS is a highly stable but with a rough orientation facility. The perturbation on main space station and payload can be so great that the implementation of such projects becomes meaningless. The incorrect orientation of the TSS at the time of catching or tossing a payload can cause that TSS/payload rendezvous may never happen or the payload will pass to incorrect orbit or trajectory. However, creating the desired control torque due to the interaction with in/out plane angles, we can achieve both high accuracy

of stabilization and attitude control systems. Thus, the introduction of a system with active control points opens up the possibility of creating a new generation of high-precision orientation and stabilization TSS.

4.1.1 Dynamics and control of TSS

Generally speaking, the dynamics and control of any TSS are quite complex. Because of their overall flexibility, the tethers are strongly susceptible to undergoing a complicated set of librations and vibrations when they are placed into a space environment and coupled with flexible satellites. The problem becomes even more challenging when the deployment and retrieval parts of a TSS mission are taken into consideration because the liberations and vibrations of tether can grow dramatically due to the effect of the Coriolis accelerations.

Over the past decades, numerous studies have been made to gain an insight into the complex dynamics and control of TSSs based on a great variety of models. The simplest, but reasonable model for a TSS is composed of a group of massive bodies connected by massless tethers, with the attitude dynamics of satellites and tether flexibility neglected, and often referred to as a "dumbbell" system when only two massive bodies are involved. The oscillatory motions of a tether can be exploited for swing-up or spin-up in some scenarios, for example, for rotating tethered formation flying. However, if not carefully controlled, the motions with large amplitudes may result in an excessively high tensional stress beyond the strength of tether material and may lead to the failure of a whole TSS. In addition to the considerations for safety, the performance requirements in TSS missions are often quite demanding from a viewpoint of control. For example, in the case of space interferometry applications, the tethered satellites must act as a single unit with precise relative position, and need to be accurately pointed towards the same inertial target while keeping a precise relative attitude for the purpose of optical beam transmission. Furthermore, the establishment of engineering feasibility is usually only the baseline requirement for the control of a TSS, in which high performance is essential to ensure the mission success. However, it is a fundamental, but open problem in control theory to synthesize the nonlinear optimal control for such a complex system. It is also necessary to notice that one peculiarity of controlling a TSS is how to apply the control action to the system. Even though the control action can be realized through thrusters, a simple but effective way is to realize the control by adequately adjusting the tether

tension, the tether length, the attachment position (offset) or the combinations of those parameters. These approaches are permitted by the TSS configuration but not feasible with other satellites [53].

4.1.2 Model and the equations of motion

As one can see from Fig. 4.1, the rocket or hypersonic airplane brings the payload to circular low earth orbit. Then, a special grapple assembly in the lower part of the rotating TSS in a perigee of the elliptical equatorial Earth orbit catches the payload. After the capture, TSS and grapple assembly lift the payload away from the previous orbit and continue their rotation around the boost facility mass center, which is now in a more circular orbit. The grapple and payload continues rotating until their highest altitude at the point where the payload must be tossed into a desired higher orbits or transfer orbit to other planets. The payload's inertial velocity has now increased by approximately twice difference between the orbiting facility's average velocity and the payload's inertial velocity. In other words, the basic idea is to boost one body into a higher orbit at the cost of deboosting the other through the momentum exchange and transfer of orbital energy between [54].

In this article, we analyze the rotating TSS orientation before and after payload's rendezvous. Tether/payload rendezvous in MXER is based on the concept of matching the position and velocity of the tether tip and the payload at one point in time and space. Unlike the traditional vehicles, where the rendezvous operations take place over span times of several minutes to several hours at very low relative velocity, the rendezvous and mating of the tether tip and the payload happens nearly instantaneously, and must be tolerant to very small velocity and position errors.

The ideal zero-relative error case is probably impossible in practice. So the tether tip must be equipped with a catch mechanism that can tolerate some level of positional and velocity error. But, these systems just allow some small tolerances. With active orientation method rotation around the mass center with desired angular velocities, we will get bigger tolerance limits, making the rendezvous windows bigger, and the operation realization more realistic. This active control can be made by a combination of electrodynamic tether/ chemical rocket, with the tether providing electric power and the rocket providing thrust to compensate the magnetic drag on the tether. It turns out that this combination

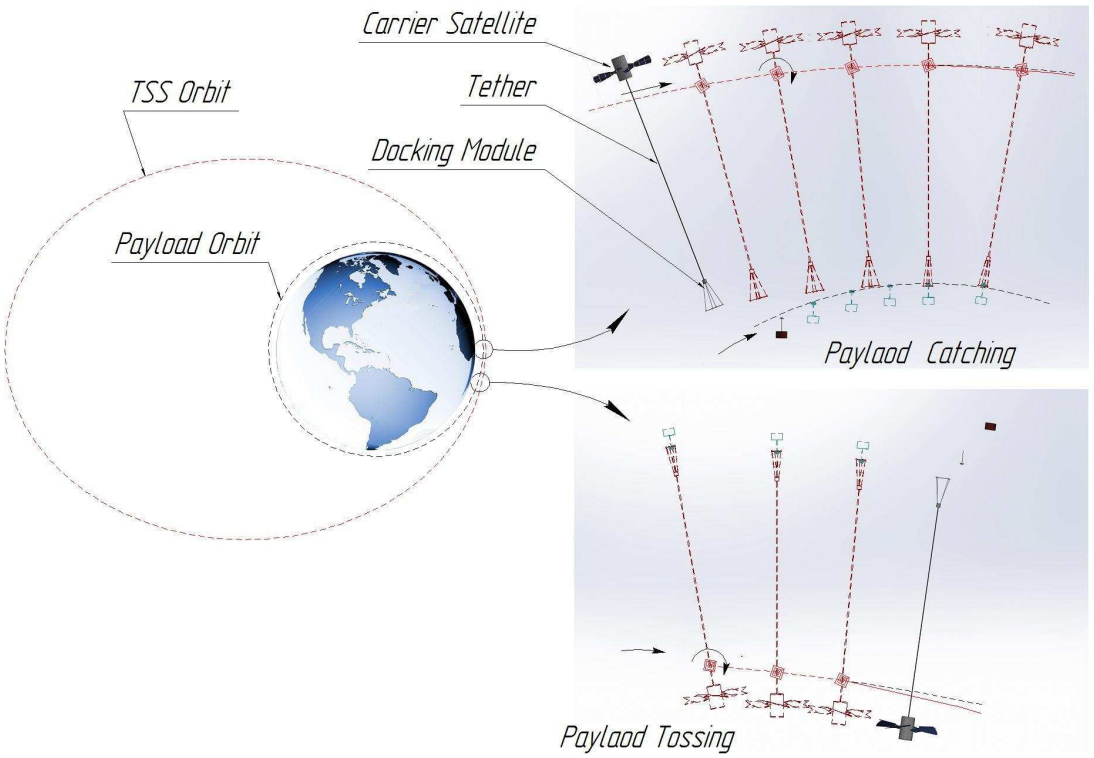

FIGURE 4.1: The Momentum-eXchenge concept illustration.

is more mass fuel-efficient than using the rocket fuel to directly generate power in a fuel cell.

We consider TSS, which consists of

- a carrier satellite mass M with the principal axes of inertia which does not coincide with the center of mass of TSS;

- a tether length l and mas m_l;

- and the docking module mass m_d without and m with the attached payload.

Because of big mass value of the carrier satellite and the tether comparing to the second end-body, we use $m_d = m$. In this work, we consider that both carrier satellite and payload are solid bodies. The TSS has two motions: rotation of mass center C around elliptical orbit and rotating motion around the mass center with a constant controlled value. We assume that variations in the orbit of the system are negligible, such that the system mass center C follows an unperturbed elliptical orbit. Lastly, we assume that the effects of the elastic vibrations of the tether are negligible and model the TSS as a rigid rod.

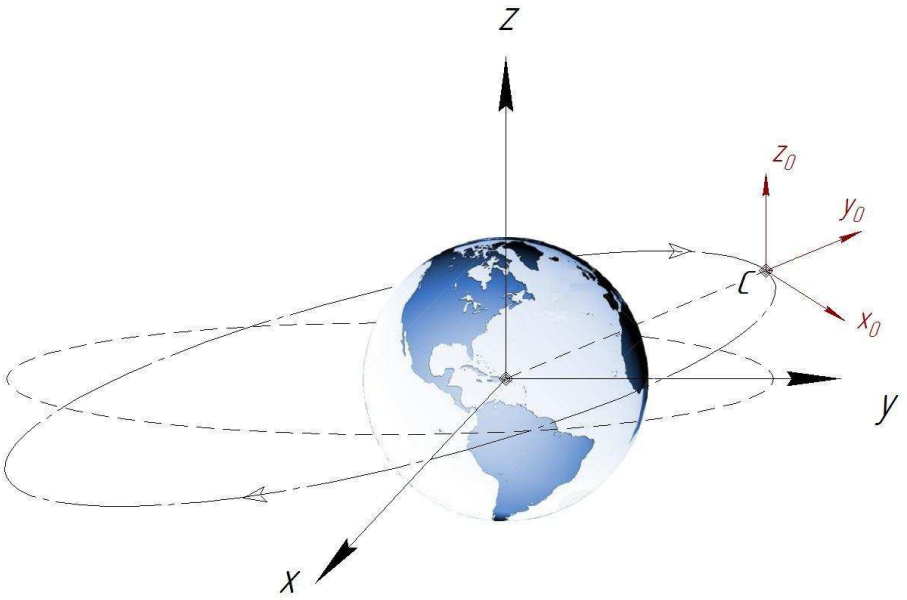

FIGURE 4.2: Orbital system coordinates.

The position of TSS relative to its mass center can be defined by fixed coordinate system $Oxyz$ and base coordinate system $Ox_0y_0z_0$. The fixed coordinate system (see Fig. 4.2) participates in the rotation of TSS relative to its main axis (axis of spinning). For determination of angular positions, we introduce semi-fixed coordinate system $Ox'y'z'$, that does not participate in spinning.

Coordinate origin of these systems take place in the inertia center Fig. 4.3 *a*. The axes of the fixed coordinates system $Oxyz$ coincide with the system's main inertial axes before its turning and are oriented such that the axis Oz is directed along the longitudinal axes of the system, and the axes Ox and Oy lie in the control surfaces of starting position of the launcher rocket. The axes of the semi-fixed coordinate system $Ox'y'z'$ after an initial orientation of TSS on orbit and before start of rotating matches with axes of base reference system. As for the base reference system, we take an orbital system, the Oy-axis of which coincides with current vertical and points upwards, and Ox-axis in the plane of orbit and directed toward the movement of TSS. The Oz-axis of this system is perpendicular to the orbital plane and completes first two axes to the right coordinate system.

Angular position of TSS relative the to axes of orbital coordinate system is defined with three angles:pitch γ, yaw β and roll α. The angle γ describes deviation of the projection of Ox-axis on the orbit plane relative to the plane of actual horizon. The angle β defines

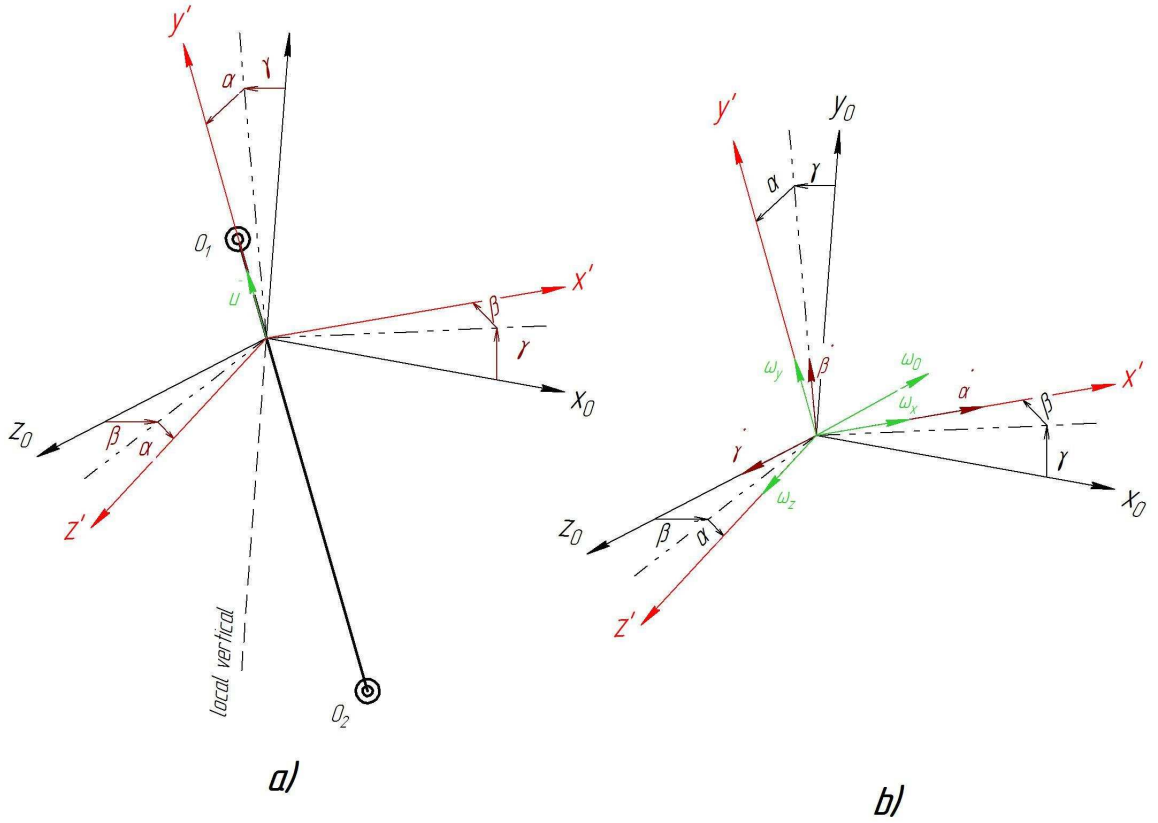

FIGURE 4.3: Angular deviations and velocities.

the deviation of the axis Ox relative to the orbit plane and α describes the deviation of the longitudinal axis Oz relative to the plane of actual horizon (see Fig. 4.3 *a*).

In our study, the angle γ does not have a practical importance because of independent spinning around center of mass in orbital plane that can be controlled by a proper control method. So we just focus on the orientation of the system around the angles α and β Fig. 4.3 *a*. These angles define the projection deviation of the main system axis Ox' on the actual horizon plane relative to the axis Oy_0 (in plane angle) and deviation of the main axis relative to this plane(out plane angle).

Considering that TSS does not have any moveable mass or any liquid filler material, the projection of angular velocities on the axis of fixed coordinate system Ox, Oy, Oz (quasi-velocities) Fig. 4.3 *b* can be presented in the form:

$$\bar{\omega} = \begin{pmatrix} \dot{\alpha} + (\dot{\gamma} - \omega_0)\sin\beta \\ \dot{\beta}\cos\alpha + (\dot{\gamma} - \omega_0)\cos\beta\sin\alpha \\ (\dot{\gamma} - \omega_0)\cos\beta\cos\alpha - \dot{\beta}\sin\alpha \end{pmatrix}$$

where $\bar{\omega} = \begin{pmatrix} \omega_x & \omega_y & \omega_z \end{pmatrix}^\intercal$ is the vector of instantaneous angular velocities and $\omega_0 = -\frac{\sqrt{\mu p}}{r^2}$ is the orbital angular velocity. Here μ, p and r are parameters of the orbit [2] .

Following the procedure of Lagrangian formalism, we consider the kinetic energy of the system given by

$$T = \frac{1}{2} M_t \left\| \bar{v}_{CI} \right\|^2 + \frac{1}{2} \left\langle \bar{\omega}, \mathbb{I}\bar{\omega} \right\rangle$$

where

- M_t is the total mass of TSS,
- $\bar{v}_{CI}$ is the absolute velocity of the center of inertia (mass),
- $\mathbb{I}$ is the tensor of inertia of TSS with respect to its center of mass.

The norm of the velocity of mass center v_{CI} (in Keplerian elliptical motion without perturbations) can be expressed as [2]

$$\left\| \bar{v}_{CI} \right\|^2 = \mu \left(\frac{2}{r} - \frac{1}{a} \right)$$

where μ, r, a are parameters of the orbit. As the result

$$T_{CI} = M_t \mu \left(\frac{2}{r} - \frac{1}{a} \right), \; M_t := \left(m_{SS} + m_{SB} + m_{Th} \right) / 2$$

The tensor of the total inertial moment in fact is the sum of three components

$$\mathbb{I} = \mathbb{I}_{CS} + \mathbb{I}_{SB} + \mathbb{I}_{Th}$$

where $\mathbb{I}_{\mathbb{CS}}$, $\mathbb{I}_{SB}$ and $\mathbb{I}_{Th}$ are known tensors of inertia of the corresponding carrier satellite, second end body and the tether. Assuming the symmetrically of the orbit station, we may represent $\mathbb{I}$ as

$$\mathbb{I} = \begin{pmatrix} \mathbb{I}_s & 0 & 0 \\ 0 & \mathbb{I}_y & 0 \\ 0 & 0 & \mathbb{I}_s \end{pmatrix}$$

Because the constant spinning motion is around the axis z, we assume that $\dot{\gamma} = \text{const}$. Denoting

$$\omega_z := (\dot{\gamma} - \omega_0)$$

we can represent the kinetic energy of the TSS rotation with respect to de mass center as follows:

$$\tfrac{1}{2}\langle \bar{\omega}, \mathbb{I}\bar{\omega} \rangle = \tfrac{1}{2} \begin{pmatrix} \dot{\alpha} + \omega_z \sin\beta \\ \dot{\beta}\cos\alpha + \omega_z \cos\beta \sin\alpha \\ \omega_z \cos\beta\cos\alpha - \dot{\beta}\sin\alpha \end{pmatrix}^{\top} \times$$
$$\begin{pmatrix} I_s & 0 & 0 \\ 0 & I_y & 0 \\ 0 & 0 & I_s \end{pmatrix} \begin{pmatrix} \dot{\alpha} + \omega_z \sin\beta \\ \dot{\beta}\cos\alpha + \omega_z \cos\beta \sin\alpha \\ \omega_z \cos\beta\cos\alpha - \dot{\beta}\sin\alpha \end{pmatrix} =$$

$$\tfrac{1}{2} \begin{pmatrix} \left[\mathbb{I}_s \left(\dot{\alpha}^2 + \omega_z^2 \sin^2\beta + \dot{\alpha}\omega_z \sin\beta\right) + \left(I_y \cos^2\alpha + I_s \sin^2\alpha\right)\right. \\ \left.\left(\dot{\beta}^2 + \omega_z^2 \cos^2\beta\right) + \dot{\beta}\omega_z \cos\beta\cos\alpha\sin\alpha\,(\mathbb{I}_y - \mathbb{I}_s)\right] \end{pmatrix}$$

So, the total kinetic energy T is

$$\begin{aligned} T = \frac{1}{2}\Big[\mathbb{I}_s\left(\dot{\alpha}^2 + \omega_z^2\sin^2\beta + \dot{\alpha}\omega_z\sin\beta\right) + \left(\mathbb{I}_y\cos^2\alpha + \mathbb{I}_s\sin^2\alpha\right)\left(\dot{\beta}^2 + \omega_z^2\cos^2\beta\right)\Big] \\ + \frac{1}{4}\dot{\beta}\omega_z\cos x_2 \sin 2x_1\,(\mathbb{I}_y - \mathbb{I}_s) + M_t\mu\left(\frac{2}{r} - \frac{1}{a}\right) \end{aligned} \tag{4.1}$$

The potential energy of the system is the sum of the energies of the carrier satellite, the tether and the second end body [2] :

$$\Pi = \Pi_{SS} + \Pi_{Th} + \Pi_{SB}$$

where

$$\Pi_{CS} = \frac{3\mu}{2r^3}\left(\mathbb{I}_{xCS} - \mathbb{I}_{yCS}\right)\cos^2\beta$$

$$\Pi_{SB} = \frac{3\mu}{2r^3}\left(\mathbb{I}_{xSB} - \mathbb{I}_{ySB}\right)\cos^2\beta$$

$$\Pi_{Th} = -\frac{\mu}{r} + \frac{\mu M l^2}{2r^3}\left(1 - \cos^2\alpha\right)$$

Here $\mathbb{I}_{xCS}$, $\mathbb{I}_{yCS}$, $\mathbb{I}_{xSB}$, and $\mathbb{I}_{ySB}$ are the projections of inertial moment of the carrier satellite and the second end body on the axes x' and y'. As a result, we have

$$\Pi = \frac{3\mu}{2r^3}\left(\mathbb{I}_{xSS} + \mathbb{I}_{xSB} - \mathbb{I}_{ySB} - \mathbb{I}_{ySS}\right)\cos^2\beta - \frac{\mu}{r} + \frac{\mu M l^2}{2r^3}\left(1 - \cos^2\alpha\right) \tag{4.2}$$

Denote for simplicity

$$\mathbb{I}_{\Pi} := \mathbb{I}_{xSS} + \mathbb{I}_{xSB} - \mathbb{I}_{ySB} - \mathbb{I}_{ySS}$$

Combination (4.1) and (4.2) allow us to obtain the Lagrange's function $L = T - \Pi$:

$$L = \frac{1}{2}\left[\mathbb{I}_s\left(\dot{\alpha}^2 + \omega_z^2\sin^2\beta + \dot{\alpha}\omega_z\sin\beta\right) + \left(\mathbb{I}_y\cos^2\alpha + \mathbb{I}_s\sin^2\alpha\right)\left(\dot{\beta}^2 + \omega_z^2\cos^2\beta\right)\right] +$$

$$\frac{1}{4}\dot{\beta}\omega_z\cos x_2\sin 2x_1\left(\mathbb{I}_y - \mathbb{I}_s\right) + M\mu\left(\frac{2}{r} - \frac{1}{a}\right) - \frac{3\mu}{2r^3}\cos^2\beta\mathbb{I}_{\Pi} - \frac{\mu}{r} + \frac{\mu M l^2}{2r^3}\left(1 - \cos^2\alpha\right)$$

The corresponding Lagrange equations are:

$$\frac{d}{dt}\frac{\partial L}{\partial \dot{x}_j} - \frac{\partial L}{\partial x_j} = \tau_j,\ j = \overline{1,2}$$

$$x_1 = \alpha\ , x_2 = \beta$$

describing the dynamic of the system under the consideration, and can be expressed in the following format:

$$\ddot{x} + D^{-1}(x)\, C(x, \dot{x})\, \dot{x} + D^{-1}(x)\, G(x) = D^{-1}(x)\, \tau$$

$$x := \begin{pmatrix} x_1 & x_2 \end{pmatrix}^\top, \ \tau := \begin{pmatrix} \tau_1 & \tau_2 \end{pmatrix}^\top$$

Here

$$D(x) := \begin{pmatrix} \mathbb{I}_s & 0 \\ 0 & \mathbb{I}_y \cos^2 x_1 + \mathbb{I}_s \sin^2 x_1 \end{pmatrix}$$

$$C(x, \dot{x}) := \begin{pmatrix} 0 & \frac{1}{2}\omega_z (\mathbb{I}_y - \mathbb{I}_s) \cos x_2 \cos 2x_1 + \dot{x}_2 \sin 2x_1 (\mathbb{I}_s - \mathbb{I}_y) \\ \frac{1}{2}\mathbb{I}_s \omega_z \sin x_2 & \mathbb{I}_y \cos^2 x_1 + \mathbb{I}_s \sin^2 x_1 - \frac{1}{2}\omega_z \sin x_2 \sin 2x_1 (\mathbb{I}_y - \mathbb{I}_s) \end{pmatrix}$$

$$G(x) := \begin{pmatrix} \sin 2x_1 (\mathbb{I}_s - \mathbb{I}_y)\, \omega_z^2 \cos x_2 + \frac{\mu M l^2}{r^3} \sin x_1 + \frac{\mathbb{I}_s}{4}\omega_z \cos x_2 \\ \\ \frac{1}{4}\omega_z \cos x_2 \sin 2x_1 (\mathbb{I}_y - \mathbb{I}_s) + \frac{3\mu}{2r^3} \sin 2x_2 \mathbb{I}_\Pi \\ + \frac{1}{2}\omega_z^2 \sin x_2 \left[\mathbb{I}_s \sin x_2 - \left(\mathbb{I}_y \cos^2 x_1 + \mathbb{I}_s \sin^2 x_1 \right) \right] \end{pmatrix}$$

We can rewrite the system in the "*state-space form*" as

$$\begin{gathered} \dot{x}_1 = x_3 \\ \dot{x}_2 = x_4 \\ \begin{pmatrix} \dot{x}_3 \\ \dot{x}_4 \end{pmatrix} = -D^{-1}(x_1, x_2)\, C(x_1, x_2, x_3, x_4) \begin{pmatrix} x_3 \\ x_4 \end{pmatrix} \\ -D^{-1}(x_1, x_2)\, G(x_1, x_2) + D^{-1}(x_1, x_2)\, \tau \end{gathered}$$

or, in the matrix form

$$\dot{X} = AX + B\mathbf{u} + h$$

$$X := (\mathbf{x}_1^\intercal, \mathbf{x}_2^\intercal)^\intercal, \ \mathbf{x}_1 := (x_1, x_2)^\intercal \tag{4.3}$$

$$\mathbf{x}_2 := (x_3, x_4)^\intercal, \ \mathbf{u} := (\tau_1, \tau_2)^\intercal$$

where

$$A = \begin{bmatrix} 0_{2\times 2} & I_{2\times 2} \\ 0_{2\times 2} & -D^{-1}(\mathbf{x}_1)\, C(\mathbf{x}) \end{bmatrix}$$

$$B = \begin{bmatrix} 0_{2\times 2} \\ I_{2\times 2} \end{bmatrix} D^{-1}(\mathbf{x}_1)$$

$$h = -\begin{pmatrix} 0_{2\times 1} \\ D^{-1}(\mathbf{x}_1)\, G(\mathbf{x}_1) \end{pmatrix}$$

The components of the control vector $\mathbf{u} := (\tau_1, \tau_2)^\intercal$ are torques created by a combination of electrodynamic tether/ chemical rocket.

Model with bounded disturbances and uncertainties Under the presence of external disturbances and internal model-uncertainties, the mathematical model see Eq. (4.3), considered above, becomes as follows:

$$\dot{X} = AX + B\mathbf{u} + h + f(X,t) \tag{4.4}$$

where the vector $f(X,t)$ characterizes the joint effect of external disturbances and internal model-uncertainties, and is supposed to be bounded, i.e., for all $X \in \mathbb{R}^4$ and all $t \geq 0$

$$\|f(X,t)\| \leq L$$

where L is assumed to be known *a* priory.

4.2 Secondary Mirror of Radio-Telescope

The radio-telescope antenna is a device that is used to receive radio-frequency radiation emitted by extraterrestrial sources and satellites. Because radio wavelengths are much longer than those of visible light, radio telescopes must be very large in order to attain the resolution of optical telescopes. Radio telescopes vary widely, but depending on their design they can be divided in one and dual reflector antennas. In dual-reflector

(Cassegrian) antennas a parabolic reflector is used as the mail reflector and a hyperboloid of revolution as the sub-reflector (secondary mirror) as shown in Fig. 1.2.

Because radio wavelengths are much longer than those of visible light, radio telescopes must be very large in order to attain the resolution of optical telescopes. The first radio telescope, built in 1937 by Grote Reber of Wheaton, Ill., U.S., was a steerable paraboloid–i.e., a device with a parabolically shaped reflector, dubbed the "dish", that focuses the incoming radio waves onto a small pickup antenna, or "feed." Radio telescopes vary widely, but they all have two basic components: (1) a large radio antenna and (2) a radiometer or radio receiver. The sensitivity of a radio telescope–i.e., the ability to measure weak sources of radio emission-depends on the area and efficiency of the antenna, the sensitivity of the radio receiver used to amplify and detect the signals, and the duration of the observation. For broadband continuum emission the sensitivity also depends on the receiver bandwidth. Because some astronomical radio sources are extremely weak, radio telescopes are usually very large and only the most sensitive radio receivers are used. Moreover, weak cosmic signals can be easily masked by terrestrial radio interference, and great effort is taken to protect radio telescopes from man-made interference.

The performance of the radiotelescope could be improved considerably using thedual reflector antennas. In dual-reflector (Cassegrian) antennas a parabolic reflector is used as the mail reflector and a hyperboloid of revolution as the sub-reflector (secondary mirror) as shown in Fig. (1.2).

In this work a Stewart platform is used to obtain desired pointing accuracy (1 arcsec) of a secondary mirror in the required position and orientation. These highly position and attitude requirements encompass six independent degrees of freedom. Usually, the tracker is supported by the telescope structure at the nominal position of half the radius of curvature of the primary reflector. The telescope structure supports all the interfaces of the tracker to the rest of the telescope system. These manipulators have attracted much attention from researchers in a large number of applications, such as machine tools, underwater exploration, aviation rescue operations , aircraft simulators, telescopes and orthopedic surgery (see [55–60]).

The platform is permanently under the action of harsh environmental conditions and parasitic dynamics, on the other hand there is always a discrepancy between the actual plant dynamics and its mathematical model used for the controller design. The performance

of a radio telescope is limited by various factors: the accuracy of a reflecting surface that may depart from the ideal shape because of manufacturing irregularities; the effect of wind load; thermal deformations that cause differential expansion and contraction; and deflections due to changes in gravitational forces as the antenna is pointed to different parts of the sky. Designing the control laws that provide the desired closed-loop system performance in the presence of these disturbances/uncertainties is a very challenging task for a control engineer. Primary success applications of Stewart platform were expounded which include kinematics, mechanic structure and primary control strategies (Robust PID control [61], inverse dynamics control [62], neuro-fuzzy control [63]) at present.

In this dissertation a new sliding mode algorithm is proposed to control the system. The sliding mode structure does not require dynamic modelling of the manipulator; the bounds of the model parameters are sufficient to construct the controller. The previous works which used the sliding mode for the manipulator are based of the linear Newton-Euler dynamic equations [64] and with estimation of inverse kinematics of platform [65].

The direct application of the lagrangian dynamic formulation, together with the space state representation in this work, results in a convenient and compact algorithmic description of the manipulator equations of motion. The algorithm is expressed by matrix operations and facilities both analysis and control implementation giving the complete representation of the mechanism performance. However the implementation of sliding mode to this system causes a near-singularity phenomena, provoking the increasing of the values of control signals. This problem is resolved by a new design of sliding mode control. This proposed controller provides the positioning of the secondary mirror of a radio-telescopes in presence of unmodelled dynamics and perturbations. The chattering reduction is handled by an adaptive type of sliding mode based on equivalent control. This methodology is associated with dynamic adaptation of sliding mode controllers (under known uncertainty bounds) where the adaptation process is continued during sliding mode, using the current estimates of the corresponding equivalent control (see [25]), that leads to minimization of chattering effect.

4.2.1 General system description

The figure 4.4 illustrates the example of secondary mirror of a radio-telescope mounted on a GSM. This device is designed to be installed on the Large Millimeter Telescope

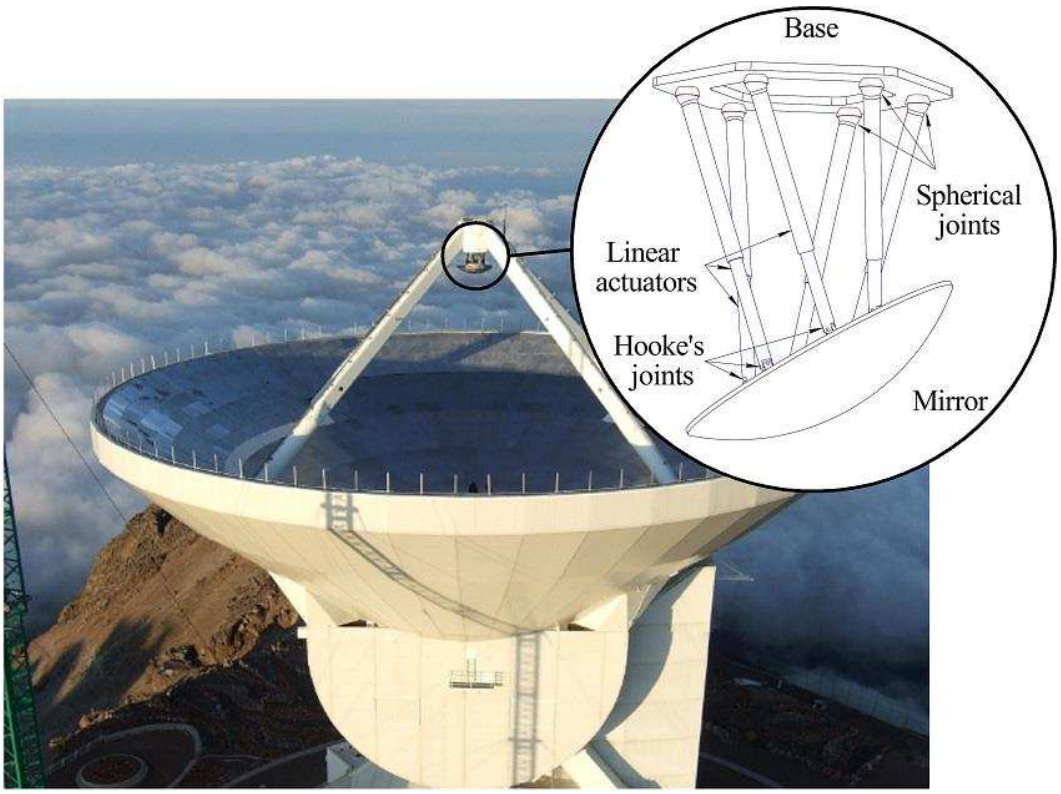

FIGURE 4.4: Secondary mirror of radio-telescope antenna with hexapod positioner.

[66]. The secondary mirror with aim of this device must keep the focus length with high position and orientation accuracy. The platform consists of a stationary base, the mirror mounted on a movable platform, and six prismatic actuators (screw joint). The mirror placed on the top platform can be moved in the six degrees of freedom: the three linear movements x, y, z and the three rotations pitch, roll and yaw. The actuators are connected by spherical joints to the base and via Hooke's joints to the moving platform.

4.2.2 Mathematical model

The simplified kinematic model of the proposed GSM is derived as in figure 4.5. Let the support legs A_iB_i, $i = \overline{1,6}$ consist of upper and lower parts, connected as translational kinematic pair, fixed to the moving platform in the points B_i through universal Hooke's joints, and to the base platform in the points A_i via spherical joints. Each leg A_iB_i has length l_i and is inclined by the angle γ_i.

Let fix the coordinate system $AXYZ$ with the base platform such that origin A coincides with the mass center of base, AX-axis passes through the joint A_3, AY is pointed by

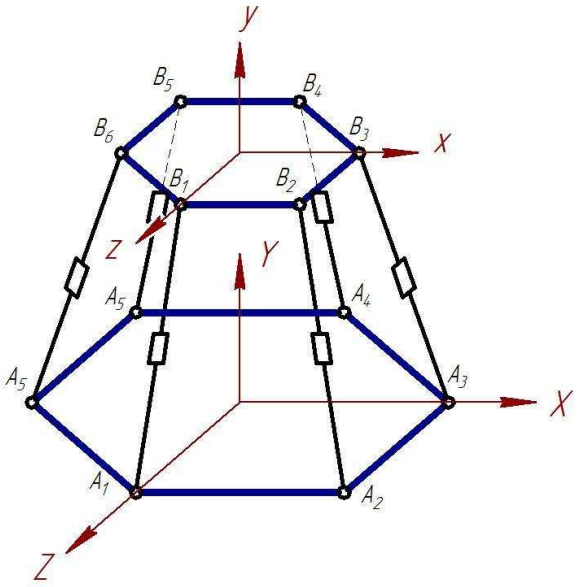

FIGURE 4.5: Kinematic geometry of the hexapod with 6 dof.

the normal to the base and the AZ generates a right system with two previous axes. Similarly we fix $Bxyz$ coordinate system with the moving platform. The position of the joints $\overline{A_1, A_6}$ and $\overline{B_1, B_6}$ in coordinate system $AXYZ$ define by next vectors.

$$\bar{A}_i = (A_{i,1}, A_{i,2}, A_{i3}) \, , \bar{B}_i = (B_{i,1}, B_{i,2}, B_{i3}) \, , \; i = \overline{1,6} \tag{4.5}$$

The position of the moving platform respect to the base defines by Euler angles φ_1, φ_2 and φ_3 (Fig. 4.6) and the vector $\bar{B} = (X_B, Y_B, Z_B)$.

The geometrical correlation between the coordinate systems $AXYZ$ and $Bxyz$ obtains by the homogeneous transformation matrix T_H [1]:

$$T_H = \begin{bmatrix} a_{1,1} & a_{1,2} & a_{1,3} & X_B \\ a_{2,1} & a_{2,2} & a_{2,3} & Y_B \\ a_{3,1} & a_{3,2} & a_{3,3} & Z_B \\ 0 & 0 & 0 & 1 \end{bmatrix}$$

Accordingly, the position of the joint B_i, in the coordinate system $AXYZ$ defines as:

[1] Find the values of $a_{i,i}$ in Appendix A

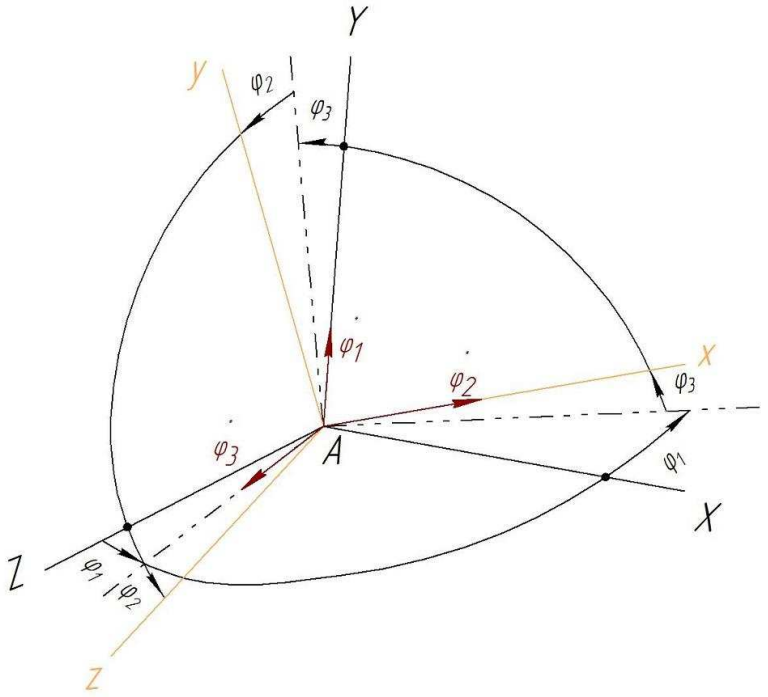

FIGURE 4.6: Coordinate system representation of Euler angles.

$$\bar{B}_i = T_H \left[B_{i,1},\ B_{i,2},\ B_{i,3},\ 1\right]^\top \tag{4.6}$$

From (4.5) and (4.6) it follows, that the generalized coordinate l_i, as a function of the magnitudes $X_B, Y_B, Z_B, \varphi_1, \varphi_2, \varphi_3$ defines by the expression

$$l_i = \sqrt{\sum_j \left(A_{i,j} - \bar{B}_i\right)^2},\ \ j = 1, 2, 3$$

4.2.3 Mechanism dynamics

For the formation of dynamic equations of the platform we use the second order Lagrange equations

$$\frac{d}{dt}\frac{\partial T}{\partial \dot{q}_i} - \frac{\partial T}{\partial q_i} = Q_i,\ \ i = 1, .., 6 \tag{4.7}$$

where

- T is the general kinetic energy of the system

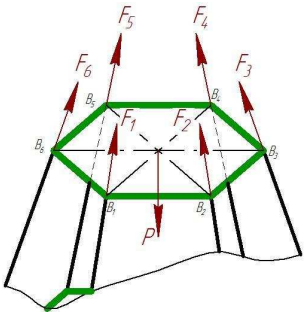

FIGURE 4.7: External forces acting on the platform.

- Q_i are the generalized forces corresponding to the i-th coordinate

- q_i are the generalized coordinates:

$$q_1 = X_B, q_2 = Y_B, q_3 = Z_B, q_4 = \varphi_1, q_5 = \varphi_2, q_6 = \varphi_3$$

Neglecting mass of the legs, the kinetic energy of the system can be expressed as

$$T = \frac{1}{2}\left[M\left(\dot{X}_B^2 + \dot{Y}_B^2 + \dot{Z}_B^2\right) + J_x\dot{\varphi}_1^2 + J_y\dot{\varphi}_2^2 + J_z\dot{\varphi}_3^2\right] \tag{4.8}$$

where M is the mass of platform and $J_{x,y,z}$ are inertial moments around the corresponding axes. The generalized forces acting on the system as in Fig. 4.7 determine as:

$$Q_1 = \sum_{i=1}^{6} F_i \cos\gamma_{i,1} \qquad Q_2 = -P + \sum_{i=1}^{6} F_i \cos\gamma_{i,2} \qquad Q_3 = \sum_{i=1}^{6} F_i \cos\gamma_{i,3}$$
$$Q_4 = \sum_{i=1}^{6} F_i \sum_{j=1}^{3} (a_{i,j,1}\cos\gamma_{i,j}) \quad Q_5 = \sum_{i=1}^{6} F_i \sum_{j=1}^{3} (a_{i,j,2}\cos\gamma_{i,j}) \quad Q_6 = \sum_{i=1}^{6} F_i \sum_{j=1}^{3} (a_{i,j,3}\cos\gamma_{i,j})$$

Here F_i represents the forces acting on the linear actuators and $P = Mg$. Let's rewrite the system by new variables: the coordinates and velocities of the point B as

$$X_B = x_1 \quad Y_B = x_2 \quad Z_b = x_3$$
$$\varphi_1 = x_4 \quad \varphi_2 = x_5 \quad \varphi_3 = x_6$$

angles and angular velocities of the point B as

$$\dot{X}_B = x_7 \quad \dot{Y}_B = x_8 \quad \dot{Z}_b = x_9$$
$$\dot{\varphi}_1 = x_{10} \quad \dot{\varphi}_2 = x_{11} \quad \dot{\varphi}_3 = x_{12}$$

and finally the control signals generated by actuators as

$$u_i = F_i, \ i = \overline{1,6}$$

The state space representation in the vector form is:

$$\begin{aligned} \dot{X}_1(t) &= X_2(t) \\ \dot{X}_2(t) &= f + G(X_1, t)\, u + \xi(X, t) \\ y(t) &= X_1(t) \end{aligned} \tag{4.9}$$

- $X_1(t), X_2(t) \in \mathbb{R}^6$ are the state of the system at time $t \in \mathbb{R}_+$;

- $X(t) := \left(X_1^\top(t), X_2^\top(t)\right)^\top \in \mathbb{R}^{12}$;

- $y(t) \in \mathbb{R}^6$ is a measurable output at time $t \geq 0$;

- $u \in \mathbb{R}^6$ is a control to be designed;

- $\xi(x, t) \in \mathbb{R}^6$ is unmeasurable term including the external as well as internal perturbations and uncertainties;

- $f = (0, -Mg, 0, 0, 0, 0)^\top$

- $G \in \mathbb{R}^{6\times 6} = [g_{k,i}](k, i = 6)$ is supposed to be exactly known [2].

Notice that in the model (4.9) only the half of coordinates ($X_1(t)$) are available in time[3].

[2] Find values $g_{k,i}$ in appendix B

[3] More detailed mathematical modelling can be found in [67]

Chapter 5

Numerical Simulations

Different simulations are carried out in this section to prove the effectiveness of the designed approaches. Firstly for an orientation and stabilization tasks of tethered satellite system and then by applying the controller and observer to the radiotelescope subreflector.

5.1 Tethered Satellite System

5.1.1 The conventional algorithm

Fig. 5.1 illustrates the finite time convergence of the state variables to the desired states in the presence of the external bounded disturbance (here we took $f = \sin(10x)$).

As we can see from Fig. 5.2 the zoomed portion of the phase portrait illustrates the *zigzag motion* of small amplitude and high frequency that control signals exhibit while in the sliding mode.

5.1.1.1 Adaptive algorithm based on "Equivalent Control Method"

To demonstrate the properties of the adaptation procedure, another simulation was performed with the following parameters:

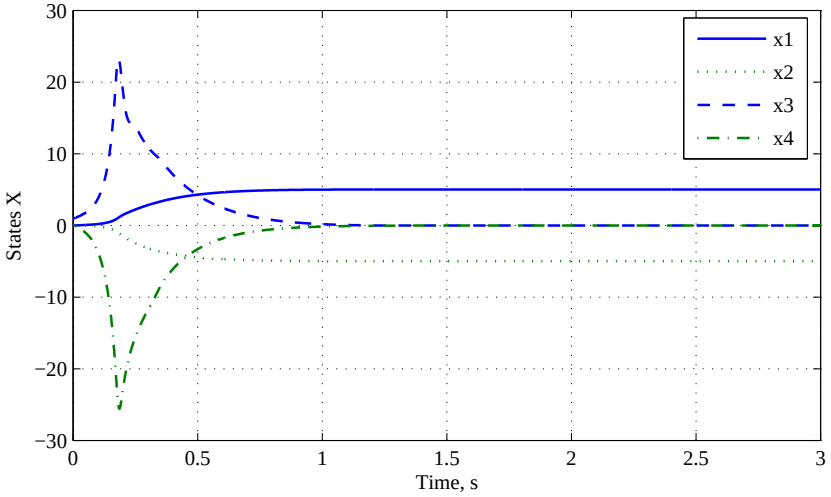

FIGURE 5.1: States evaluation under SMC.

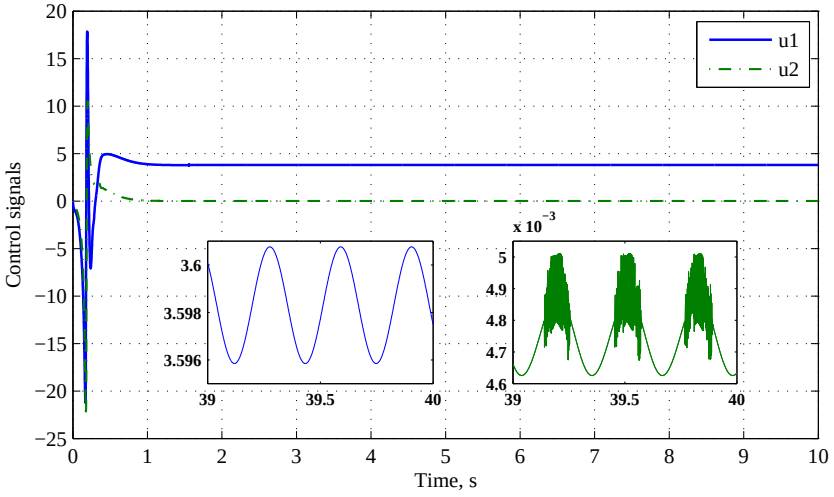

FIGURE 5.2: Control signals in conventional SMC.

$$\gamma_0 = 3,\ \mu = 0.04,\ \alpha = 0.95$$

$$k_1^+ = 10,\ k_2^+ = 1, k_{1,2}(0) = 2.8$$

One can see that the control signals have the chattering phenomenon with amplitudes much smaller than the conventional control.

Here is clearly (see Fig. 5.2 and Fig. 5.4) that gain parameter $k(t)$, defining the chattering amplitude in the sliding mode (after the reaching time t_{reach}), continues decreasing attaining after $0,3$ *sec.* and follows the amplitude of the external perturbation signal f.

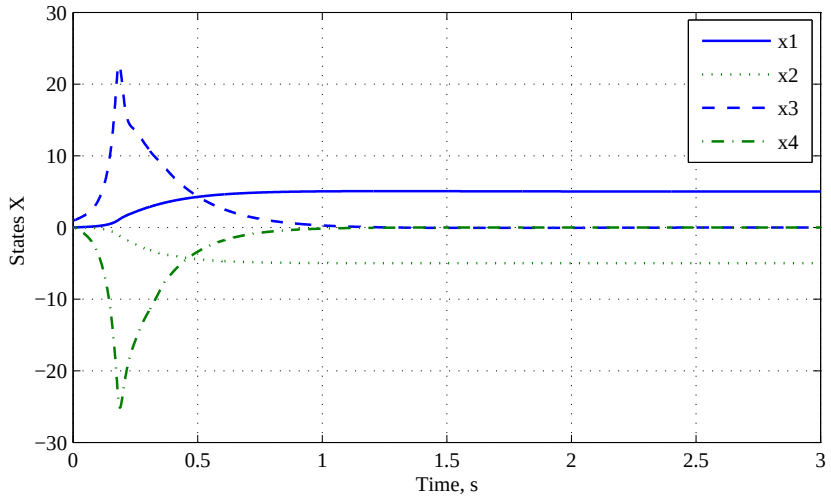

FIGURE 5.3: States variables in Equivalent Control method.

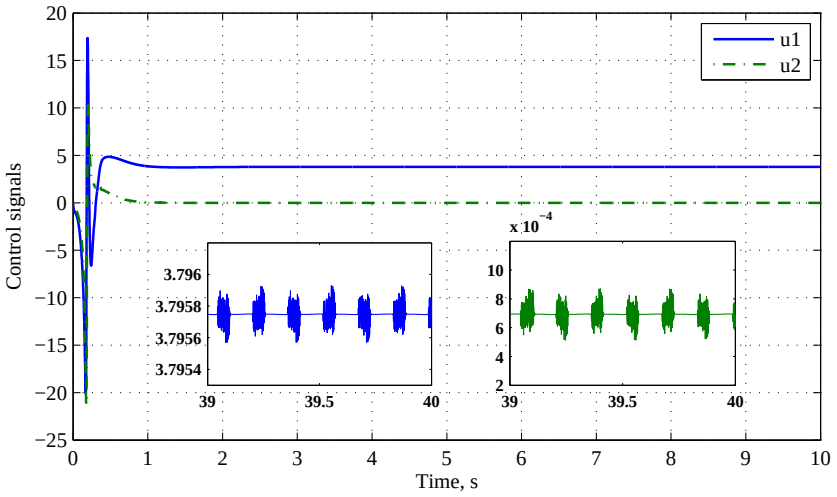

FIGURE 5.4: Control signals under the adaptive gain-learning

Notice that, in the simulation with lower frequencies, the chattering effect improvement for adaptive sliding mode control may attach ten times with respect to the standard SMC.

5.1.2 Adaptive Sliding Mode Controller Based on Super-Twist Observer

The parameters, participating in the controller realization, are given in Table 1.

Table 1. Numerical values of the parameters in the suggested control scheme.

$p_0 = 0,2$	$c_2 = 6$	$L_f = 20$	$\gamma = 90$	$\mu = 3.98 \times 10^{14}$	$x_1^*[\text{rad}] = 5$
$p_1 = 1$	$\epsilon = 1$	$\xi^+ = 10$	l [m] $= 2000$	M [kg] $= 2000$	$x_2^*[\text{rad}] = 0$
$p_2 = 1$	$\alpha = 200$	$n = 2$	$\mathbb{I}_s[\text{kg} \cdot \text{m}^2] = 5000$	ω_z [rad/s] $= 2$	$x_3^*[\text{rad/s}] = 0$
$c_1 = 0,1$	$e_2^+ = 40$	$L_g = g_{-1}^+ = 1$	$\mathbb{I}_y[\text{kg} \cdot \text{m}^2] = 3000$	r [m] $= 2 \times 10^6$	$x_4^*[\text{rad/s}] = 0$

From the figures 5.5 and 5.6 one can see the behavior of the real states X and $\dot{X}$ of the controlled tethered system closed by the suggested adaptive SM controller based on the angular velocities estimation. Practically in 2.0 seconds the controlled variables reach the desired values. The angular position as well as their derivative estimates show quick approachment to the real values.

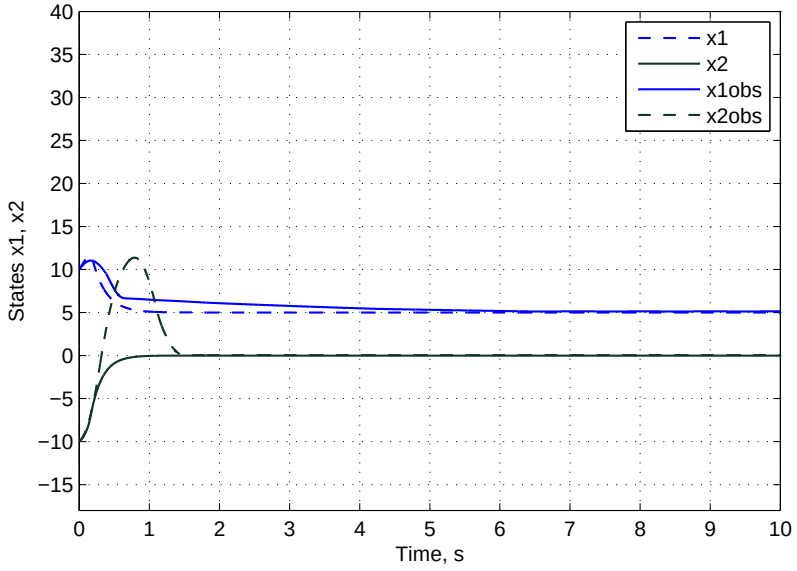

FIGURE 5.5: The comparison of angular positions between estimated and real values.

As it was expected, the control actions attains their their behavior at fast rate corresponding to the desired regular regime: u_1 obtains the constant value and u_2 enters into "*chattering regime*" around zero value (see Fig. 5.7).

Fig. 5.8 depicts the behavior of two sliding surfaces $\sigma_1(X(t))$ and $\sigma_2(X(t))$ which practically in 2.0 seconds obtain 0-values that corresponds the "beginning" of the sliding process.

Finally, Fig. 5.9 illustrates the time-variations of the adaptive control parameters $k = k\left(\hat{x}\left(t\right), t\right)$, $\lambda = \lambda\left(\hat{x}\left(t\right), t\right)$ providing the desired dynamics of the considered closed-loop system.

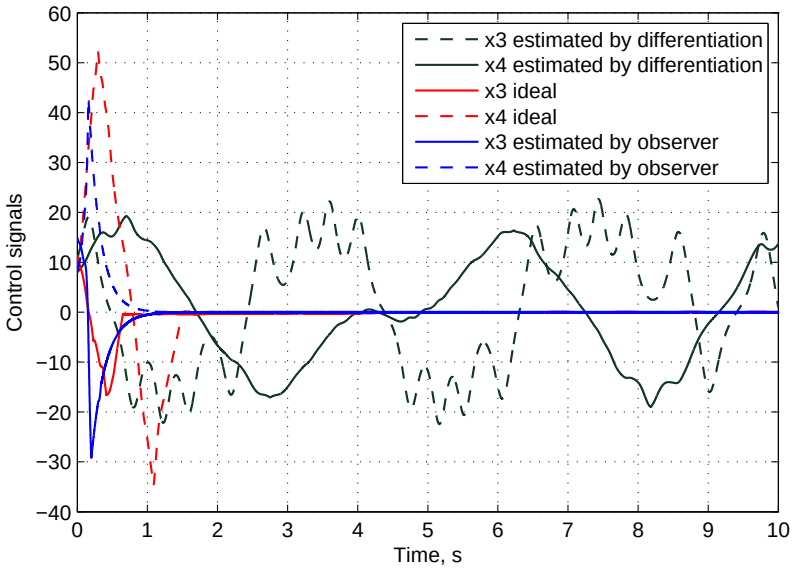

FIGURE 5.6: Angular velocities and their estimates.

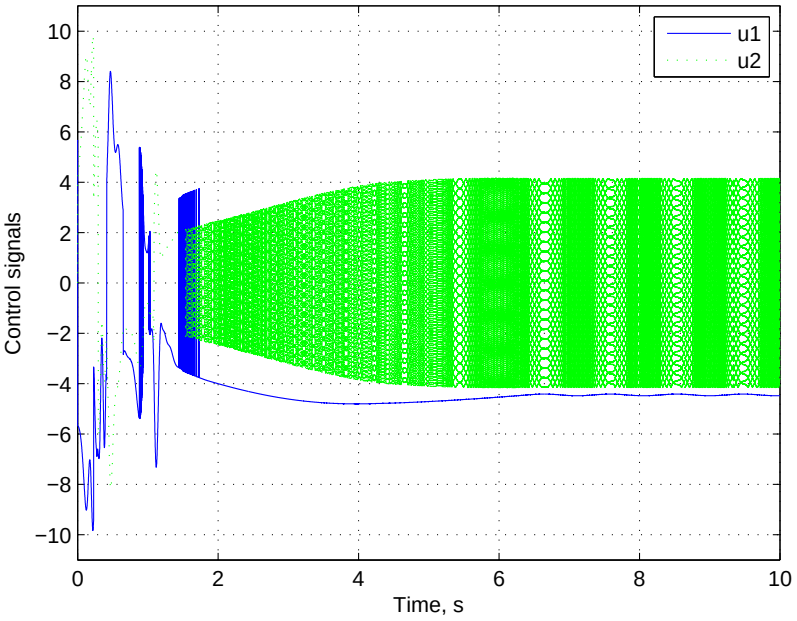

FIGURE 5.7: Control signals representation.

Comparing the suggested adaptive SM observer with a standard differentiator containing a preliminary smoothing (low-pass filtering) in the input, one can observe in Fig. 5.6 that with an essential noise term the standard technique applying to the considered example becomes practically unworkable. Fig. 5.10 show that the control, corresponding the standard low-pass filtering with differentiation, never reaches the "chattering regime".

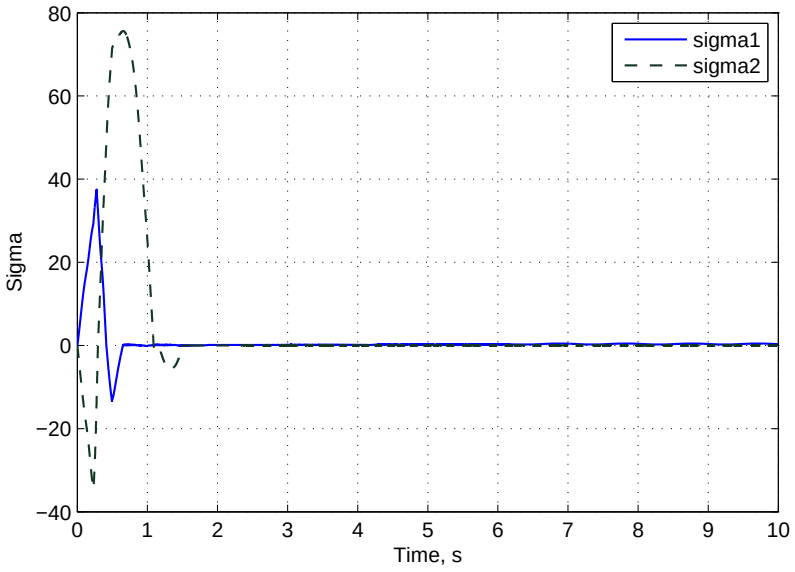

FIGURE 5.8: Two sliding surfaces $\sigma_1(X(t))$ and $\sigma_2(X(t))$.

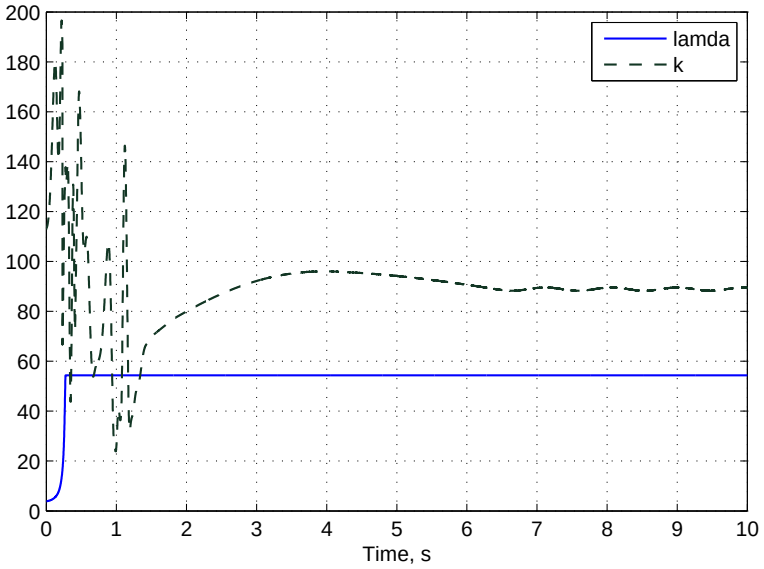

FIGURE 5.9: The comportment of the adapted parameters k and λ.

This explicitly demonstrates that the behavior of the close-loop system with classical control is too far from desired one.

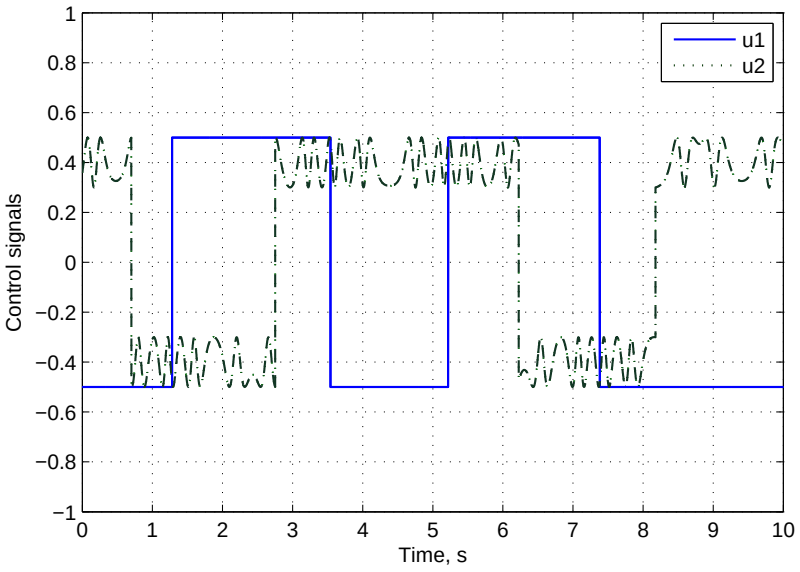

FIGURE 5.10: Control signals for classical differentiator with preliminary low-pass filtering.

5.1.3 Pareto-Optimal Adaptive SMC with SM Observer

The results of the subsection *2.5*, could be proved as well. For that we use the Pareto-optimal parameters:

Table 2. Numerical values of the parameters in the Pareto-optimal control

$p_0 = 0,2$	$\epsilon = 0.5$	$\alpha = 50$
$p_{1opt} = 0.1040$	$\xi^+ = 10$	$\gamma = 70$
$p_{2opt} = 0.6960$	$L_f = 20$	

The comparison of figures (5.11) and (5.12) demonstrates the improvement of adaptive control by the Pareto optimization method. On one hand the state tracking time has been reduced and on the other hand the chattering effect of the sliding observer has been reduced.

5.2 Secondary mirror of Radio-telescope

We begin with the simulation of the system by applying a simple PID controller. As it was expected, Fig. 5.13 demonstrates that this method can not come up successfully

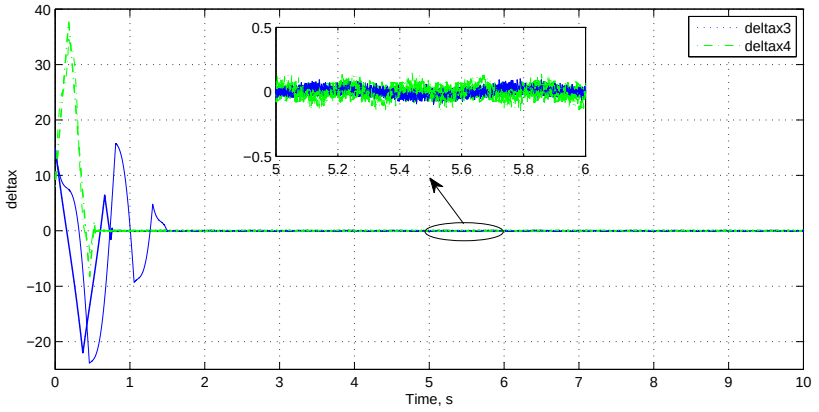

FIGURE 5.11: States tracking in conventional control.

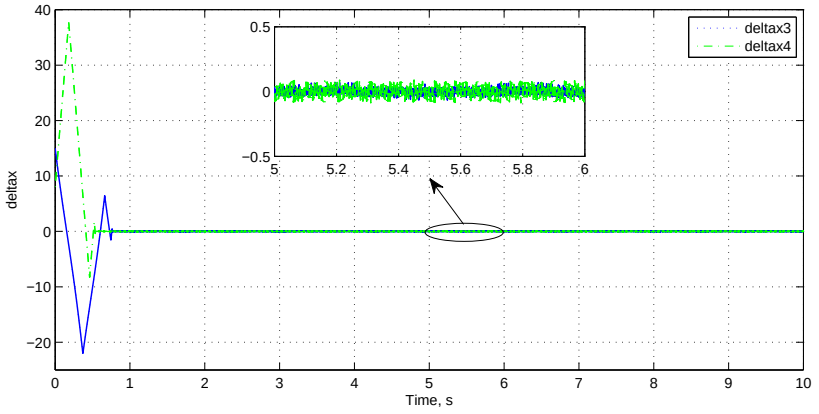

FIGURE 5.12: States tracking with Pareto-optimization control.

with the control task of the system. The adaptive version of PID control based on Neural idea [68] handles better this task (see figure 5.14). On one hand this is because of the additional external perturbation injected to the system and on the other hand because of near-singularity condition of the matrix $G(X)$.

5.2.1 Near-Singularity Elimination and Equivalent Control

As one can see from the Fig 5.15, applying the conventional SMC to the platform system (4.9) provokes a huge control signals, do to the near singularity proporties of the matrix $G(X)$. The proposed regulizated control however (2.23) provides a significant improvement of control signal behaviour. The figure 5.16 shows the stabilization of the control signals and the near-singularity elimination.

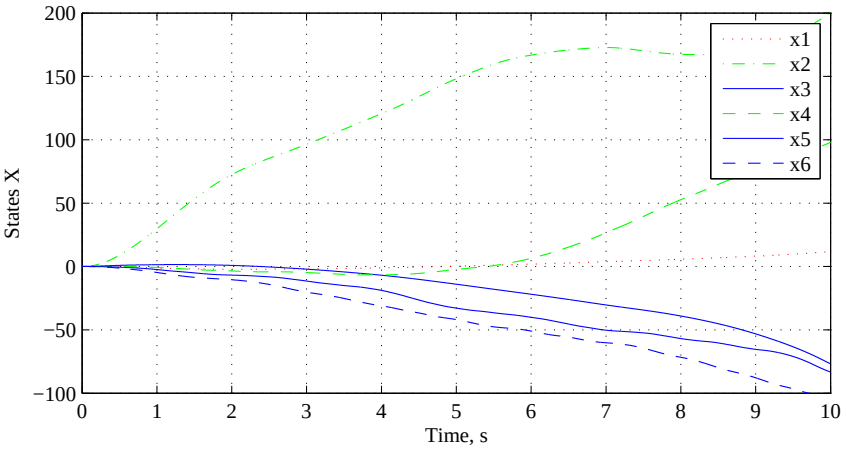

FIGURE 5.13: States evaluation under PID control.

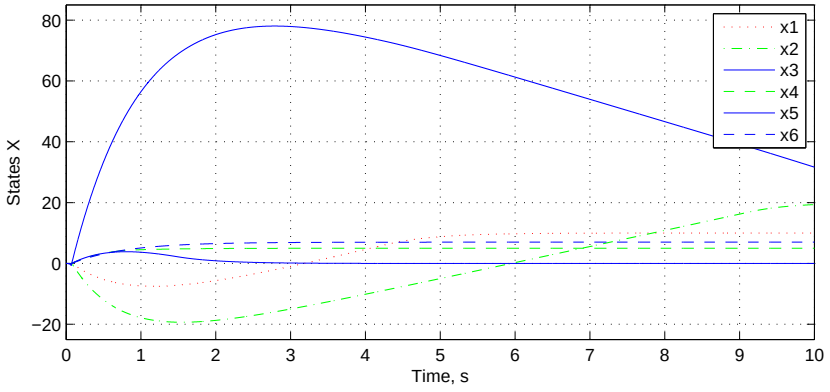

FIGURE 5.14: States evaluation under Adaptive PID control.

Figures 5.17 and 5.18 illustrate the finite time convergence of the state variables and their derivatives to the desired magnitudes in the presence of the external bounded disturbance all states reach the desired values approximately after 5 seconds.

Equivalent sliding mode control To demonstrate the properties of the adaptation procedure for chattering reduction, another simulation was performed with the following parameters:

$$\gamma_0 = 3,\ \mu = 0.04,\ \alpha = 0.95$$

$$k_1^+ = 10,\ k_2^+ = 1, k_{1,2}(0) = 2.8$$

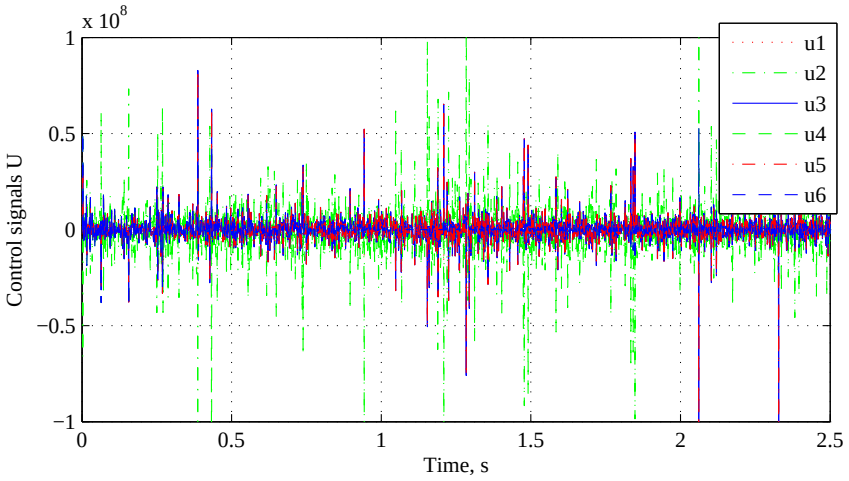

FIGURE 5.15: Control signals with original matrix G.

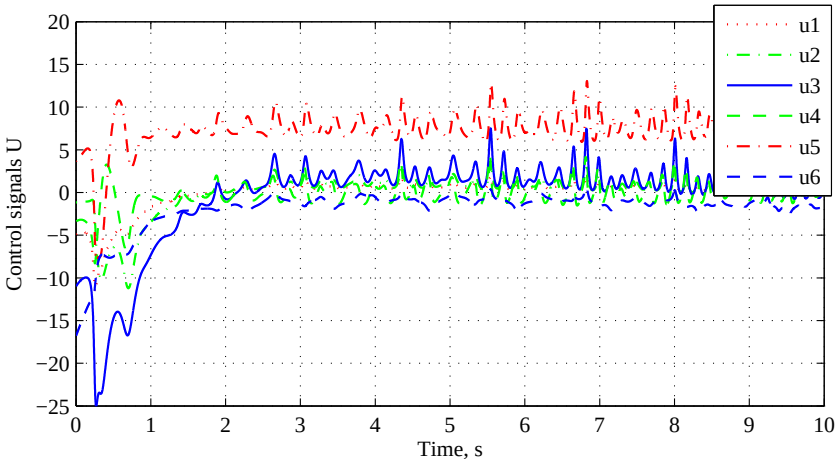

FIGURE 5.16: The normalized control signals with G_1.

One can see that the control signals have the chattering phenomena with amplitudes much smaller than the conventional control.

It can be clearly seen (Fig. 5.16 and Fig. 5.19) that gain parameter $k(t)$, defining the chattering amplitude in the sliding mode (after the reaching time t_{reach}), continues decreasing attaining after $0,3$ *sec.* and follows the amplitude of the external perturbation signal f. Notice that, in the simulation with lower frequencies, the chattering effect improvement for adaptive sliding mode control may attach ten times with respect to the standard SMC.

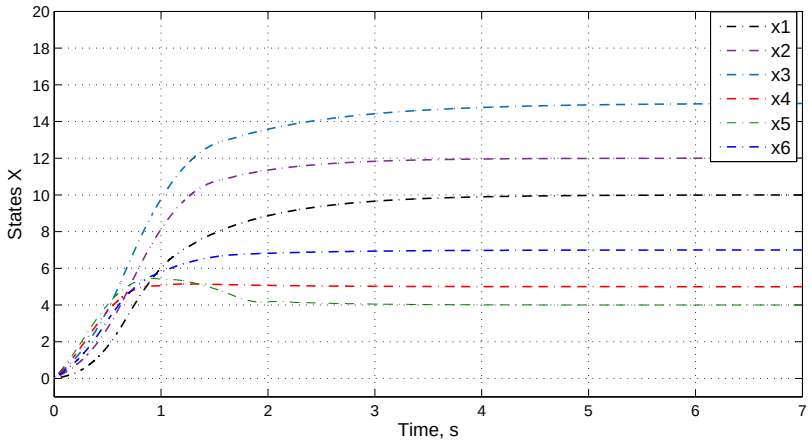

FIGURE 5.17: States evaluation under SMC.

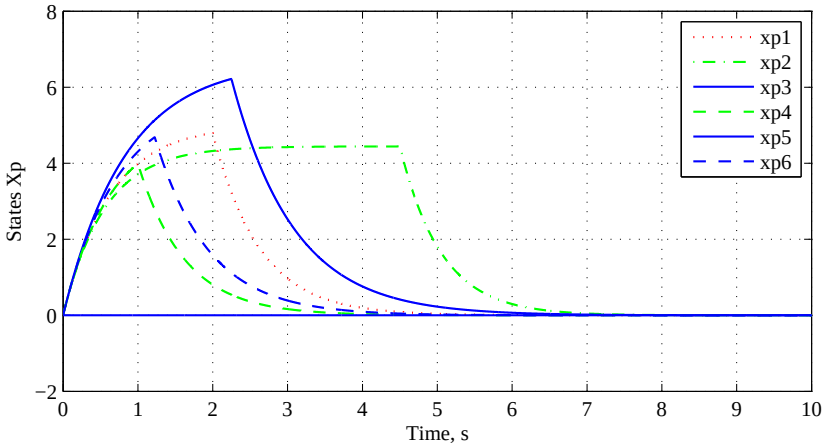

FIGURE 5.18: States $\dot{X}$ evaluation under SMC.

5.2.2 Adaptive Sliding Mode Controller Based on Super-Twist Observer

From the figures 5.20 and 5.21 one can see the behavior of the real states X and $\dot{X}$ of the stewart platform orientation controlled by the suggested adaptive Sliding Mode Controller based on the velocities estimation. Practically in 6.0 seconds the controlled variables reach the desired values. The coordinates as well as their derivative estimates show quick approachment to the real values.

As it was expected, the control actions attains their their behavior at fast rate corresponding to the desired regime: (see Fig. 5.22).

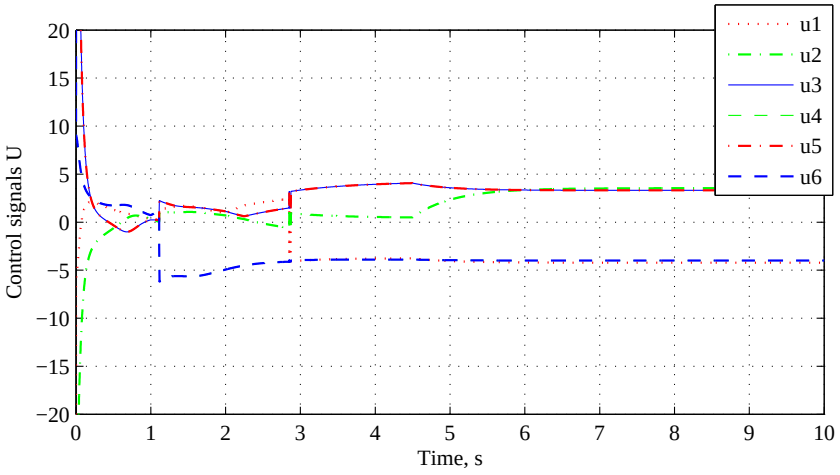

FIGURE 5.19: Control signals under filtered sliding mode control.

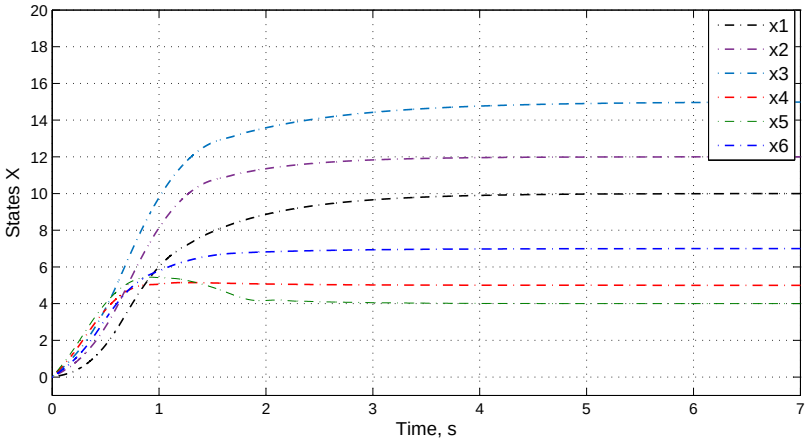

FIGURE 5.20: Lineal and angular coordinates.

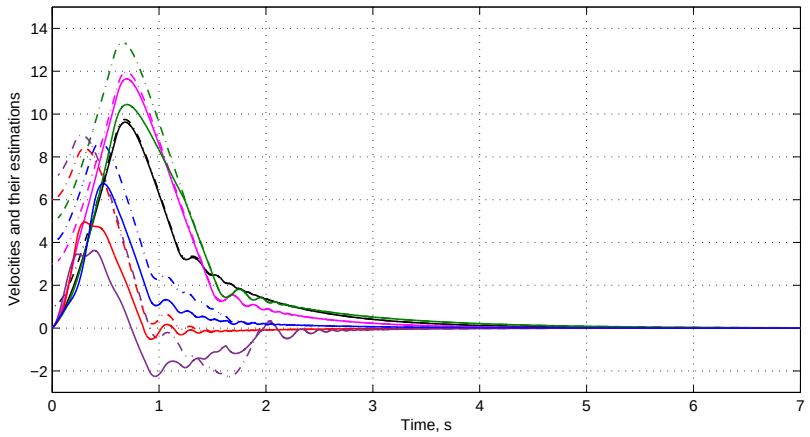

FIGURE 5.21: The comparison of Angular velocities and their estimates (every color represents one state and its estimation).

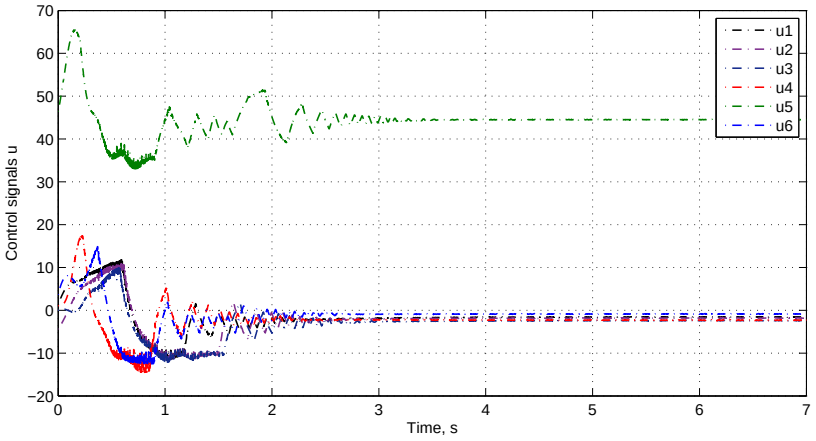

FIGURE 5.22: Control signals representation.

Chapter 6

Summary and Recommendations for Future Work

Tethered satellite systems have a great deal of potential for a wide range of future space-based applications. Although a great deal of research has already been conducted on the dynamics and control of TSS and its tracking, there remain a number of open areas of study that must be addressed before TSS can be widely put to use. The objective of the work presented in this dissertation is to address several of these open areas of study, and in the process identify new avenues down which TSS dynamics and control research should progress. The original contributions provided by this dissertation are summarized below, and we also present recommendations for future work on TSS dynamics and control.

6.1 Summary of Contributions

The description, design and performance of Stewart manipulator tethered satellite systems (TSS) was studied. The rendezvous of rotating TSS and payload that should be tossed into higher orbit was considered as a tracking problem. An adaptation methodology was used to find the control gain of a sliding-mode control providing the minimization of the chattering effect. The application of this methodology to the conventional control enables reducing of the control action magnitude to smaller value along with a finite-time convergence.

The characteristics of this six degree of freedom platform applied for the orientation of an radio telescope sub-reflector were also studied and the mathematical model was described. The new sliding mode control design was used to control the system in presence of unmodelled dynamics and perturbations and eliminate the near-singularity properties of the model. The stability analyse and the performance of the controller were studied. The same equivalent control technique was used to reduce the chattering effects.

Then We presented a new approach to the SMC-designing which uses the state estimates, obtained on-line by the Super-Twist observer. The parameter of the controller and the observer may be time-varying and depending on available current measurements. The problem of the Gough-Stewart Platform orientation in a required positions considered and numerically resolved showing very high efficiency of the suggested approach.

The numerical examples clearly illustrated the positive effect of the gain-coefficient adaptation in both contoller and observer.

6.2 Recommendations for Future Work

The work presented in this dissertation addresses only a handful of the open areas of research in TSS dynamics and control. Many issues have yet to be adequately addressed, and the work in this dissertation raises several new questions on its own. In this section, we make recommendations for ways in which the work presented in this dissertation can be extended in future TSS dynamics and control research.

The first way in which the work in this dissertation can be extended is to refine the top-level system model. Despite the fact that the system model presented is taken as the top-level system model, it contains several assumptions about the physical system that could be relaxed to make the model a better abstraction of reality. Most of these assumptions are related to the physical environment in which the TSS operates; recall that the only external forces acting on the system in the top-level system model are the gravitational force of the central body and the electrodynamic force. Other external forces, such as atmospheric drag and solar radiation pressure, could be added to the model, along with other effects like thermal expansion of the tether due to crossings between shadow and sunlight. The gravitational and electrodynamic force models can themselves be extended by using higherorder spherical harmonic expansions of the gravitational and magnetic

fields of the central body. Modeling all of these external forces would make the top-level system model a better representation of an actual TSS, and would therefore provide an even better substitute for experimental data until it can be collected.

The fact that experimental data from an actual TSS is not readily available does not mean that data cannot be collected to validate some aspects of the system model. For example, the string model for the tether can be applied to any type of vibrating string, not just a TSS. would greatly enhance the level of confidence in modeling of TSS dynamics.

One significant way in which the control analysis presented can be extended is to perform a more thorough controllability analysis of the system for the case in which the electrodynamic force is the only control input. It may be possible to perform certain types of control maneuvers using only the electrodynamic force, and knowing these maneuvers could prove useful because they would require no propellant. Along the same lines, it would be useful to determine optimal control laws that minimize the total control input required to control the pendular motion, thereby minimizing the required propellant. Both open- and closed-loop optimal control laws could be developed. Some hybrid control strategy could be developed that uses a combination of electrodynamic forcing and thrusters on the end bodies. The electrodynamic force could be used as the only control input for times when the pendular motion can be controlled adequately using only the electrodynamic force, and thrusters on the end bodies could be employed only in situations for which they are needed to make the system controllable. One final way in which the control analysis presented can be extended is to include the orbital motion in the system model and determine methods of controlling the orbital motion and the motion of the tether simultaneously, perhaps using only the electrodynamic force.

Appendix A

Values of $a_{i,k}$

A *Values of* $a_{i,k}$.

$$a_{1,1} = \cos\varphi_1 \cos\varphi_3 - \sin\varphi_1 \cos\varphi_2 \cos\varphi_3$$

$$a_{1,2} = \sin\varphi_1 \cos\varphi_3 + \cos\varphi_1 \cos\varphi_2 \sin\varphi_3$$

$$a_{1,3} = \sin\varphi_2 \sin\varphi_3$$

$$a_{2,1} = -\cos\varphi_1 \sin\varphi_3 - \sin\varphi_1 \cos\varphi_2 \cos\varphi_3$$

$$a_{2,2} = -\sin\varphi_1 \sin\varphi_3 + \cos\varphi_1 \cos\varphi_2 \cos\varphi_3$$

$$a_{2,3} = \sin\varphi_2 \cos\varphi_3$$

$$a_{3,1} = \sin\varphi_1 \sin\varphi_2$$

$$a_{3,2} = -\cos\varphi_1 \sin\varphi_2$$

$$a_{3,3} = \cos\varphi_2$$

Appendix B

Values of $g_{k,i}$ and $a_{k,i,j}$

B *Values of* $g_{k,i}$ *and* $a_{k,i,j}$.

$$g_{1i} = M^{-1}\cos\gamma_{i,1}; \qquad g_{2i} = M^{-1}\cos\gamma_{i,2}; \qquad g_{3i} = M^{-1}\cos\gamma_{i,3}$$
$$g_{4i} = J_x^{-1}\left(a_{i,1,1}\cos\gamma_{i,1} + a_{i,1,2}\cos\gamma_{i,2} + a_{i,1,3}\cos\gamma_{i,3}\right)$$
$$g_{5i} = J_y^{-1}\left(a_{i,2,1}\cos\gamma_{i,1} + a_{i,2,2}\cos\gamma_{i,2} + a_{i,2,3}\cos\gamma_{i,3}\right)$$
$$g_{6i} = J_z^{-1}\left(a_{i,2,1}\cos\gamma_{i,1} + a_{i,3,2}\cos\gamma_{i,2} + a_{i,3,3}\cos\gamma_{i,3}\right)$$

where $\gamma_{i,k}$ is the angle between A_iB_i and the axes AX, AY and AZ define as:

$$\cos\gamma_{i,j} = \cos\gamma_{i,j}\left(X_B, Y_B, Z_B, \varphi_{1,2,3}\right) = \frac{\bar{B}_i - A_{i,j}}{\sqrt{\sum_j \left(A_{i,j} - \bar{B}_i\right)^2}}$$

and

$$a_{i,1,1} = B_{i,1}\left(-\sin\varphi_1\cos\varphi_3 - \cos\varphi_1\cos\varphi_2\cos\varphi_3\right)$$
$$+B_{i,2}\left(\cos\varphi_1\cos\varphi_3 - \sin\varphi_1\cos\varphi_2\sin\varphi_3\right)$$
$$a_{i,1,2} = B_{i,1}\sin\varphi_1\cos\varphi_2\cos\varphi_3$$
$$-B_{i,2}\cos\varphi_1\sin\varphi_2\sin\varphi_3 + B_{i,3}\cos\varphi_2\sin\varphi_3$$
$$a_{i,1,3} = B_{i,1}\left(\sin\varphi_1\cos\varphi_2\sin\varphi_3 - \cos\varphi_1\sin\varphi_3\right) + B_{i,2}$$
$$\left(\cos\varphi_1\cos\varphi_2\cos\varphi_3 - \sin\varphi_1\sin\varphi_3\right) + B_{i,3}\sin\varphi_2\cos\varphi_3$$

$$a_{i,2,1} = B_{i,1}\left(\sin\varphi_1 \sin\varphi_3 - \cos\varphi_1 \cos\varphi_2 \cos\varphi_3\right)$$
$$-B_{i,2}\left(\cos\varphi_1 \sin\varphi_3 + \sin\varphi_1 \cos\varphi_2 \cos\varphi_3\right)$$
$$a_{i,2,2} = B_{i,1} \sin\varphi_1 \sin\varphi_2 \cos\varphi_3 -$$
$$B_{i,2} \cos\varphi_1 \sin\varphi_2 \cos\varphi_3 + B_{i,3} \cos\varphi_2 \cos\varphi_3$$
$$a_{i,2,3} = B_{i,1}\left(\sin\varphi_1 \cos\varphi_2 \sin\varphi_3 - \cos\varphi_1 \cos\varphi_3\right) - B_{i,2}$$
$$\left(\sin\varphi_1 \cos\varphi_3 + \cos\varphi_1 \cos\varphi_2 \sin\varphi_3\right) - B_{i,3} \sin\varphi_2 \sin\varphi_3$$

$$a_{i,3,1} = -B_{i,2} \sin\varphi_1 \sin\varphi_2$$
$$a_{i,3,2} = \cos\varphi_2\left(B_{i,1} \cos\varphi_3 - B_{i,2} \cos\varphi_1\right) - B_{i,3} \sin\varphi_2$$
$$a_{i,3,2} = -B_{i,1} \sin\varphi_2 \sin\varphi_3$$

.

Appendix C

Singular configuration

C.1 Grassmann geometry

We recall the definition of a Plucker vector for a line; for two points M_1, M_2 on the line and a reference point O, the Plucker vector, of dimension 6, is [26]

$$P_r = [M_1M_2, OM_1 \times OM_2] = [M_1M_2, M_2M_1 \times OM_2] = [p, q]$$

A line is represented by any vector λP_r where λ is an arbitrary non-zero scalar. A 6-dimensional vector will represent a line if $p.q = 0$ and q is not the zero vector. Two lines with Plucker vectors $P_r^1 = [p1, q1]$, $P_r^2 = [p2, q2]$ intersect if and only if $p_1.q_2 + q_1.p_2 = 0$. Plucker vectors with $p = 0$ do not represent real lines and are associated with a line at infinity. All lines at infinity belong to a plane, the plane at infinity. A point may also be represented by the Plucker coordinates $(\mathbf{U}3b1, r)$ so that its coordinates are $r/\mathbf{U}3b1$. If $\mathbf{U}3b1 = 0$, then the point is at infinity, and a point $(0, r)$ at infinity is on the line at infinity $(0, q)$ if and only if r.$q = 0$. Consequently a point at infinity that belongs to the two lines at infinity $(0, s_1)$, $(0, s_2)$ has coordinates $(0, s1 \times s2)$.

The representation of a line by its Plucker coordinates is redundant because the dimension of this vector is 6, although only 4 parameters are needed to define a line. This redundancy

may be decreased by introducing the normalized Plucker vector Prn defined by:

$$P_{rn} = \left[\frac{M_1 M_2}{\|M_1 M_2\|}, \frac{OM_1 \times OM_2}{\|M_1 M_2\|} \right]$$

The columns of the full inverse kinematic jacobian matrices of most parallel robots are constructed from the Plucker vectors, normalized or not, of lines associated with links of the manipulator. The singularity of this matrix therefore means that there will be a linear dependence between these vectors. If n Plucker vectors are linearly independent, they will span a variety with dimension$n \leq 6$; if some of them are linearly dependent, the dimension of the variety will be less than n. H. Grassmann (1809-1877) showed that linear dependence of Plucker vectors induced geometric relations between the associated lines, so that a set of n Plucker vectors creates a variety with dimension $m < n$. He established the geometrical conditions on a set of $n + 1$ lines so that the induced variety has dimension n.

Grassmann's geometrical conditions allows us to design an algorithm for finding the singular configurations of any type of parallel robot whose full inverse kinematic jacobian consists of Plucker vectors. We will consider all sets of n lines that are associated with the vectors, and then determine what should be the pose of the moving platform so that the n lines satisfy one of the geometrical conditions which ensure that they span a variety of dimension $n - 1$, thereby leading to a singularity of the robot.

C.2 Variety and Geometry

We now list the geometric conditions that ensure that the dimension of the variety spanned by a set of $n + 1$ Plucker vectors is n, for each possible dimension n of the variety. Note that we will often mention the case of intersecting lines; these include parallel lines, which intersect at infinity.

We shall start with the dimensions going from 1 to 3 (figure C.1); for the variety of dimension 1 (called a point) there is just one Plucker vector and one line. A variety of dimension 2, called a line, may be constituted either by two Plucker vectors for which the associated lines are skew, i.e. they do not intersect and they are not parallel, or be spanned by more than two Plucker vectors if the lines that are associated with the vectors

form a planar pencil of lines, i.e. they are coplanar and possess a common point (possibly at infinity, to cover the case of coplanar parallel lines).

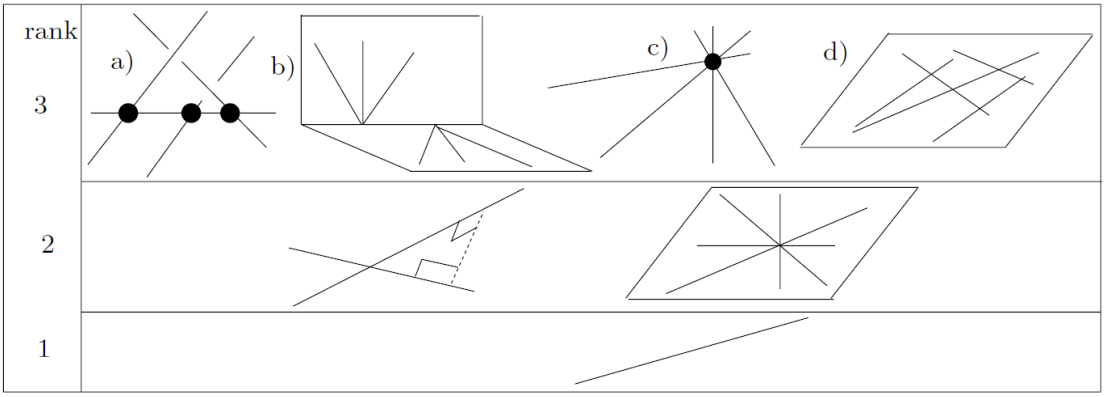

FIGURE C.1: Grassmann varieties of dimension 1,2,3.

A variety of dimension 3, called a plane, is the set of lines $\mathcal{F}$ that are dependent upon 3 lines $\mathcal{F}_1$,$\mathcal{F}_2$,$\mathcal{F}_3$. It is possible to show that all the points belonging to the lines F lie on a quadric surface $\mathcal{Q}$. This quadric degenerates to a pair of planes $\mathcal{P}_1$,$\mathcal{P}_2$ if any two of the three lines $\mathcal{F}_1$,$\mathcal{F}_2$,$\mathcal{F}_3$ intersect.

- condition 3d: all the lines are coplanar, but do not constitute a planar pencil of lines; $\mathcal{F}_1$,$\mathcal{F}_2$,$\mathcal{F}_3$ are coplanar and $\mathcal{P}_1$,$\mathcal{P}_2$ are coincident .

- condition 3c: all the lines possess a common point, but they are not coplanar; $\mathcal{F}_1$,$\mathcal{F}_2$,$\mathcal{F}_3$ intersect at the same point, possibly at infinity (this covers the case of parallel lines).

- condition 3b: all the lines belong to the union of two planar pencils of non coplanar lines that have a line L in common; $\mathcal{F}_2$,$\mathcal{F}_3$ intersect at a point p, and $\mathcal{L}$ intersects $\mathcal{F}_1$ at a. Two different cases may occur:

• $\mathcal{P}_1$,$\mathcal{P}_2$ are distinct and intersect along the line L. The set of dependent lines are the lines in $\mathcal{P}_1$ that go through a, and the lines in $\mathcal{P}_2$ that go through p

• $\mathcal{P}_1$,$\mathcal{P}_2$ are distinct and parallel. This occurs if two of the lines $\mathcal{F}_i$are parallel; L is a line at infinity, and the set of dependent lines are two planes of parallel lines

- condition 3a: all the lines belong to a regulus; $\mathcal{F}_1$,$\mathcal{F}_2$,$\mathcal{F}_3$ are skew

Condition 3a must be explained in more detail. Consider three pairwise skew lines in space. The lines which intersect all three of these skew lines define a set, called a regulus.

This set of lines, the regulus, constitutes a surface, a hyperboloid; the three skew lines are said to be the generators or transversal of the surface. In 1645, Sir Christopher Wren showed that apart from the regulus, a second set of lines generates the same hyperboloid; this second set is called the complementary regulus. The hyperboloid therefore is a surface that is doubly ruled. The lines of the reguli possess an interesting characteristic: all the lines of a regulus intersect all the lines of the other regulus and none of its own regulus.

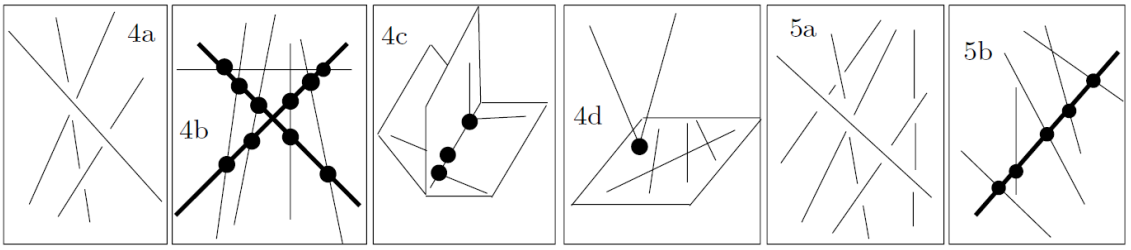

FIGURE C.2: Grassmann varieties with dimension 4 and 5. The varieties are generated by the thin lines.

We now list the geometrical conditions that characterize the varieties of dimension 4 and 5 (figure C.2). A variety if dimension 4, called a congruence, corresponds to a set of lines which satisfies one of the following 4 conditions:

- condition 4d: all the lines lie in a plane or meet a common point that lies within this plane. This is a degenerate congruence.

- condition 4c: all the lines belong to the union of three planar pencils of lines, in different planes, but which have a common line. This is a parabolic congruence.

- condition 4b: all the lines intersect two given skew lines. This is a hyperbolic congruence.

- condition 4a: the variety is spanned by 4 skew lines such that none of these lines intersects the regulus that is generated by the other three. This is an elliptic congruence.

A variety $\mathcal{C}$ of dimension 5, called a linear complex, is defined by two 3-dimensional vectors $(c, \bar{c})$ as the set of lines L with Plucker coordinates $(l, \bar{l})$ such that $\bar{c}.l + \bar{c}.l = 0$. The complex may be

-singular (5b) if $\bar{c}.c = 0$. All the lines of the complex intersect the line with Plucker coordinates $(c, \bar{c})$.

- general or non singular (5a) if $\bar{c}.c \neq 0$

The degree of freedom associated with a linear complex is a screw motion with axis defined by the line with Plucker vector $(c, c - pc)/\left\|c\right\|$, where $p = c.c/\left\|c\right\|$ is the pitch of the motion. All coplanar lines of a non singular complex are in a plane that is normal to the helical motion at a point, and intersect this point, thereby constituting a planar pencil of lines.

Bibliography

[1] V. I. Popov. *Sistems of Orientation and Stabilization of spacecrafts*. Mashinostroenie, Moscow, 2 edition, 1986. in russian.

[2] M. Griffin and J. French. *Space Vehicle Design, Second Edition*. AIAA, 2004.

[3] B. S. Alioshin, Veremeyenko K. K., and Chernomorsky A. I. *Orientation and Navigation of movable objects*. FISMATLIT, Moscow, 2006. in russian.

[4] J. J. E. Slotine and W. Li. *Applied Nonlinear Control*. Prentice-Hall, 1991.

[5] K. Park and J.L. Crassidis. A robust gps receiver self survey algorithm. *J. Inst. Navigation*, 53(4):259–268, 2006.

[6] S. Merlo, M. Norgia, and S. Donati. *Handbook of Optical Fibre Sensing Technology*, volume 53, chapter Fiber gyroscope principles, pages 331–347. Wiley, Chichester, 2002.

[7] F. Landis Markley and John L. Crassidis. *Fundamentals of Spacecraft Attitude Determination and Control*. Springer, New York, 2014.

[8] H.B. Hablani. Momentum accumulation due to solar radiation torque, and reaction wheel sizing, with configuration optimization. *In: Proceedings of the Flight Mechanics/Estimation Theory Symposium*, pages 3–22, 1992.

[9] Eugene Lavretsky and Kevin A. Wise. *Robust and Adaptive Control with Aerospace Applications*. Springer-Verlag, London, 2013.

[10] V.I. Utkin. *Sliding Modes in Control and Optimization*. Spronger Verlag, 1992.

[11] ROBERT P. HOYT. Stabilization of electrodynamic space tethers. *TETHERS UNLIMITED, INC.*, pages 1–9, 2001.

[12] V. V. Beletsky and E. M. Levin. *Dynamics of Space Tether Systems*. Advances in the Astronautical Sciences, 1993.

[13] Dimitry Petrovich Kim. *Automatic Control Theory*. Fismatlit, Moscow, 2 edition, 2004. in russian.

[14] A. Levant. Sliding order and sliding accuracy in sliding mode control. *Journal of Control 58*, pages 1247–1263, 1993.

[15] G. Bartolini, A. Ferrara, E. Usai, and V.I. Utkin. On multi-input chattering-free secondorder sliding mode control. *IEEE Transactions on Automatic Control*, pages 1711–1717, 2000.

[16] S. Laghrouche, P. Plestan, and A. Glumineau. Higher order sliding mode control based on integral sliding surface. *Automatica*, pages 531–537, 2007.

[17] K.J. Astrom and B. Wittenmark. *Adaptive Control*. Addison-Wesley, NY, 2 edition, 1989.

[18] E. Dubrovskii. Application of the adaptation principle for control systems with variable structure. *In: Proceedings of National Conference on Control*, 1967.

[19] F. Plestan, Y. Shtessel, V. Brageault, and A. Poznyak. Sliding mode control with gain adaptation: Application to an electropneumatic actuator. *Control Engineering Practice*, 21:679–688, 2013.

[20] Y. J. Huang, Kuo T. Ch., and Sh. H. Chang. Adaptive sliding-mode control for nonlinearsystems with uncertain parameters. *IEEE TRANSACTIONS ON SYSTEMS, MAN, AND CYBERNETICS—PART B: CYBERNETICS*, 38(2):208–212, 2008.

[21] C. Hall and Y. Shtessel. Sliding mode disturbance observer-based control for a reusable launch vehicle. *AIAA Journal of Guidance, Control, and Dynamics*, 29(2): 1315–1328, 2006.

[22] H. Lee and V.I. Utkin. Chattering suppression methods in sliding mode control systems. *In: Annual Reviews in Control*, pages 178–188, 2007.

[23] V. Utkin and A. Poznyak. *Adaptive Sliding Mode Control, In the book Advances in Sliding Mode Control: Concept, Theory and Implementation*, volume 440 of *Lecture Notes in Control and Information Sciences*, chapter 3, pages 21–53. Springer-Verlag Berlin Heidelberg, 2013.

[24] A. Poznyak. *Advanced Mathematical Tools for Automatic Control Engineers, vol.2: Stochastic Technique*. Elsevier, Amsterdam, Netherlans, 2009.

[25] V. Utkin and A. Poznyak. Adaptive sliding mode control with application to super-twist algorithm: Equivalent control method. *Automatica*, 49:39–47, 2013.

[26] J. P. Merlet. *Parallel Robots*. Springer, INRIA, Sophia-Antipolis, France, 2 edition, 2006.

[27] E.F. Fichter. A stewart platform based manipulator: general theory and practical construction. *Int. J. of Robotics Research*, 5(2):157–181, 1986.

[28] K. Sugimoto, J. Duffy, and K.H. Hunt. Special configurations of spatial mechanisms and robot arms. *Mechanism and Machine Theory*, 17(2):119–132, 1982.

[29] Cauchy A. Deuxieme memoire sur les polygones et les polyedres. *Journal de l'Ecole Polytechnique*, pages 87–98, May 1813.

[30] P. Deuflhard. A modified newton method for the solution of ill-conditioned systems of nonlinear equations with application to multiple shooting. *Numer. Math.*, pages 289–315, 1974.

[31] E. Mastorakis Nikos. Sliding mode disturbance observer-based control for a reusable launch vehicle. *in: Proceedings of the 6th WSEAS Int. Conf. on EVOLUTIONARY COMPUTING*, pages 29–35, 2005.

[32] John Hauser, Shankar Sastry, and Kokotovic Petar. Nonlinear control via approximate input-output linearization: The ball and beam example. *IEEE TRANANSACTIONS ON AUTOMATIC CONTROL*, 37(3):392–399, 1992.

[33] V.I. Filippov. *Differential Equations with Discontinuous Right-Hand Sides, Mathematics and Its Applications*. Kluwer Academic, 1988.

[34] Y. Shtessel, Ch. Edwards, L. Fridman, and A. Levant. *Sliding Mode Control and Observation*. Birkhauser, 2014.

[35] S. Keshtkar and A. Poznyak. Tethered space orientation via adaptive sliding mode. *Int. J. Robust. Nonlinear Control*, (accepted), 2015. doi: 10.1002/rnc.3371.

[36] Kazantzis Nikolaos and Kravaris Costas. Nonlinear observer design using lyapunov auxiliary theorem. *Systems and Control Letters*, 34(5):241–247, 1998.

[37] Hu Xiaosong, Sun Fengchun, and Zou Yuan. Estimation of state of charge of a lithium-ion battery pack for electric vehicles using an adaptive luenberger observer. *Energies*, 3:1586–1603, 2010.

[38] Vadim Utkin, Martin Buss, and Sachit Rao. An adaptive sliding mode observer for induction machines. *American Control Conference*, pages 1947–1951, 2008.

[39] Christopher Edwards and Chee Pin Tanb. Sensor fault tolerant control using sliding mode observers. *Control Engineering Practice*, 14:897–908, 2006.

[40] H. Weiss and J.B. Moore. Improved extended kalman filter design for passive tracking. *IEEE Trans. Autom. Contr.*, AC-25:897–908, 1980.

[41] D. D. Gobbo, M. Napolitano, P. Famouri, and M. Innocenti. Experimental application of extended kalman filtering for sensor validation. *IEEE Transactions on Control Systems Technology*, 9:376–380, 2001.

[42] Huh K. Fathy H.K. Jung, J. and J.L. Stein. E optimal robust adaptive observer design for a class of nonlinear systems via an h-infinity approach. *American control conference*, In Proceedings of the 2006:3637–3642, 2006.

[43] Sang-Min Kima, Woo-Yong Hanb, and Sung-Joong Kima. Design of a new adaptive sliding mode observer for sensorless induction motor drive. *Electric Power Systems Research*, 70:16–22, 2004.

[44] Yuhong Zheng, Hossam A. Abdel Fatta2, and Kenneth A. Loparo. Non-linear adaptive sliding mode observer-controller scheme for induction motors. *Int. J. Adapt. Control Signal Process*, 14:245–273, 2000.

[45] Jingchuan Li, Longya Xu, and Zheng Zhang. An adaptive sliding-mode observer for induction motor sensorless speed control. *IEEE TRANSACTIONS ON INDUSTRY APPLICATIONS*, 41(4):1039–1047, 2005.

[46] Christopher Edwards, Sarah K. Spurgeon, and Ron J. Patton. Sliding mode observers for fault detection and isolation. *Automatica*, 36:541–553, 2000.

[47] Christopher Edwards and Xing-Gang Yan. Nonlinear robust fault reconstruction and estimation using a sliding mode observer. *Automatica*, 43:1605–1614, 2007.

[48] L. Fridman, A. Mokhtari, and A. Benallegu. High-order sliding-mode observer for a quadrotor uav. *Int. J. Robust Nonlinear Control*, 18:427–440, 2008.

[49] H.T. Kung, F. Luccio, and F. P. Preparata. On finding the maxima of a set of vectors. *Journal of the ACM*, 22(4):469–676, 1975.

[50] C. Arnold Barry. *Pareto Distributions*. CRC Press, Riverside, CA, 2 edition, 2015.

[51] C. Gasdaska, J. Spence, and A. Young. Testing of carbon nanotube field emission cathodes. *AIAA, 40th Joint Propulsion Conference*, pages 2004–3427, 2004.

[52] R. L. Forward, T. J. Bogar, M. E. Bangham, and M. J. Lewis. Hypersonic airplane space tether orbital launch (hastol) system: Initial study results. *IAF 50th International Astronautical Congress*, pages S6–16, 1999.

[53] Hao Wen, P. Jin Dongping, and Y. Hu Haiyan. Advances in dynamics and control of tethered satellite systems. *Acta Mech Sin*, 2008. doi: 10.1007/s10409-008-0159-9.

[54] R. L. Forward. Tether transport from leo to the lunar surface. *AIAA Paper*, pages 23–34, 1991.

[55] X. S. Su and et all. Singularity analysis of fine-tuning stewart platform for large radio telescope using genetic algorithm. *Mechatronics*, 5:413–425, 2003.

[56] N. Leroy and et all. Dynamic modeling of a parallel robot. application to a surgical simulator. *IEEE Int. Conf. on Robotics and Automation*, 198, Flight Simulation: 4330–4335, 1975.

[57] W.P. Koevermans and et all. Design and performance of the four d.o.f. motion system of the nlr research flight simulator. *AGARD Conf. Proc.n*, 198, Flight Simulation: 17(1)–17(11), 1975.

[58] A. Dubowsky and et all. The design and implementation of a laboratory test bed for space robotics. *ASME Design Automation Conf.*, pages 99–108, 1994.

[59] M. Girone, G. Burdea, and et al. A stewart platform-based system for ankle telerehabilitation. *Special Issue on Personal Robotics, Autonomous Robots*, 10:203–212, 2001.

[60] L. E. Bruzzone, R. M. Molfino, and R. P. Razzoli. Modelling and design of parallel robot for laser cutting applications. *Proceedings of IASTED International Conference on Modelling, Identification and Control*, pages 518–522, 2002.

[61] R. M. Jan, C. S. Tseng, and R. J. Liu. Robust pid control design for permanent magnet synchronous motor: a genetic approach. *Electr. Power Syst. Res.*, 7:1161–1168, 2007.

[62] S. H. Lee, J. B. Song, W. Ch. Choi, and D. Hong. Position control of a stewart platform using inverse dynamics control with approximate dynamic. *Mechatronics*, pages 605–619, 2003.

[63] C. Elmas, O. Ustun, and H. H. Sayan. A neuro-fuzzy controller for speed control of a permanent magnet synchronous motor drive. *Exp. Syst. Appl.*, 1:657–664, 2008.

[64] W. Dongsu and G. Hongbin. Adaptive sliding control of six-dof flight simulator motion platform. *Chinese Journal of Aeronautics*, pages 425–433, 2007.

[65] P.R. Kumar and B. Bandyopadhyay. Stabilization of stewart platform using higher order sliding mode control. In *Electrical Computer Engineering (ICECE), 2012 7th International Conference on*, pages 945–948, Dec 2012.

[66] F. P. Schloerb, L. M. Stepp, and Gilmozzi R. The large millimeter telescope, in ground-based and airborne telescopes ii. *Proc. of SPIE*, 7012:1117–1129, 2008.

[67] Yu. T. Kaganov and A. P. Karpenko. Mathematical modeling of dynamics and kinematics of robot manipulator "tranl". *Nauka Y Obrazovanie, Russia*, 519(6): 1–14, 2009. in Russian.

[68] Fin Lin, Robert D. Brandt, and George Saikalis. Self-tuning of pid controllers by adaptive interaction. *Proceedings of the American Control Confrence*, pages 3676–3682, June 2000.

Publications

Accepted in indexed journals

- S. Keshtkar and A. Poznyak; "Tethered space orientation via adaptive sliding mode"; Int. J. Robust. Nonlinear Control, 2015. doi: 10.1002/rnc.3371.
- S. Keshtkar, E. Hernandez , A. Oropeza and A. Poznyak; "Orientation of Radio-Telescope Secondary Mirror via Sliding Mode Control"; Neurocomputing 2016.
- S. Keshtkar and A. Poznyak; "Adaptive Sliding Mode Controller Based on Super-Twist Observer for Tethered Satellite System"; Int. J. of Control, 2016.

In Review

- S.Keshtkar, E. Hernandez, A. Oropeza, A. Poznyak; "Subreflector of Radio-Telescope Positioning on Gough-Stewart Platform via SM Techniques". Aut. and Rem. Cont.
- Sajjad Keshtkar,Javad Keshtkar and Alexander Poznyak; "Tracking of New Solar Photovoltaic via Integral Sliding Mode"; IET Control Theory and Applications.

Conference

- Sajjad Keshtkar,Najmeh Keshtkar and Alexander Poznyak; "Magnetic Control of Tethered Cube-Satellite stabilized by rotating"; CCE 2014.
- Sajjad Keshtkar, Eusebio Hernandez , Armando Oropeza and Alexander Poznyak; Orientation of Radio–Telescope Secondary Mirror via Parallel Platform; CCE 2015.
- S. Keshtkar, J. Keshtkar and A. Poznyak; "Adaptive Sliding Mode Control for Solar Tracker Orientation", ACC, Boston 2016.